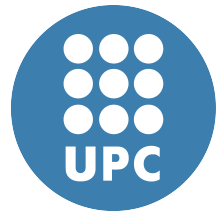

Ultrashort laser pulse measurement for multiphoton microscopy

Ivan Amat-Roldan

Dissertation
at the
Institute of Photonic Sciences (ICFO)
Super-resolution Light Microscopy & Nanoscopy Lab
Group of Prof. Pablo Loza-Alvarez
and
Universitat Politècnica de Catalunya - BARCELONATECH

En el desván antiguo de raída memoria,
detrás de la cuchara de palo con carcoma,
tras el vestuario viejo ha de encontrarse, o junto al muro
desconchado, en el polvo
de siglos. Ha de encontrarse acaso más allá del pálido gesto de una mano
vieja de algún mendigo, o en la ruina del alma
cuando ha cesado todo.

Yo me pregunto si es preciso el camino
polvoriento de la duda tenaz, el desaliento súbito
en la llanura estéril, bajo el sol de justicia,
la ruina de toda esperanza, el raído harapo del
miedo la desazón invencible a mitad del sendero que conduce al torreón
derruido.

Yo me pregunto si es preciso dejar el camino real
y tomar a la izquierda por el atajo y la trocha,
como si nada hubiera quedado atrás en la casa desierta.
Me pregunto si es preciso ir sin vacilación al horror de la noche,
penetrar el abismo, la boca del lobo,
caminar hacia atrás, de espaldas hacia la negación
o invertir la verdad, en el desolado camino.

O si más bien es preciso el sollozo de polvo en la confusión del verano
terrible, o en el trastornado amanecer del alcohol con trompetas de sueño
saberse de pronto absolutamente desiertos, o mejor,
es quizá necesario haberse perdido en el sucio trato del amor,
haber contratado en la sombra un ensueño,
comprado por precio una reminiscencia de luz, un encanto
de amanecer tras la colina, hacia el río.

Admito la posibilidad de que sea absolutamente preciso
haber descendido, al menos alguna vez, hasta el fondo del edificio oscuro,
haber bajado a tientas el peligro de la desvencijada escalera, que amenaza a
ceder a cada paso nuestro,
y haber penetrado al fin con valentía en la indignidad, en el sótano oscuro.
Haber visitado el lugar de la sombra,
el territorio de la ceniza, donde toda vileza reposa
junto a la telaraña paciente. Haberse avecinado en el polvo,
haberlo masticado con tenacidad en largas horas de sed
o de sueño. Haber respondido con valor o temeridad al silencio
o la pregunta postrera y haberse allí percatado y rehecho.

Es necesario haberse entendido con la malhechora verdad
que nos asalta en plena noche y nos devela de pronto y nos roba
hasta el último céntimo. Haber mendigado después largos días
por los barrios más bajos de uno mismo, sin esperanza de recuperar lo perdido,
y al fin, desposeídos, haber continuado el camino sincero y entrado en la noche absoluta con
valor todavía.

El precio de la verdad,
Carlos Bousoño.

ACKNOWLEDGEMENTS

First of all, I would like to acknowledge Pablo Loza-Alvarez for putting his efforts and trust in my capabilities as a PhD candidate for his research Group. I would specially like to thank him his patience and dedication along many hours spent in the lab teaching me how to mount amazingly complex optical set ups and injecting my mind with the sweet poison of ultrashort laser pulses. Along these years I have had the privilege of learning key insights and discussing next to him the real dynamics of such bursts of coherent photons that are ultrashort laser pulses, which are just unbelievably singular in the way the propagate onto space and matter, in the form they are born, in all the manners they can be transformed. All this has absolutely changed the way I see the world and all the things there are in it to achieve a better and better understanding of the beautiful physics hidden in everything that surrounds me, I can deeply say that I have already experienced the marvellous potential ultrashort laser light has to offer to the world. Secondly, I need to profoundly thank David Artigas, my closest alliance when going from the lab to the paper sheet. His critical spirit, the way he shapes the concepts and the challenges he has kept throwing at me has also enabled to engross my brain assets from a highly complementary prospective. Probably, these three things are completely unfair when it comes to enumerate his contribution to my character, which has been very extensive. There is many other people to remember, particularly Iain Cormack who underwent through my inexperienced perception of the world along my first PhD years, and as a senior postdoc had to suffer many stupid questions and hassles from me. My special thoughts go to

thank Lluis Torner, a visionary man, who has successfully devoted himself to the huge challenge of building ICFO. I hope you accomplish your mission at full range and even beyond yourself! I would particularly like to finally thank Dolors Mateu for her inestimable help and boundless kindness along these years.

In the personal side of my stuff, I have no pages to thank, cheer and hug many of my companions and PhD-travellers like Emilio, Gemma, Rodri, Pedro, Silvia, Merca, Elda,… for all the hours playing “mus” in the campus, for all the nights and mornings, for all the life we shared together growing, enjoying life and making mistakes, too. For all this, you will always remain at the bottom of my heart, where I sometimes remember that happy times do exist forever. I would like to particularly thank Sotiris, an entering PhD at the time I was finishing this work who is specially cheerful, enthusiastic and hard-worker. Thanks Sotiris for giving my faith back on research in many desperate moments!

To all of you who know me (particularly Mingo, Javi, César, Iker, Jaume, Santi, Luque, Bernat, Alberto, Ángel, Emilio, …) , thanks for holding on me, I know I can be the worst person in the world at many times, but I try keeping on solving it (although I see no equations…). Many thanks dudes, the next one is on me! ☺

INDEX

ABSTRACT (ENGLISH, CASTELLANO, CATALÀ). 3

1 Titanium-Sapphire Laser. 7

1.1 Introduction. **8**

1.2 Titanium-Sapphire as a lasing material. **8**
1.2.1 General material properties. **8**
1.2.2 Coupling of electronic and vibronic energy states. **10**
1.2.3 Absorption and Fluorescence spectra in Ti^{3+}:Al_2O_3. . . . . **.15**

1.3 Pulse generation in Titanium-Sapphire. **16**
1.3.1 Introduction to pulse generation. **16**
1.3.2 Cavity equations and normal mode formulation. **17**
1.3.3 Cavity-plus-atom equations of motion. **20**
1.3.4 Temporal modulation of light in the resonator. **21**
1.3.5 Active mode locking. **23**
1.3.6 Theory of active mode locking. **25**
1.3.7 Passive Mode Locking. **25**
1.3.8 Kerr Lens Mode Locking. **28**
1.3.9 Dispersion and its compensation. **29**
1.3.10 Pulse generation in a Ti:Sapphire laser. **32**
1.3.11 Theory of pulse generation in Ti:Sap Laser
by kerr-lens mode locking. **33**

1.4 Conclusions. **37**

2 Ultrashort laser pulses and life sciences. 41

2.1 Introduction. **42**

2.2 Scope of his thesis. **43**

2.3 The meaning of measuring. **45**
2.3.1 General concept. . . . . **.45**

2.3.2 The challenge of measuring an ultrashort laser pulses. **46**

2.4 Other applications of ultrashort laser pulses. **47**

2.5 Limitations and timeliness of this thesis. **48**

3 Ultrashort pulse measurements in the time domain: State-of-the-art (part 1) **51**

3.1 Introduction to time domain techniques. **52**

3.2 Pulse characterization in the time domain. **52**
3.2.1 Autocorrelation. **52**
3.2.2 Interferometric Autocorrelation. **55**
3.2.3 MOSAIC. **60**
3.2.4 IRIS. **61**
3.2.5 PICASO. **61**

3.3 Conclusions. **63**

4 Methods for the complete measurement of ultrashort laser pulses: State-of-the-art (part 2) **67**

4.1 Introduction to complete measurement. **68**

4.2 Methods for complete measurement. **70**
4.2.1 Time-Frequency domain. **70**
4.2.1.1 Introduction. **70**
4.2.1.2 Sonogram. **71**
4.2.1.3 Spectrogram. **73**
4.2.1.4 FROG. **73**
4.2.2 Other remarkable FROG schemes. **80**
4.2.2.1 Introduction. **80**
4.2.2.2 GRENOULLE: simplified and single shot FROG. **80**
4.2.2.3 XFROG: two different pulses. **81**
4.2.2.4 Blind-FROG: two unknown pulses. **82**
4.2.3 Interferometric Techniques. **82**
4.2.3.1 Introduction. **82**
4.2.3.2 SPIDER. **83**
4.2.3.3 Retrieval algorithm of SPIDER. **87**
4.2.4 Other techniques. **88**
4.2.4.1 Introduction. **88**

4.2.4.2 IFROG. 88
4.2.4.3 VAMPIRE. 89
4.2.4.4 MIIPS. 91
4.2.4.5 PRISM. 94

4.3 Conclusions. 95

5 New methods for pulse measurement in collinear geometry 105

5.1 Introduction. 106

5.2 Analysis of the collinear image. 108

5.3 CFROG: removing fringes. 110
5.3.1 Introduction. 110
5.3.2 Simulation. 110
5.3.3 FAST-CFROG: sampling strategy. 113
5.3.4 Experimental results. 115

5.4 MEFISTO: direct pulse measurement. 118
5.4.1 Introduction. 118
5.4.2 Theory of MEFISTO. 119
5.4.3 Simulation. 122
5.4.4 Practical considerations. 133

5.5 Experimental results from MEFISTO measurements. 137
5.5.1 MEFISTO vs CFROG. 137
5.5.2 Sub-7fs. 140
5.5.3 Pulses from a single mode fiber. 142

5.6 Conclusions. 146

6 New analytical method for measurement of two unknown pulses in collinear geometry 151

6.1 Introduction. 152

6.2 Analysis of the image from two different pulses. 153

6.3 Experimental and practical considerations. 160

6.4 Blind-MEFISTO results. 163

6.5 Other X-MEASUREMENTS. 168

6.6 Future directions of MEFISTO. 169

6.7 Conclusions. 172

7 Measuring ultrashort pulses inside a Multiphoton Microscope. 175

7.1 Introduction. 176
7.1.1 The problem. 178
7.1.2 Reported solutions. 180

7.2 Forward characterization with CFROG. 182

7.3 Relevance of the forward characterization. 187

7.4 Backwards characterization with specimen and comparing CFROG and MEFISTO. 188

7.5 Conclusions. 196

8 Summary of this thesis. 207

8.1- Major contributions. 208
8.1.1 List of papers related to this thesis. 213
8.1.2 List of papers with the research group. 213
8.1.3 Public patents with the research group. 214

Tell me, O muse, of that ingenious hero
who travelled far and wide
after he sacked the famous town of Troy.

Odyssey, Homer.

The road to excess leads to the palace of wisdom...
for we never know what is enough
until we know what is more than enough.

William Blake

ABSTRACT

In this thesis, we address specific efforts towards developing the precise aspect of ultrashort laser pulse measurement in the context of biomedical research. The motivation for pursuing these new developments was triggered by the vision of developing fundamental tools that will enable to control matter by means of light with exquisite precision with the added difficulty of being next to biological samples which are extremely sensitive and fragile. For this, light matter interaction needs to be extremely well controlled to avoid undesired effects, like cell damage due to the high peak intensity values of ultrashort laser pulses, as well as promoting specific physical processes like two-photon fluorescence excitation of a desired fluorophore embedded in some biochemical environment.

We focus in the two major bottlenecks regarding ultrashort laser pulse measurements for multiphoton microscopy, that aim for developing (1) new techniques for full characterization of ultrashort pulses under different experimental conditions and (2) new material with specific nonlinear properties that enable to obtain ultrashort pulse measurements that properly catch the temporal shape of light and at the same time can be readily found in biomedical lab, specially cost effective, non fragile and non-toxic. Combination of these two complementary strategies provides a new ground where it is possible to characterise an ultrashort pulse at the sample plane of a multiphoton microscope in a regular biomedical research facility.

Importantly, we approach ultrashort pulse characterisation by developing a different theoretical framework to the state-of-the-art and we propose few initial experiments that preliminary support our theoretical statements in the form of new optical techniques. These findings are then experimentally tested under different conditions, such different optical setups and different pulsed regimes in order to evaluate the feasibility of the tools to measure ultrashort pulses in conditions that were prohibitive at the time this thesis was started. The scope of this thesis outlines the potential of such techniques, but further efforts shall be addressed to assess feasibility, robustness and further limitations.

ABSTRACT

(ESPAÑOL)

En esta tesis dirigimos esfuerzos para desarrollar técnicas que permitan la medición de pulsos láser ultracortos en el contexto de la investigación biomédica. La motivación para la búsqueda de estos nuevos desarrollos fue provocada por la visión de desarrollar herramientas fundamentales que permitan controlar en un futuro las interacciones luz-materia con una precisión exquisita, con la dificultad añadida de estar al lado de las muestras biológicas, las cuales son extremadamente sensibles y frágiles. Para esto, la interacción luz-materia necesita estar muy bien controlada para evitar efectos no deseados, como el daño celular debido a los altos valores de intensidad de pico de los láseres de pulsos ultracortos, así como la promoción de procesos físicos específicos como excitación selectiva de un fluoroforo concreto mediante fluorescencia de dos fotones en un contexto bioquímico determinado.

Nos centramos en dos cuellos de botella relacionados con la medición de pulsos láser ultracortos en microscopía multifotónica: (1) nuevas técnicas para la caracterización completa de pulsos ultracortos en diferentes condiciones experimentales y (2) encontrar un nuevo material con propiedades no lineales que permita obtener mediciones de los pulsos ultracortos y que al mismo tiempo pueda encontrarse fácilmente en un laboratorio de biomedicina, de bajo coste, resistente y no tóxico. La combinación de estas dos estrategias complementarias proporciona un nuevo estado-del-arte en el que es posible caracterizar un pulso ultracorto en el plano de la muestra de un microscopio multifotónico en un centro de investigación biomédica regular.

Es importante destacar que presentamos un marco teórico diferente al estado de la técnica para la caracterización de pulsos láser ultracortos y proponemos algunos experimentos iniciales que corroboran dichos planteamientos teóricos y permiten introducir nuevas técnicas ópticas de medida. Estos son posteriormente probados experimentalmente en diferentes condiciones con distintos niveles de complejidad y en diferentes regímenes de pulsos con el fin de evaluar la viabilidad de las herramientas para medir pulsos ultracortos en condiciones que eran antes prohibitivas en el momento en que se inició esta tesis. El alcance de esta tesis describe el potencial de estas técnicas, aunque más esfuerzos se deberán dirigir a evaluar la viabilidad, solidez y limitaciones adicionales en un entorno práctico.

ABSTRACT

(CATALÀ)

En aquesta tesi dirigim esforços per desenvolupar tècniques que permetin el mesurament de polsos làser ultracurts en el context de la recerca biomèdica. La motivació per a la recerca d'aquests nous desenvolupaments va ser provocada per la visió de desenvolupar eines fonamentals que permetin controlar en un futur les interaccions llum-matèria amb una precisió exquisida, amb la dificultat afegida d'estar al costat de mostres biològiquesl les quals són extremadament sensibles i fràgils. Per això, la interacció llum-matèria necessita estar molt ben controlada i evitar efectes no desitjats, com el dany cel·lular a causa dels alts valors d'intensitat de pic dels làsers de polsos ultracurts, així com la promoció de processos físics específics com excitació selectiva d'un fluoròfor concret mitjançant fluorescència de dos fotons en un context bioquímic donat.

Ens centrem en dos colls d'ampolla relacionats amb la mesura de polsos làser ultracurts en microscòpia multifotónica: (1) noves tècniques per a la caracterització completa de polsos ultracurts en diferents condicions experimentals i (2) trobar un nou material amb propietats no lineals que permeti obtenir mesures de polsos ultracurts i que al mateix temps es pugui desar fàcilment en un laboratori de biomedicina, de baix cost, resistent i no tòxic. La combinació d'aquestes dues estratègies complementàries proporciona un nou estat-del-art en el qual és possible caracteritzar un pols ultracurt en el pla de la mostra d'un microscopi multifotónic en un centre d'investigació biomèdica.

És important destacar que presentem un marc teòric diferent a l'estat de la tècnica per a la caracterització de polsos làser ultracurts i proposem alguns experiments inicials que corroboren aquests plantejaments teòrics i permeten introduir noves tècniques òptiques de mesura. Aquests són posteriorment provats experimentalment en diferents condicions amb diferents nivells de complexitat i en diferents règims de polsos per tal d'avaluar la viabilitat de les eines per mesurar polsos ultracurts en condicions que eren abans prohibitives en el moment en què es va iniciar aquesta tesi. L'abast d'aquesta tesi descriu el potencial d'aquestes tècniques, encara que més esforços s'hauran d'adreçar a avaluar la viabilitat, solidesa i limitacions addicionals en un entorn pràctic.

CHAPTER 1

Titanium-Sapphire Laser.

1 Titanium-Sapphire Laser.

1.1 Introduction.

Titanium-doped sapphire (Ti^{3+}:sapphire) is a widely used gain medium for tunable lasers and femtosecond solid-state lasers based on transition-metal-doped material that has many advantages. It was introduced in 1986 (Moulton, 1986), and thereafter Ti:sapphire lasers quickly replaced most dye lasers, which had previously dominated the fields of ultrashort pulse generation and widely-tuneable lasers. Importantly, Ti:sapphire lasers are very convenient for many applications of physics as they can easily be tuned to the required wavelength and allow working at very high levels due to their good beam quality and high output power of typically several watts.

1.2 Titanium-Sapphire as a lasing material.

1.2.1 General material properties.

All this advantages and applications can be explained as Ti^{3+}:sapphire gain medium accumulates a number of properties that are not easily found in other materials at the same time. In what follows, we list the main properties of the Ti^{3+}:sapphire laser medium.

Firstly, and probably the most singular by itself, the Ti^{3+} ion has a very large gain bandwidth (much larger than that of rare-earth-doped gain media), allowing the generation of very short pulses and also wide wavelength tenability. The maximum gain and laser efficiency are obtained around 800 *nm*. The possible tuning range is from 650 to 1100 *nm*, but different mirror sets are normally required for covering this large range, and exchanging mirror sets is a tedious task. However, latest

developments in material sciences and optical materials have allowed reducing the number of mirrors by using ultrabroadband chirped mirrors.

Secondly, Sapphire (monocrystalline Al_2O_3) has an excellent thermal conductivity, and this alleviates thermal effects even at high laser powers and intensities. This is particularly important for some mode-locking schemes that will be explained below.

Thirdly, there is also a wide range of possible pump wavelengths where powerful diode-pumped solid state lasers are available, even though they are located in the green spectral region. In most cases, several watts of pump power are used, sometimes even 20 W. Originally, Ti:sapphire lasers were in most cases pumped with 514 nm argon ion lasers, which can deliver high average powers but are very inefficient, expensive to operate and bulky. The appearance of other kinds of green lasers now available, and frequency-doubled solid-state lasers based on neodymium-doped gain media also contributed to the spreading of the Ti:sapphire. The pump wavelength is, after this development, typically 532 nm, with a negligibly reduced pump absorption efficiency compared to 514 nm.

Fourthly, the upper-state lifetime of Ti:sapphire is short (about 3.2 μs) and the saturation intensity is very high. This means that the pump intensity needs to be high so that a strongly focused pump beam with high beam quality is required.

Fifthly, Ti:sapphire has relatively a high cross sections in spite of the huge emission bandwidth. This fact, together with the short upper-state lifetime, reduces the tendency of Ti:sapphire lasers for Q-switching instabilities, which is a significant advantage for mode-locking schemes. Additional properties of Ti^{3+}:sapphire crystals can be read from Table 1.1.

Properties of Ti^{3+}:sapphire crystals	**Value**
chemical formula	$Ti^{3+}:Al_2O_3$
crystal structure	hexagonal
mass density	3.98 g/cm^3
Moh hardness	9
Young's modulus	335 GPa
tensile strength	400 MPa
melting point	2040 °C
thermal conductivity	33 W/(m K)
thermal expansion coefficient	$5 \times 10^{-6} K^{-1}$
thermal shock resistance parameter	790 W/m
birefringence	negative uniaxial
refractive index at 633 nm	1.76
temperature dependence of refractive index	$13 \times 10^{-6} K^{-1}$
Ti density for 0.1% at. doping	$4.56 \times 10^{19} cm^{-3}$
fluorescence lifetime	3.2 µs
emission cross section at 790 nm	$41 \times 10^{-20} cm^2$

Table 1.1. Quantitative physical properties of Ti^{3+}:sapphire crystals. (from http://www.rp-photonics.com/titanium_sapphire_lasers.html)

1.2.2 Coupling of electronic and vibronic energy states.

In Ti^{3+}:sapphire laser gain media, which is doped with transition metal ions, there is a strong interaction of the electronic states of 3d electrons with lattice vibrations like phonons (Moulton, 1986; Wall and Sanchez, 1990) as illustarated in Fig. 1.1(a).

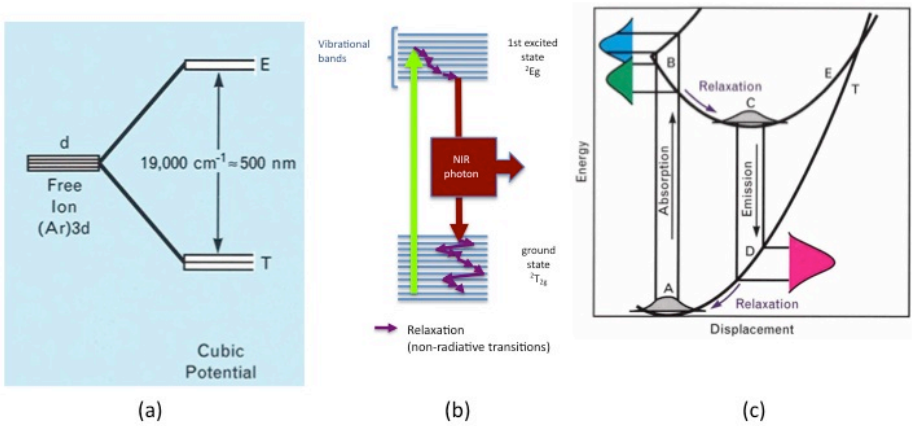

Figure 1.1. (a) A simplified energy-level diagram of Ti^{3+}. The electronic configuration of the free ion is that of an argon shell plus a single 3d electron. The crystal field of the sapphire lattice removes the fivefold degeneracy of the ground-state level of the free ion to a triplet T ground state and a doublet E excited state. (b) Excitation and emission diagram in Ti3+ ion where a blue-green photon have enough energy to pump the free electron from the triplet T ground state to the doublet E state. The large bands formed by vibronic states allow tuning the emission of photons to a number of wavelengths of a remarkable bandwidth. Within the laser cavity (c) The Ti:Al_2O_3 configurational diagram shows the relationship between the energy of the electronic states with respect to the displacement of the Ti^{3+} ion. Absorption is indicated by the vertical transition from A to B and occurs in the blue and green region of the spectrum as indicated to the left. The emission of light is indicated by the transition from C to D and occurs in the red to infrared region of the spectrum as indicated at the right. (a) and (c) pictures are from K.F. Wall and A. Sanchez in 1990.

The simplified excitation and emission process is illustrated in Figure 1.1(b), which includes the excitation with a green wavelength, around 500nm as illustrated in Figure 1.1(a), followed by a vibronic relaxation process onto the Sapphire lattice, red-NIR photon emission, and another vibronic relaxation process. This vibrational–electronic, or *vibronic*, interaction leads to a strong homogeneous broadening and thus to a large gain bandwidth as shown in Fig. 1.1(c). In the early years of laser technology, vibronic lasers were sometimes called phonon-terminated lasers. The Ti^{3+}:sapphire laser has only one d electron, and can only exist

in two energy levels as shown in Fig. 1.2. However, as the laser operates on a vibronic transition, it resembles a four-level laser. The possibility of excited state absorption of radiative transitions is eliminated due to the energy level structure of the Ti^{3+} ion, in that it has no d-state energy levels above the upper laser level.

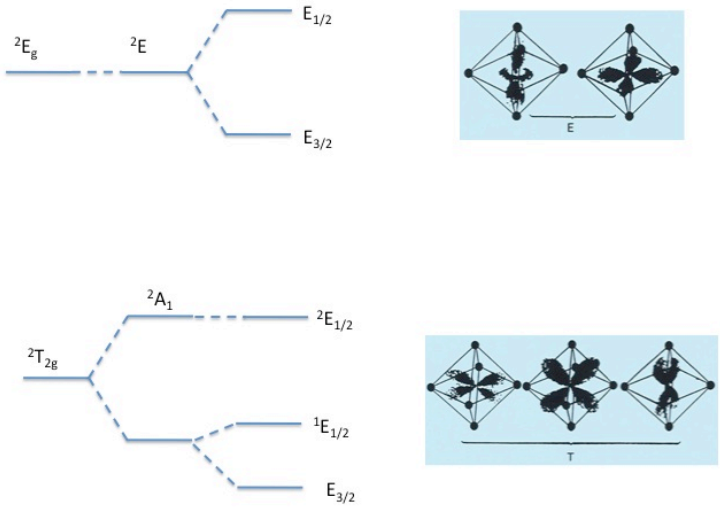

Figure 1.2. The left side of the pictures shows the two level states of the doublet state E and the three level triplet states T. The right side of the figure (acknowledged from reference Wall and Sanchez, 1990) shows the orientation of the 3d electronic orbitals with respect to the octahedrally coordinated nearest-neighbor oxygen atoms.

Particularly, the wide tuning range of the laser is possible because of a large shift between the $E_{3/2}$ excited state and the $^2T_{2g}$ ground state. The upper and lower level of the ^2E_g state can be split above the $^2T_{2g}$ ground state as seen in Fig.1.2.

In titanium-doped sapphire the Ti^{3+} ions substitute for the aluminium ions and exist in only the 3+ charge state. The energy levels of the Ti^{3+} ions are particularly simple to analyze because only a single d electron is in the outermost shell while the remaining 18 electrons have the filled-shell configuration of a neutral argon atom. When the titanium ions are placed in a host crystal, the electrostatic field of neighbouring atoms, or

the crystal field, removes the five-fold angular momentum degeneracy of the single d electron. In Ti:Al_2O_3 the 3d electron electrostatically interacts with the electronic charges of six surrounding oxygen ions that are positioned at the corners of an octahedron, as shown in Figure 1.2. In three of the five angular momentum states of the 3d electron (designated as the triplet T), orbitals do not point directly at the neighbouring oxygen atoms; these states have lower energy than the two states in which the orbitals point directly at the oxygen atoms (the doublet designated as E). This difference in energy corresponds to the energy of a green photon (of about 500 nm or 19,000 cm^{-1}), which is able to cause transitions from the ground state T to the excited state E.

In addition to this, electronic energy levels of the Ti^{3+} ions are obviously perturbed by the sapphire host lattice of Al_2O_3. When the Ti^{3+} ion is in the excited state, the overall energy of the system can be lowered if the position of the Ti^{3+} ion displaces itself with respect to the surrounding oxygen atoms (the Jahn-Teller effect, Abragam et al. 1986). This displacement removes the degeneracy of the two excited angular momentum states, which leads to a splitting of the green absorption band. Also, as the Ti^{3+} ion moves to its new equilibrium position, it kicks the surrounding lattice and excites vibrations (or phonons); this action is why the Ti:Al_2O_3 laser is called a *vibronic laser*.

The coupling between the displacements (vibrational energy levels or phonons of the surrounding sapphire lattice) with the electronic energy states of the Ti^{3+} ions is vital to operate the laser as shown in Figure 1.1(c). In this Figure, pathway from A to B indicates the absorption of a blue-green photon, whereas going from C to D shows the emission of one near-infrared photon. The purple arrow, going from B to C or D to A indicates the relaxation by the emission of a phonon.

Two important consequences of this must be noted. Firstly, population inversion in the near infrared emission band, which is mandatory for amplification and can be a bottleneck for amplification if the excited state gets full, is more easily achieved compared to other systems because the emission terminates on high vibrational levels of the ground state, which are unpopulated because of the fast vibrational relaxation rate

proportional to $1/\tau$ (for Ti:Al_2O_3 at room temperature τ is 3.2 μs, which remarkably faster compared to other lasing materials like 230 μs for Nd:YAG and 3 ms for Ruby). Secondly, large emission bandwidth and broad tunability is related to the link that exists between the broad probability of Ti^{3+} ion localization at the bottom of the E potential and the number of possible vertical transitions to several vibrational levels of the T potential as the width of the emission bandwidth depends on the details of the potential curves.

Ti^{3+} ions have no close energy states and further excitation of 3d electron levels is highly inefficient as they lie far above the E levels. This means that Ti^{3+} ion exhibits no excited state absorption (ESA); higher energy levels are far enough removed and therefore green light (pump photons) or red light (laser photons) cannot cause transitions from the E level to higher levels. The situation with other 3d transition metal ion lasers is more complex, and ESA is present at some level.

Another important feature in the design of a laser is the stimulated emission cross section (or gain cross section) denoted as σ and measured in units of area relates the number of transitions from the upper to the lower level caused by a particular flux of photons. The total gain per unit length of an amplifier is given by $N\sigma$, where N is the population inversion density. For a high gain amplifier and a low-threshold oscillation, the larger the value of σ the better. Importantly, it is possible to accurately estimate σ for a material by measuring the fluorescence profile Δf and the fluorescence lifetime τ as stimulated emission cross section is given by (Siegman, 1971):

$$\sigma = \frac{3}{4\pi^2}\frac{\lambda^2}{n^2\tau\Delta f} \tag{1.1}$$

where λ is the peak of the fluorescence curve, n is the index of refraction, and Δf is the full width at half maximum of the fluorescence curve in frequency. From small-signal gain measurements in a Ti:Al_2O_3 amplifier we have determined the value of σ to be 3.0 x 10^{-19} cm^2 (Wall et. al, 1990).

1.2.3 Absorption and Fluorescence spectra in $Ti^{3+}:Al_2O_3$

One of the most singular advantages of Ti:sapphire laser is the broad absorption band in pump and emitted fluorescence (see Figure 1.3) as mentioned above. Particularly, the peak absorption of this material is around 490nm and this is why Argon laser (as they have a number of wavelengths within the blue-green region which are suitable to pump the medium, particularly at 488 and 514.5 nm, among other secondary with less emitted power, like 454.6 nm, 457.9 nm, 465.8 nm, 476.5 nm, 496.5 nm, 501.7 nm, 528.7 nm) was originally the preferred pumping for this type of lasers.

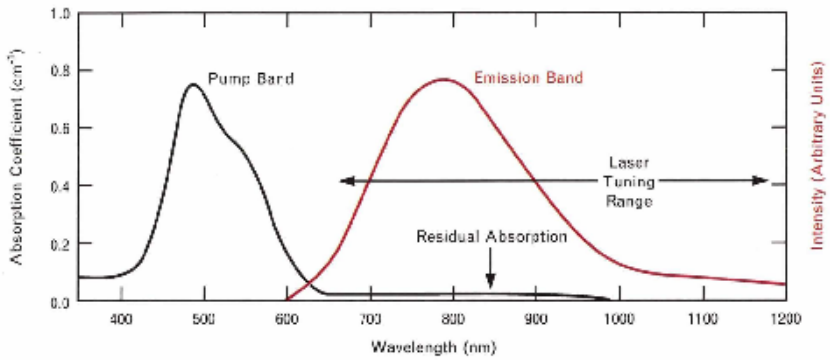

Figure 1.3. The emission and absorption bands of $Ti:AI_20_3$. The absorption band, which peaks near 490 nm, occurs in the blue-green region of the spectrum and allows $Ti:Al_2O_3$ to be pumped by argon-ion lasers, frequency-doubled Nd:YAG lasers, copper-vapor lasers, or flashlamps. The emission band peaks near 790 nm. A weak absorption band that overlaps the emission band is known as the residual absorption (figure from Wall and Sanchez, 1990).

Other suitable lasers can be found in those emitting in the green and yellow like copper-vapour at 510 and 578nm, respectively. However, this has been substituted by doubling frequency of Neodymium YAG lasers, with an emission peak around 532nm, as they are all solid state and this makes them more reliable, less bulky and simpler to operate. The excitation/emission in $Ti^{3+}:Al_2O_3$ spectra are shown in black and red in Figure 1.3, respectively.

1.3 Pulse generation in Titanium-Sapphire.

1.3.1 Introduction to pulse generation.

Currently, pulsed light is an important tool for studying nonlinear light-matter interactions (multiphoton phenomena) as it enables studying materials in new manners. Particularly, ultrashort laser pulses enable to produce high order nonlinear phenomena and minimize the damage on the interacting sample if the amount of energy deposited in the material is below its breakdown threshold. These advantages are extremely important for studying biological specimens as will be seen onto this thesis.

Pulse generation has been an intensive research topic since Charles Hard Townes produced the first continuous wave maser, the ancestor of the laser at the microwaves range in 1953. Many years later, Nicolaas Bloembergen got also a shared Nobel Prize in 1981 for his research of nonlinear optics, and particularly for his mathematical formalism that is still in use. However, years before Bloembergen became a Nobel laureate high intensity sub-picosecond lasers were already available in many labs. The first laser working at the femtosecond regime was built by Shank in 1974 and utilized a dye as a gain medium. The actual good reason to work with dye lasers was their huge fluorescence bandwidth. Much of the original work on ultrashort pulse generation was thus done with dye lasers (Shank and Ippen, 1974; Fork et al. 1981; and Valdmanis et al. 1985). However, dye lasers suffer from significant disadvantages such as rapid degradation during operation and limited output power fundamentally caused by the fact that the gain medium is an organic dye and undergoes through high intensity fields during operation that produce molecular changes or even damage. More importantly for the researchers, dye lasers required the awkward handling of poisonous and often even carcinogenic materials. The dyes themselves and also the solvents used are sometimes highly toxic, like dimethylsulfoxide (DMSO) for cyanide dyes, which was particularly hazardous as it significantly accelerates the

transport of dye molecules into the skin. Fortunately, this changed as soon as Titanium-sapphire lasers evolved and most labs changed to this solid-state technology for the many reasons mentioned above.

In order for all this to happen, it was necessary to develop a deep understanding in many fields and particularly a correct mathematical modelling of the oscillation dynamics of light in resonant cavities passing through an amplification medium (laser cavities). This advancement assisted researchers to understand how laser cavities work and which their limitations were at a given point of time. This knowledge was key to design a range of improved laser cavities and develop new types of lasers, like pulsed lasers.

1.3.2 Cavity equations and normal mode formulation.

In this section we develop an approximation of cavity equations that result in normal mode formulation by assuming some ideal condtions as no cavity losses and orthonormal nature of laser modes, which are not valid for real laser cavities, but cavity equations can help development of the essential laser insight necessary to understand how a laser works. These equations can be readily derived from Maxwell's equations and obtain the real vector electric field in the cavity. We begin in general by using the two main expressions:

$$\nabla \times \varepsilon(r,t) = -\frac{\partial b(r,t)}{\partial t} \tag{1.1}$$

and

$$\nabla \times h(r,t) = j(r,t) + \frac{\partial d(r,t)}{\partial t} \tag{1.2}$$

where

$$b(r,t) = \mu_0[h(r,t) + m_a(r,t)], \tag{1.3}$$

$$d(r,t) = \in \varepsilon(r,t) + p_a(r,t) \tag{1.4}$$

and

$$j(r,t) = \sigma\varepsilon(r,t). \tag{1.5}$$

Equations (1.3) and (1.4) are the constitutive relations that model the response of the elements within the cavity, where $\in$ is the dielectric

constant which includes the dielectric permeability of the host crystal (around 1.3267 for Ti:sapphire crystal at 633nm) and any other dielectric material inside the laser cavity. The electric and magnetic dipole moments, $p_a(r,t)$ and $m_a(r,t)$, which are dependant on polarization, model the atomic transitions (i.e. laser transitions) that may be present. The conductivity σ of Equation 1.5 stands for ohmic losses inside the laser cavity, which can be extended to include scattering and coupling losses as well.

We then compute the curl of Eq. 1.1 and in combination to the rest of equations plus the identity $\nabla \times \nabla \times \varepsilon = \nabla(\nabla \cdot \varepsilon) - \nabla^2 \varepsilon$. If we further assume that inside the closed cavity there are no free charges , which means that $\nabla \cdot \varepsilon = 0$, we obtain the full vector wave equation:

$$\frac{\partial^2 \varepsilon(r,t)}{\partial t^2} + \frac{\sigma}{\in}\frac{\partial \varepsilon(r,t)}{\partial t} - \frac{1}{\mu_0 \in}\nabla^2 \varepsilon(r,t) = -\frac{1}{\in}\left[\frac{\partial^2 p_a(r,t)}{\partial t^2} + \frac{\partial}{\partial t}\nabla \times m_a(r,t)\right] \tag{1.6}$$

This equation, named vector wave equation, enables to compute how the cavity fields $\varepsilon(r,t)$, on the left side, are driven by any electric and magnetic atomic polarizations, on the right side of Eq. 1.6.

Eq.1.6 is in general solved by means of the normal mode expansion, which assuming that we can write the cavity fields as an expansion in a set of normal modes or eigenmodes $u_r(r)$ in the form:

$$\varepsilon(r,t) = \sum_n \hat{E}_n(t) u_n(r) \tag{1.7}$$

where $E_n(t)$ are scalar functions of time only. The normal modes $u_r(r)$ in this expansion are assumed to be solutions of Laplace's equation, $\left[\nabla^2 + {k_n}^2\right] u_n(r) = 0$, which satisfy the boundary conditions of the particular cavity. These cavity modes are therefore the transveral eigenmodes of the cavity as they satisfy both the wave equation and the boundary conditions only for discrete values of the separation constant or eigenvalue k_n, which can be written as $k_n = \omega_n \sqrt{\mu_0 \in}$, where ω_n are the resonant frequencies of the empty cavity, leaving out any effects of the

atomic polarizations p_a or m_a. The laser cavity can in principle support a large number of longitudinal (along the cavity axis) and transverse (transverse to the cavity axis) modes.

Eq. 1.7 shows how the output of the laser is obtained as combination of different cavity transversal eigenmodes, $u_n(r)$, and longitudinal eigenmodes that depend on $\hat{E}_n(t)$. This relationship can be made more evident by Fourier analysis:

$$\hat{E}_n(t) = \int_{-\infty}^{\infty} e_n(\omega)\exp(-\omega t)d\omega \tag{1.8}$$

where ω is the angular frequency related to the optical wavelength by $k_n = \omega_n\sqrt{\mu_0 \in}$. This approach assumes the Slowly Varying Envelope Approximation, which means that that the envelope of the pulse is much slower than the carrier frequency, ω_o. In other words, the bandwidth of the pulse is much lower than the optical frequency, which is true in general. As there is only a discrete number of transversal eigenmodes we can substitute the integral by a summation as follows:

$$\hat{E}_n(t) = \sum_{p=-\infty}^{\infty} e_n(\omega_p)\exp(-j\omega_p t) \tag{1.9}$$

By unifying Eq.1.7 and 1.9, we obtain the following expression:

$$\varepsilon(r,t) = \sum_n u_n(r)\sum_p e_n(\omega_p)\exp(-j\omega_p t) \tag{1.10}$$

which contains the transversal wave information within the u_n term and the time-varying information within the e_n term. In order to better understand the process of time-varying electric field, we can reduce Eq.1.10 by assuming that there is only one allowed transversal eigenmode. This simplifies the previous expression to the following:

$$\varepsilon(r,t) = u_0(r)\sum_p e_0(\omega_p)\exp(-j\omega_p t) \tag{1.11}$$

which illustrates how the temporal output of the laser can be modelled by linear superposition of frequency modes. For the case in which more transversal modes are present the average temporal profile can be modelled as the contribution of all the spatial components, as we are assuming propagation in a linear medium.

1.3.3 Cavity-plus-atom equations of motion.

The temporal component of the electric field, however, is a complex issue as it depends in other factors in addition to cavity modes. In order to gain insight in the way a laser works, basic laser dynamics can be modelled by taking into account three major relationships: the distribution of the electric field inside the gain medium, how occurs inversion of population in the medium at atomic level and the interaction with the cavity that makes the electric field oscillate under certain conditions. These relationships have been specified for many laser systems and one of the most general approaches is found in the complete cavity-plus-atom equations of motion for the laser (Siegman, 1986). This can be written as three coupled differential equations for each cavity mode that relate the cavity mode itself *E(t)*, the atomic polarization *P(t)*, and the population difference *ΔN(t)* for a specific cavity mode. These can be written as follows:

$$\frac{\partial^2 E(t)}{\partial t^2} + \gamma_c \frac{\partial E(t)}{\partial t} - \omega_c{}^2 E(t) = -\frac{1}{\in}\frac{\partial^2 P(t)}{\partial t^2} + \sqrt{\frac{8\gamma_e}{\in V_c}}\frac{dE_e(t)}{dt} \tag{1.12a}$$

$$\frac{d^2 P(t)}{dt^2} + \Delta\omega_a \frac{dP(t)}{dt} + \omega_a{}^2 P(t) = \kappa \Delta N(t) E(t) \tag{1.12b}$$

$$\frac{d\Delta N(t)}{dt} + \frac{\Delta N(t) - \Delta N_0}{T_1} = -\frac{2^*}{\hbar\omega} E(t)\frac{dP(t)}{dt} \tag{1.12c}$$

The advantage of this approach is that simultaneously relates and isolates the main processes that undergo within a laser cavity when it oscillates. In brief, equation 1.12a, cavity mode equation, sets the conditions of the allowed modes inside the cavity and how coupling from an external driving signal $E_e(t)$ into the laser cavity occurs. Cavity mode equation relates to the structure of the cavity to keep electromagnetic waves inside for oscillation, in simple cases, this is dependent on the distance between the mirrors that limit the length of the cavity and the curvature of the mirrors to compensate undesired losses produced by diffraction. The external driving signal is related to the pumping of energy within the cavity. This external signal will strongly affect the working regime of the

laser. Some lasers like Nd:YAG will have a flash lamp that pumps incoherent light into the laser medium that produces spontaneous emission of the laser medium to initiate light oscillation. Equation 1.12b, atomic polarization equation, relates the atomic polarization with the circulating electric field inside the cavity. Atomic polarization links the quantum nature of the laser medium with the propagating electric field inside the cavity. This equation 1.12b is particularly important as it is a semiclassical approach that links the quatum nature of the photons, allowed energy levels inside the laser medium and its polarization dependence if required. Finally, Equation 1.12c, atomic population equation, sets the rate of change of energy caused by the cavity fields in the form of stimulated transitions.

These three equations are the starting point for many laser analysis in literature as they correspond to one of the simplest analysis applied to a single cavity mode and a two-level atomic system in which atoms are quantized while fields are not, known as semiclassical quantum theory. Another advantage of this approach relies on the fact that these equations are time-dependant only, as cavity modes are eliminated by normal mode formulation of transversal eigenmodes as will be explained below. Thus, it provides the ability to adapt to many laser problems independently of the cavity geometry, as this is treated by the cavity eigenmodes. Each transversal eigenmode will have a subset of temporal solutions (also named longitudinal modes) that compete inside the cavity. In general, we can say that lasers can operate at four different regimes: continuous wave (CW), mode-locking, cavity-dumping and Q-switching.

1.3.4 Temporal modulation of light in the resonator.

The above equations enable to predict the complex behaviour of light oscillation in different circumstances and allowed to design an extended number of laser types. Fundamentally, the study of such equations enabled tailoring a laser cavity, for example, by just adding few elements to it, and taking into account the properties of the gain medium among

many others elements of the cavity. These elements, like optic modulators control the way inversion population occurs (in Q-switching) or the way the different laser modes compete to build up inside the cavity (in mode-locking), naturally changed the way the lasers were built. Although laser dynamics inside cavities is an extremely interesting topic is slightly beyond the scope of this thesis, so I will focus in briefly introducing the most important approaches to produce mode-locking, and particularly, explain a bit more in detail how mode-locking is achieved in most commercial Titanium-Sapphire lasers. Detailed reviews can be found in references of Siegman, 1971 and Haus, 2000.Laser cavity equations show that a laser cavity can be modelled as a resonator with gain, losses, active elements to allow the resonator working off its cavity eigenmodes, and passive elements that enable to modify the cavity eigenmodes of the resonator. In Figure 1.4 there are two examples of typical schemes of laser cavities with (a) active mode locking, in which a modulator is added to the gain medium and resonator (mirror plus output coupler) and (b) passive mode-locking, in which one of the mirrors is changed by a saturable absorber mirror that produces two effects: reflection and passive modulation of the pulses of the laser.

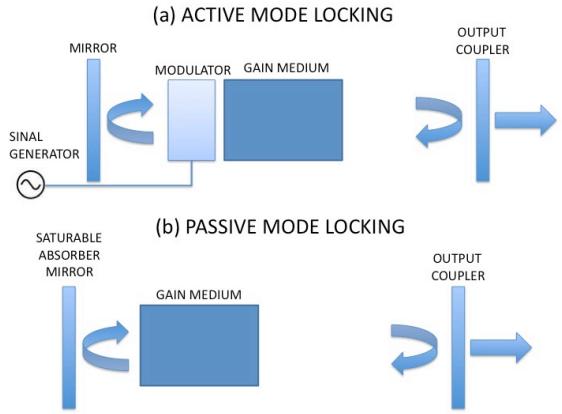

Figure 1.4. two examples of typical schemes of laser cavities with (a) active mode locking, in which a modulator is added to the gain medium and resonator (mirror plus output coupler) and (b) passive mode-locking, in which one of the mirrors is changed by a saturable absorber mirror that reflects and passively modulates the pulses of the laser.

In summary, methods for producing mode locking in a laser may be classified as either active or passive depending on the additional elements we add to the cavity. Active methods typically involve using an external signal to induce a modulation of the intra-cavity light. Passive methods do not use an external signal, but rely on placing some element into the laser cavity that causes self-modulation of the light.

1.3.5 Active mode locking.

Active mode locking consists in adding an active (meaning that it requires an external electric signal to operate) element within the cavity, like an acousto-optic or electro-optic modulator as shown in Figure 1.4(a). Light shall pass the modulator when the losses are at a minimum. A pulse that matches the right cavity round-trip time is thus formed, as shown in Figure 1.5. Although the wings of the pulse experience only little attenuation, the pulse is tailored little by little in every roundtrip of the pulse travelling inside the cavity and this effectively leads to pulse shortening until an equilibrium point is reached (called steady-state) among all the competing effects like gain narrowing which tends to broaden the pulse.

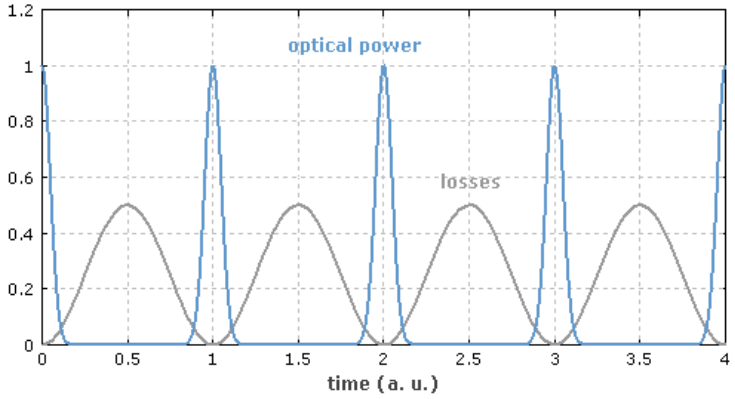

Figure 1.5. Schematic setup of an actively mode-locked laser (from http://www.rp-photonics.com/img/active_mode_locking.png).

The pulse duration is typically in the picosecond range and is only weakly dependent on parameters such as the strength of the modulator signal. This weak dependence arises from the fact that the pulse-shortening effect of the modulator becomes less effective for shorter pulse durations, whereas other effects that broaden the pulse, like chromatic dispersion, become more effective.

1.3.6 Theory of active mode locking.

For simplicity, we will develop the laser dynamic equations for a specific number of setups to illustrate how active mode-locking enables pulse generation. This explanation will be the base for our final mathematical development of Kerr lens mode-locking that is normally used for generating femtosecond pulses in Ti:sapphire medium. For this, we assume that our cavity is an optical Fabry-Pérot resonator formed by two mirrors. This has longitudinal modes sparated in frequency by $\Delta\Omega = 2\pi/T_R$, where T_R is the roundtrip time of the cavity. In general, several axial modes will be lasing if the gain level is above threshold and central model will be at ω_0. A cosinusoidal modulation od the central mode at frequency $\Omega_M = \Delta\Omega$ produces sidebands at $\omega_0 \pm \Delta\Omega$. These injection lock the adjacent modes, which in turn lock their neighbours. Denote the amplitude of the axial mode of frequency $\omega_0 \pm n\Delta\Omega$ by An. The amplitude changes within each pass through the amplifier of loss 1-l and peak gain 1+g, where l<<1 and g<<1, and can be written as follows:

$$\Delta A_n = \left(\frac{g}{1 + \left(n\Delta\Omega / \Omega_g \right)^2} - l \right) A_n + 0.5M\left(A_{n-1} - 2A_n + A_{n+1} \right) \qquad (1.13)$$

where M is the modulation. This expression can be transformed into a standard operator when the following three approximations apply:

1) The frequency dependent gain can be expanded to second order in $n\Delta\Omega$.

2) The discrete frequency spectrum with Fourier components at $n\Delta\Omega$ are replaced by a continuum spectrum.

3) The sum $(A_{n+1} - 2A_n + A_{n-1})/\Delta\Omega^2$ can be approximated by second derivative with respect to the frequency if the spectrum is very dense, as normally model-locking involves thousands of modes.

In that context, Eq.1.13 can be rewritten as follows:

$$\Delta A(\Omega) = (g - l)A(\Omega) - g\left(\Omega/\Omega_g\right)^2 A(\Omega) + 0.5M\Omega_m{}^2 d^2A/d\Omega^2 \qquad (1.14)$$

where $\Omega_M = \Delta\Omega$ is the modulation frequency. In the steady-state, the change of the pulse in one roundrtrip is zero. Hence, the mode-locked pulse must be a solution of Eq.1.14 when is equal to zero. This solution is a gaussian pulse in the form of

$$A(\Omega) = E_0 \exp\left(-\Omega^2\tau^2\right) \qquad (1.15a)$$

where

$$\tau^4 = 2g/\left(M\Omega_m{}^2\Omega_g{}^2\right). \qquad (1.15b)$$

This is the Kuizega-Siegman formula (Siegman, 1971) for the pulse width, which is proportional to the inverse of the geometric mean of the gain bandwidth and the modulation frequency. The eigen value of the equation provides the expression for the net gain, $g - l = 0.5M\Omega_m{}^2\tau^2$. We can observe that the gain is greater than the loss. This is allowed and does not cause instabilities, since the modulator increases the loss in the pulse wings.

1.3.7 Passive Mode Locking.

Passive mode-locking techniques are those that do not require an external signal (i.e. active element) to the laser, such as the driving signal of the modulator shown in Figure 1.4(a), to produce pulses. Passive mode-locking relies on the use of an intracavity passive element that causes that the light inside the cavity changes without any driving signal. A

commonly used device to achieve this self-coupling with light is a saturable absorber as shown in Figure 1.4(b).

A saturable absorber is an optical device that exhibits an intensity-dependent transmission, as shown in Figure 1.6. For passive mode-locking, a saturable absorber will selectively absorb low-intensity light, and transmit light which is of sufficiently high intensity and produces an analogous effect of the modulator in active mode-locking, in which for every roundtrip, the tails of the pulse get attenuated and the pulse is effectively shortened until an equilibrium point is reached. Such devices produce much shorter and stable pulses than electronically driven modulators, as electronics are much slower and underperform in comparison to some optical components.

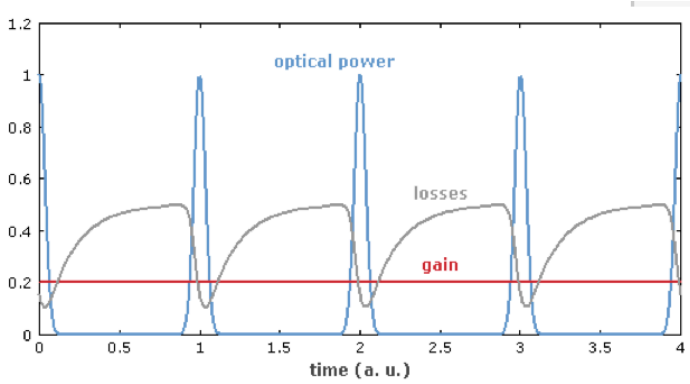

Figure 1.6 Temporal evolution of optical power and losses in a passively mode-locked laser with a slow saturable absorber. The saturable absorber causes a loss modulation which is fast for the leading wing of the pulse, whereas recovery of the absorber takes some longer time (from http://www.rp-photonics.com/passive_mode_locking.html).

As cavities contain many eigenmodes, at the initial moments of starting the laser, the light inside the cavity is somehow composed by purely random intensity fluctuations experienced by a CW laser and any random intense spike will be transmitted preferentially by the saturable absorber. As the light travels inside the cavity selective amplification of the high-intensity spikes takes place, at the same time that low-intensity light gets absorbed. After many round trips a competition among the high-intensity spikes occur until one of them reach the intensity saturation. After this

point the spike above the intensity saturation is amplified empting the energy in the laser medium (population inversion decreases), reducing the gain for the lower intensity spikes which start to disappear. Equilibrium is reached when the gain for the spike is equal to the losses, leading to mode-locking of the laser and the generation of a highly stable train of light pulses.

Saturable absorbers started as liquid organic dyes, but currently they can also be made from doped crystals and semiconductors. Semiconductor absorbers tend to exhibit very fast response times (~100 fs), which is one of the requiriment to obtain short duration of the pulses in a passively mode-locked laser. The most important type of absorber for passive mode locking is the semiconductor saturable absorber mirror, called SESAM. This is a compact semiconductor device, the parameters of which can be adjusted in very wide ranges, so that appropriately designed SESAMs can be used to mode-lock very different kinds of lasers, in particular solid-state lasers, including different kinds of semiconductor lasers.

The concept of “saturable absorbers” has been crucial for the development of passive mode locking and as a consequence it has been further extended as there are also passive mode-locking schemes that do not rely on materials that directly display an intensity dependent absorption. These methods rely on nonlinear optical effects in intracavity components that are used to provide a way of selectively amplifying high-intensity light in the cavity, and attenuation of low-intensity light. Such components are named to be “artificial saturable absorbers” because they do not have the real material properties but they produce an analogous effect inside the cavity.

One of the most successful schemes is called Kerr-lens mode-locking (KLM), also sometimes called "self mode-locking". This uses a nonlinear optical process, the optical Kerr effect, which results in high-intensity light being focussed differently than low-intensity light. By careful

arrangement of an aperture in the laser cavity, this effect can be exploited to produce the equivalent of an ultra-fast response time saturable absorber as explained below.

1.3.8 Kerr Lens Mode Locking.

Ultrashort pulses from Ti:sapphire lasers can be generated with passive mode locking, usually in the form of Kerr lens mode locking (KLM). This is a passive mode locking technique that uses an artificial saturable absorber based on the Kerr lens effect in the gain medium. This approach exploits the reduction in the beam size for high optical intensities in the gain medium to promote one eigenmode of the cavity. This can be achieved under two different regimes: (1) hard aperture KLM, the Kerr lens reduces the optical losses at an aperture which the beam must pass in each resonator round trip; (2) soft aperture KLM, the Kerr lens leads to a better overlap of laser and pump beam, and thus to a higher gain for the peak of the pulse.

The first Kerr Lens Modelocked Ti:sapphire laser was constructed by Prof. Wilson Sibbett and co-workers in University of Saint Andrews in 1990 (Sibbett, 1991 y pon también la referencia de optics-lett. De Spence) which was first presented as a late paper at The Conference of Lasers and Electro-Optics, probably the most referenced conference in lasers still at the time of this Thesis (Spence et al, 1990).

The combination of KLM with a SESAM allows for reliable self-starting of the pulse generation process. Pulse duration of 100 fs can be readily achieved and is typical available in commercial laser systems and even pulse durations around 10 fs are possible for commercial devices.

Typical output powers of mode-locked Ti:sapphire lasers are of the order of 0.3–2 W depending on the pumping laser, whereas continuous-wave versions sometimes generate several watts. A typical pulse repetition rate

is 80 MHz, but devices with multi-gigahertz repetition rates are also commercially available, which can be used as frequency comb sources.

1.3.9 Dispersion and its compensation.

Another important issue in ultrashort pulse generation (mode-locked lasers of femtosecond pulses) is related to the chromatic dispersion of the cavity that tends to broaden the temporal width of the pulse as each wavelength undergoes a different optical path. Particularly, chromatic dispersion is mostly introduced by the gain medium and other optical components inside the laser cavity. Chromatic dispersion is normally not desirable because it tends to broaden and chirp the generated pulses. Dispersion compensation can be achieved by introducing optical components with anomalous dispersion. In the case of bulk lasers, such components are usually either special dispersive dielectric mirrors (e.g. in the form of monolithic Gires–Tournois interferometers or chirped mirrors), or prism pairs (Fork, 1984) as shown in Figure 1.7 that enable introducing negative dispersion to the propagating light beam.

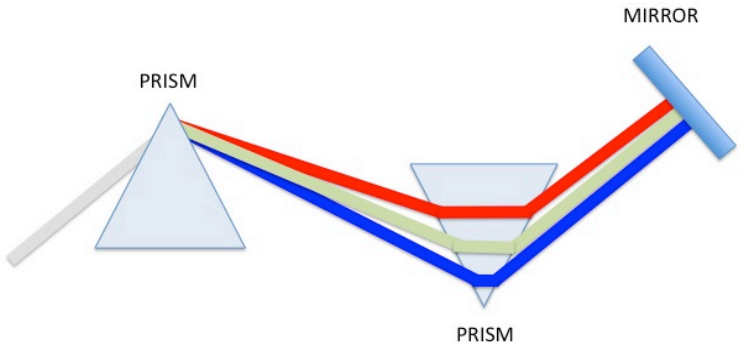

Figure 1.7. Classical arrangement of prism pairs to introduce negative dispersion of a broadband pulse as detailed by Fork in 1984.

Chromatic dispersion of an optical medium is the phenomenon that the phase velocity and group velocity of light propagating in a transparent medium depend on the optical frequency. Chromatic dispersion of

second and higher order is defined via the Taylor expansion of the wavenumber k (change in spectral phase per unit length) as a function of the angular frequency ω (around some center frequency ω_0, e.g. the mean frequency of some laser pulses):

$$k(\omega) = k_0 + \frac{\partial k}{\partial \omega}\left(\omega - \omega_0\right) + \frac{1}{2}\frac{\partial^2 k}{\partial \omega^2}\left(\omega - \omega_0\right)^2 + \frac{1}{6}\frac{\partial^3 k}{\partial \omega^3}\left(\omega - \omega_0\right)^3 + \ldots \tag{1.16}$$

where k_0 the zero-order term describes a common phase shift; the first-order term contains the inverse group velocity (i.e., the group delay per unit length) and describes an overall time delay without an effect on the pulse shape, $k' = \partial k/\partial \omega = 1/v_g$; the second-order (quadratic) term contains the second-order dispersion, or group delay dispersion (GDD) per unit length or Group Velocity Delay (GVD), $k'' = \partial^2 k/\partial \omega^2$, which affects the temporal width of the pulse; the third-order (cubic) term contains the third-order dispersion (TOD) per unit length, $k''' = \partial^3 k/\partial \omega^3$,which also spreads the energy of the pulse by generating small pulses, so-called 'satellites', around the main pulse. GDD and TOD reduce the peak intensity, which is fundamental for efficiently exploiting nonlinear effects of light. Measuring these effects on the delivered pulse at the sample plane of a nonlinear microscope is the main focus of this thesis.

In general, the chromatic dispersion is often estimated by the "dispersion parameter" which relates to the second derivative of the wave number with respect to the angular frequency within a particular wavelength as follows:

$$D_\lambda = -\frac{2\pi c}{\lambda^2}\frac{\partial^2 k}{\partial \omega^2} = -\frac{2\pi c}{\lambda^2}k'' \tag{1.17}$$

where λ is the wavelength, ω is the angular frequency, k is the wave number and c is the speed of light in vacuum. There are circumstances in which dispersion of third and higher order can be used and they are called "higher-order dispersion parameters". In most cases, broadband light is affected by normal (or positive) chromatic dispersion (for k">0) and anomalous (or negative) dispersion (for k"<0). Normal dispersion,

where the group velocity decreases with increasing optical frequency, occurs for most transparent media in the visible spectral region. Anomalous dispersion sometimes occurs at longer wavelengths, like in silica (the basis of most optical fibers) for wavelengths longer than the zero-dispersion wavelength of around 1.3 μm.

Dispersion has an important impact on the propagation of pulses, because a pulse always has a finite spectral width (bandwidth), so that dispersion can cause its frequency components to propagate with different velocities. Normal dispersion, for example, leads to a lower group velocity of higher-frequency components, and thus to a positive chirp, whereas anomalous dispersion creates negative chirps. The frequency dependence of the group velocity also has an effect on the pulse duration. If the pulse is initially unchirped, dispersion in a medium will always increase its duration (dispersive pulse broadening). For an originally unchirped Gaussian pulse with the duration τ_0, the pulse duration is increased as it propagates according to the following formula:

$$\tau = \tau_0 \sqrt{1 + \left(4 \log_n(2) z k'' / \tau_0^2\right)^2} \tag{1.18}$$

where z is the amount of dispersive material in which the pulse is propagated.

Alternatively, in Figure 1.7 we observe how the scheme proposed by Fork produces that the red spectral components of the pulse travel through a longer optical path (because it propagates through more glass) compared to the blue spectral parts, introducing as a result a negative dispersion to the pulse.

For pulses with durations below roughly 30 *fs*, it is necessary to control not only the second order dispersion but also the dispersion of higher orders. It may then be important, for example, choosing the appropriate material for a prism pair, or an optimized geometry of a prism compressor. This has produced hybrid devices composed by a grating pattern on a prism called GRISMs (Kane and Squier, 1997), which make

possible an optimized ratio of the strength of second- and third-order dispersion.

Therefore, proper dispersion management enables that the broad band of optical wavelengths undergo the same, or at least, very similar optical path in every roundtrip to synchronize of all of them and get a Fourier Transform limited pulse at the output of the cavity, which is the shortest pulse for a given bandwidth as all optical components are at the same phase.

1.3.10 Pulse generation in Ti:sapphire lasers.

Currently, there are many commercial systems that provide ultrashort lasers pulses. The most common one is the Ti:sapphire laser that is based on kerr-lens mode locking with a dispersion compensation stage based on a pair of prisms. The general scheme of commercial system is illustrated in Fig.1.8.

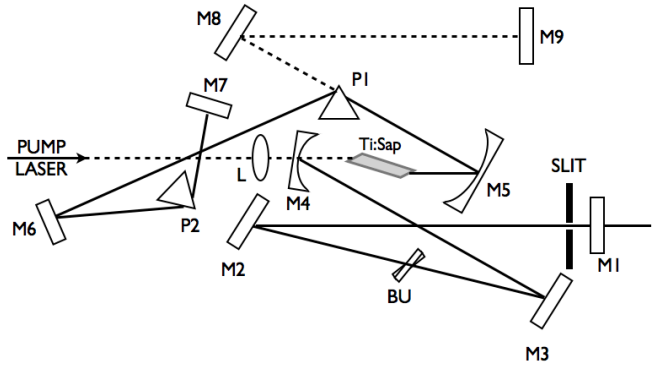

Figure 1.8. Schematic of Ti:sapphire laser. (M) Mirror, (P) Prism, (BU) Butterfly and (L) Lens.

On the left side of Fig.1.8 we can see the pump laser, which is in general a doubled Nd:YaG laser, as it operates at 532nm near one of the absortion peaks of Ti:sapphire. Ti:sapphire crystal acts as gain medium, saturable absorver by kerr-lens effect of the virtual pinhole as explained above. Pair of Prisms P1 and P2 compensate for cavity and material dispersion. A number of mirrors make a compact cavity and M1 is an

output coupler that transmits about 1% of the cavity power. Butterfly (BU) is used to generate "seed noise" and enhance the generation of modes inside the cavity to trigger the competition among modes until mode locking is achieved. The slit prior to M1 allows fine tunning of the pulse duration and spatial profile of the output beam. Several alignment controls of position and tilt angles are available in all the components to adjust and tune the system approximately from 690nm to 960nm.

1.3.11 Theory of pulse generation in Ti:sapphire Laser by kerr-lens mode locking.

The key feature of commercial Ti:sapphire lasers lies in achieving passive mode-locking by replacing the active modulator by a saturable absorber as mentioned above and shown in Fig.1.4(b). In order to extend the theory behind active mode locking (presented in subsection above) to passive mode locking, we need to understand the behaviour of laser dynamics in time. For this purpose, Eq.1.14 can be firstly generalized to include transient behaviour, where change per roundtrip need not to be zero. For non-zero, Eq.1.12 will result in different $A_n(\Omega)$, the spectrum of the n-th pass. If the evolution is slow compared to a roundtrip, the differentce equation can be replaced by a differential equation in terms of the long term variable T. Even though the pulse is characterized in terms of its spectrum, slow variation of the spectrum can be described in terms of time-varying spectrum. We can then write the following differential equation:

$$\frac{1}{T_R}\frac{\partial}{\partial T}A(T,\Omega) = (g-l)A(T,\Omega) - g\left(\frac{\Omega}{\Omega_g}\right)^2 A(T,\Omega) + 0.5M\Omega_m{}^2\frac{\partial^2 A(T,\Omega)}{\partial\Omega^2} \tag{1.19}$$

To solve this equation and compute the transient behaviour, it is possible to express the excitation by an expansion in terms of Hermite-Gaussian functions as it is a complete set of functions:

$$A(T,\Omega) = \sum C_n(T)H_n(\Omega\tau)\exp\left(-\Omega^2\tau^2/2\right) \tag{1.20}$$

Then, we rewrite Eq.1.17 as a number of differential equations:

$$\frac{dC_n}{dT} = \left(g - l - \left(n + \frac{1}{2} \right) M\Omega_m{}^2 \tau^2 \right) C_n = -nM\Omega_m{}^2 \tau^2 \tag{1.21}$$

This expression provides a clear picture of the behaviour of pulse perturbations as a combination of Hermite-Gaussians of order $n \geq 1$. The dynamics of amplitude perturbations of the pulse itself represented by $n=0$ term of Hermite-Gaussian expansion require a separate study. Such a perturbation, when in phase with the main pulse, lowers the gain through gain saturation (generally with a relaxation time much longer than the pulse). This provides net loss to the perturbation that then decays. On the contrary, a perturbation in anti-phase raises the gain and thus the original pulse amplitude is restored. This interplay between gain and resonator response can also lead to damped relaxation oscillations of the pulse-train envelope, a phenomenon we shall not discuss any further. A perturbation $n=0$ in phase-quadrature with the pulse does not affect the energy to first order and does not affect the gain and its decay rate is zero. Hence it is not stabilized. Amplified spontaneous emission noise kicks the phase back and forth, which means that the phase experiences a random walk.

The description of mode-locking in terms of a pulse spectrum that evolves with time can be further transformed into a description of a pulse with a temporal envelope that evolves on a time scale much longer than the pulsewidth. We can write the classical dual relationship between time and frequency, $a(t) = \int d\Omega \exp(j\Omega t) A(\Omega)$, and further Fourier Transform Eq.1.15 to obtain the temporal evolution of the time-varying pulse shape:

$$\frac{1}{T_R} \frac{\partial}{\partial T} A(T,t) = (g - l) a(T,t) + g \left(\frac{1}{\Omega_g} \right)^2 \frac{\partial^2}{\partial t^2} a(T,t) - 0.5 M\Omega_m{}^2 t^2 a(T,t) \tag{1.22}$$

It can be directly seen, as expected, that general form of Eq.1.15 and 1.18 is equivalent and Hermite-Gaussian functions are also a solution as a consequence of the fact that the Fourier transforms of Hermite–Gaussians are themselves Hermite–Gaussians. The pulse shape of steady state

mode-locking in time is also a Gaussian, $A(t) = E_0 \exp\left(-t^2/2\tau^2\right)$. In time domain, the modulation provides a time dependant loss. Whenever the loss goes below the gain level, the curvature of the envelope becomes negative. The transition between net gain and net loss marks the point of inversion on the pulse envelope.
Active modelocking does not lead to ultrashort pulses because frequency of modulation cannot be raised arbitrarily. Harmonic mode-locking allows for modulation frequencies at a harmonic of $2\pi/T_R$. When this is done the shortening of the pulse within each roundtrip can be enhanced. However, if the energy of the individual pulses is to be kept high, only one pulse must be allowed to circulate in the resonator. This can be accomplished through the use of step-recovery diodes for the modulation source. However, the bandwidth of optical modulators is limited and thus modulation with ultrashort electrical pulses runs into difficulties. Modulation by a passive, saturable absorber is much more effective in pulse shaping. Since the pulse itself produces the shape of the modulation function, considerably tighter modulation becomes feasible. Each time the pulse passes through the resonator it is multiplied by a time function. If the process is treated in the frequency domain, the multiplication in the time domain becomes convolution in the frequency domain. The resulting master equation involves convolution integrals. For this reason, a description of passive mode-locking has been presented in the time domain.

In Ti:sapphire laser the effect of a fast saturable absorber is produced by Kerr focusing: the high intensity part of the beam is focused by the Kerr effect, whereas the low intensity parts remain unfocused. If such a beam is passed through an aperture, the low intensity parts are attenuated, thereby shortening the pulse. The modulation of the saturable absorber s(t) in transmission through the saturable absorber can be written as:

$$I_s(t) = \frac{I_{s0}}{1 + I(t)/I_{sat}} \tag{1.23}$$

where I_{s0} is the unsaterated loss and thus less than 1, I(t) the time-varying intensity and I_{sat} the saturation intensity of the absorber. If saturation is relatively weak, this can be expanded by Taylor series as:

$$I_s(t) = I_{s0} - I_{s0} I(t)/I_{sat} \tag{1.24}$$

The intensity multiplied by the effective area of the mode A_{eff} gives the power in the mode. We can then normalize the mode amplitude and rewrite Eq.1.17 as follows:

$$I_s(t) = I_{s0} - \frac{I_{s0}|E(t)|^2}{I_{sat}A_{eff}} = I_{s0} - \gamma|E(t)|^2 \tag{1.25}$$

where $I(t) = |E(t)|^2 / A_{eff}$ and γ is the self amplitude modulation coefficient. Therefore, the equation of passive mode-locking with a fast saturable absorber, i.e. Kerr lens effect, can be obtained by including the saturable loss in Eq.1.20 and omitting the active modulation term. The unsaturated loss I_{s0} can be incorporated into the loss coefficient and this results in the following expression:

$$\frac{1}{T_R}\frac{\partial}{\partial T}E(t) = (g-l)E(t) + \frac{g}{\Omega_g{}^2}\frac{\partial^2}{\partial t^2}E(t) + \gamma|E(t)|^2 E(t) \tag{1.26}$$

The solution of this

$$E_0(t) = E_0 sech(t/\tau) \tag{1.27}$$

where

$$\tau^2 = 2g/\gamma E_0{}^2 \Omega_g{}^2 \tag{1.28a}$$

and

$$l - g = g/\Omega_g{}^2 \tau^2 \tag{1.28b}.$$

Eq.1.28a is related to the active mode-locking term of Eq.1.15b, where $\tau^4 = 2g/\left(M\Omega_m{}^2\Omega_g{}^2\right)$, as can be directly observed. The comparison also explains why passive mode-locking can result in much shorter pulsewidths for the same filter bandwidth. As the pulse gets shorter, the curvature of the modulation increases as $1/\tau^2$, whereas it remains unchaged for active mode-locking. In other words, the net gain is negative preceding and following the pulse. At the pulse peak, the gain is positive due to the bleaching of the saturable absorber and as hyperbolic

secant pulse has exponential wings the system behaves linearly in the wings since the intensity is small. The second order differential equation dictates exponential solutions for any bounded pulse. The solution of Eq.1.26 is not stable unless gain saturation is explicitly included. This gain saturation can be cumulative and this allows to assume that the gain is approximately constant during the passage of one pulse. The solution is also stabilized if the full saturation behavior, as modeled in Eq.1.23, is taken into account, but then no closed form solutions have been found.
This situation is more realistic and this is why no assumptions can be made when characterising ultrashort laser pulses. If it were possible to ensure that the temporal shape of the electric field at the output of a Ti:sapphire laser is hyperbolic secant, this would impose constrains on the allowed spectral intensity and full characterization of ultrashort pulses could be highly simplified. As this is not the case, no assumptions can be made on the spectral profile of ultrashort pulses and completely general methods were needed. Furthermore, as pulse propagates through an optical setup, chromatic dispersion, spatiotemporal distortions and nonlinear effects (like self-phase modulation) that change not ony the phase but also the spectral intensity. Therefore, it was absolutely mandatory to develop fully general means to characterize such temporal bullets of light that are faster than any electronic device as we will comment on the next chapters.

1.4 Conclusions.

In summary, this chapter explains how ultrashort laser pulses can be produced by hosting of a suitable Ti:sapphire crystal as lasing material within a properly designed laser cavity. However, at the end we raise the point that such unique light entities are distorted as they propagate through media and optical elements, which is in general produced by chromatic dispersion and other nonlinear effects. The effects of chromatic dispersion diminish, and can even destroy, coherence of the optical pulse and might avoid accomplishing a particular application, like

life science imaging or multiphoton microscopy. Chromatic dispersion (among other effects) mainly occurs as a consequence of the intrinsic spectral broad bandwidth of ultrashort laser pulses. The broader the pulses are the more unique, but the more fragile. As a solution, ultrashort laser pulses need to be rebuilt at the localization were the physical interaction occurs to produce the desired effect in an optimal manner, like a contrast mechanism to generate an image. For this, particular optical schemes have been introduced to produce negative second-order dispersion, which are extendable to third-order by few changes. In the early age of ultrashort laser pulses, theoretical models based on light oscillation within particular laser cavities proved that temporal intensity could be approximated by a squared hyperbolic secant, which has some similarities with a Gaussian like pulse. These were good approximations as technology and science were not as developed as today. However, as optical setups get more complex and applications start to emerge it is mandatory to achieve perfect light control to let engineers develop automated and reliable systems that do not need dedicated experts to use devices based on ultrashort laser pulse technology.

Therefore, controlling the shape of ultrashort laser pulses is becoming one of the current bottlenecks of this technology for many applications that range from coherent imaging or spectroscopy, to laser micromachining or nanosurgery, or to quantum control applications among others. In this line, it is becoming fundamental to measure the actual shape at any desired location of the light path and to find strategies that offer enough flexibility to control spatiotemporal delay experienced by all the light components of an ultrashort laser pulse and beam. This thesis addresses one of the topics and focuses in developing direct and reliable strategies to measure the actual shape of an ultrashort laser pulse in a flexible and general manner.

References

A Abragam and B Bleany, Electron Paramagnetic Resonance ofTransition Ions. New York: Dover Publications, pp. 790-792 (1986).

RL Fork, BI. Greene and CV Shank, "Generation of optical pulses shorter than 0.1 ps by colliding pulse modelocking," *Appl. Phys. Lett.* **38** pp. 671-672 (1981).

RL Fork, OE Martinez, and JP Gordon, "Negative dispersion using pairs of prisms", *Opt. Lett.* **9** p. 150-152 (1984).

HA Haus, " Mode-Locking of Lasers", *IEEE J. Sel. Top. Quantum Electron.* **6** pp. 1173-1185 (2000).

S Kane and J Squier, "Grism-pair stretcher–compressor system for simultaneous second- and third-order dispersion compensation in chirped-pulse amplification", *J. Opt. Soc. Am. B* **14** pp. 661-665 (1997).

WE Lamb Jr., "Theory of an optical laser," *Phys. Rev.* **134** pp. A1429–A1450 (1964).

PF Moulton, "Spectroscopic and laser characteristics of Ti:Al_2O_3," *J. Opt. Soc. Am. B* 3 (1), pp. 125-133 (1986)

CV Shank and E. P. Ippen, "Subpicosecond kilowatt pulses from a modelocked cw dye laser", *Appl. Phys. Lett.* 24, pp. 373-375 (1974).

W Sibbett, "Self modelocking: Ultimate simplicity in ultrashort pulse generation," *Optics & Photonics News* **2** pp. 37-38 (1991).

AE Siegman, An Introduction to Lasers and Masers. *McGraw- Hill, New York*, pp. 402-408 (1971).

DE Spence, PE Kean, and W Sibbett, "Sub-100fs Pulse Generarion from a Self-Modelocked Tiranium-Sapphire laser," *Postdeadline paper, CLEO '90*, Anaheim, CA (1990).

KF Wall, RL Aggarwal, RE Fahey, and A. Srrauss, "Small Signal Gain Measurements in a Ti:Al_2O3 Amplifier," *IEEE J. Quantum Electron.* **24** pp. 1016-1021 (1988).

JA Valdmanis, RL Fork, and JP Gordon, "Generation of optical pulses as short as 27 femtoseconds directly from a laser balancing self-phase modulation, group-velocity dispersion, saturable absorption, and saturable gain," *Opt. Lett.* **10** pp. 131-133 (1985).

KF Wall and A Sanchez, “TItanium Sapphire Lasers,” *Lincoln Laboratory Journal* **3** pp. 447-462 (1990).

CHAPTER 2

Ultrashort laser pulses and life sciences.

2 Ultrashort laser pulses and life sciences.

2.1- Introduction.

The last decades have seen tremendous progress in the development of lasers systems that deliver ultrashort pulses. Nowadays, every year we can find in the market cheaper, more powerful and more robust systems that were at the edge of the state-of-the-art just a few years ago. This tremendous leap on the access to sophisticated laser sources is currently pushing the number of applications in which it makes sense to use this type of light and the number of potential users. In spite of such tremendous progress and hard work, much more needs to be known and investigated in order to explain and utilize the unique properties of ultrashort laser sources. We can definitely state that currently, we are watching just at the tip of the iceberg of what ultrashort pulses has to offer. Analogously to an iceberg which typically exhibits only one ninth of its total volume, a closer look should reveal for the curious observer the amazingly huge volume we were neglecting by our firstly naïve picture, which was indeed superficial.

2.2 – Scope of this thesis.

In this thesis, we address specific efforts towards developing the precise aspect of ultrashort laser pulse measurement in the context of biomedical research. High resolution imaging of cells by means of ultrashort laser pulses was firstly reported by Denk and Webb in their Science paper (Denk, 1990). This work opened a new line of research generally named multiphoton microscopy that exploits the interaction of high peak intensity light (ultrashort light pulses) with cells and markers. This further triggered the vision of developing fundamental tools that will enable to control matter by means of light with exquisite precision with the added difficulty of being next to biological samples, which are extremely sensitive and fragile. For this, light matter interaction needs to be extremely well controlled to avoid undesired effects, like cell damage due to the high peak intensity values of ultrashort laser pulses, as well as promoting specific physical processes like two-photon fluorescence excitation of a desired fluorophore embedded in some biochemical environment. Particularly, it is necessary to control the temporal shape of the ultrashort pulse at the focal plane of a multiphoton microscope to ensure that the dose of light is the desired one, and for this, methods to measure the temporal shape of ultrashort laser light in the focal plane needed to be developed at the time in which this thesis was started.

The findings of this thesis should become the basis for one particular range of new tools in which temporal/spectral properties of ultrashort pulses will be of paramount importance. For this, we face the challenge of measuring ultrashort laser pulses in an accurate, robust and flexible manner.

We focus in the two major bottlenecks regarding ultrashort laser pulse measurements for multiphoton microscopy, that aim for developing (1) new techniques for full characterization of ultrashort pulses under different experimental conditions and (2) new material with specific nonlinear properties that enable to obtain ultrashort pulse measurements that properly catch the temporal shape of light and at the same time can

be readily found in biomedical lab, specially cost effective, non fragile and non-toxic.
Combination of these two complementary strategies provides a new ground where it is possible to characterise an ultrashort pulse at the sample plane of a multiphoton microscope in a regular biomedical research facility.

Importantly, we approach ultrashort pulse characterisation developing a different theoretical framework to the state-of-the-art and we propose a few initial experiments that preliminary support our theoretical statements in the form of new optical techniques. These findings are then experimentally tested under different conditions, such different optical setups and different pulsed regimes in order to evaluate the feasibility of the tools to measure ultrashort pulses in conditions that were prohibitive at the time this thesis was started. The scope of this thesis outlines the potential of such techniques, but further efforts shall be addressed to assess feasibility, robustness and further limitations.

More specifically, for new techniques for measuring ultrashort pulses at the focus of a microscope, firstly, I will provide some basic concepts regarding ultrashort pulse laser generation and mathematical modelling, then two chapters focused in the state-of-the-art of ultrashort pulse characterisation is introduced in Chapters 3-4, and subsequently, two big issues at the time this thesis started are detailed: (a) lack of an analytical general pulse measurement technique with few optical components, which is addressed along Chapters 5-7 and (b) lack of biocompatible and efficient materials that is also disclosed onto Chapter 7.
Final conclusions and a vision of future are presented in Chapter 8.

2.3- The meaning of measuring.

2.3.1 General concept.

Mankind has been always challenged to find the edges of nature. In order to know and control nature, there has been always the need to relate a concept with respect to a quantity. In this manner the concept would remain static whereas its quantity can be dynamic. Throughout this long pathway, mankind has been always wondering how far it could go, how small (or big) can it go before an obstacle is found, a new edge, a new opportunity... to twist reality.
This dissertation explores new manners to measure one of the fastest events ever made by mankind, and how, in order to measure such type of fast events, you need at least, something as fast or short as itself.

In general, in order to measure or quantify anything we require having a reference to compare with. Therefore, it is desirable that this reference is shorter or smaller than the object being measured. For example, measuring the optical table in the laboratory, which can typically range a few meters in length, would need an apparatus with resolution below meters, i.e. centimetres. The smaller the reference, the more accurate can be the measurement.

In contrast to this common actions that anyone performs in a daily basis without any effort, measuring ultrashort pulses is an extremely difficult task because they are one of the shortest events that mankind can produce in a controlled manner. This fact makes measurement of an ultrashort pulse a current challenge and the ultrashort pulse to be measured be the best “reference” or “unit”.

2.3.2 The challenge of measuring an ultrashort laser pulses.

The focus of this thesis will be on the measurement of *ultrashort laser pulses* that have durations shorter than the response time of any electronic instrument. Thus, one can never directly measure the electric

field envelope by using only a photodetector. This topic is still being a subject of intense research for more than 40 years (Maier, 1966; Weber, 1967; Armstrong, 1967, Diels 1978a-b) and although ultrashort pulses were available in the late 1960's it took almost 25 years to find a general method to completely characterize them with no assumptions.
Ultrashort pulses are, at the time this thesis has been written, at least five orders of magnitude faster than oscilloscopes, three orders of magnitude faster than photodiodes, and one order of magnitude faster than the fastest streak cameras. It was soon realized that the only event remotely fast enough to measure an ultrashort pulse was the pulse itself.

2.4 Other applications of ultrashort laser pulses.

For the time being, main ultrashort pulse applications (apart from multiphoton microscopy of use in biology and medicine) can be found in different fields like micro-machining as they allow drilling sub-micron holes with high precision in all types of materials by exploiting high multiphoton absortion a producing photoablation, a physical phenomenon that literally breaks electronic bonds of molecules and produces the evaporation the material because of the tremendous energy deposition of high intensity light. This occurs prior to any thermal effect and has the advantage of making sharp and neat edges, as opposite to pulses of tens of picoseconds which normally produce some type of unaccurate cleveage due to thermal effects occurring when transforming part of the high peak intensity light into thermal relaxation in the bulk material.
More than ten years ago, Ahmed H. Zewail was awarded with the Nobel prize for using ultrashort laser pulses to observe chemical reactions at the time scales they occur (femtoseconds), opening a new field in the area of physical chemistry: femtochemistry. Major contribution of femtochemistry is to provide details about the intermediate products that

form during chemical reactions, which cannot be deduced from observing the starting and end products.
Another application, which can be also used as an imaging technique but it exploits ultrashort laser pulses by means of a different physical process, is generation and detection of Terahertz radiation. This can be used for (1) medical imaging as it has a relatively low photon energy for damaging tissues and DNA, and it has the ability to penetrate up to few millimetres; (2) security, as it penetrates plastics and fabrics and can be used in surveillance; (3) manufacturing, for quality control; and (4) scientific purposes, like spectroscopy, THz tomography and submillimetre astronomy.
Probably, one of the latest applications found for femtosecond lasers has been the called "optical frequency comb" that enables spectroscopist to have a wide range of highly pure, evenly spaced set of optical frequencies and produce very precise spectroscopy studies. For this, Theodor W. Hänsch and John L. Hall shared half of the 2005 Nobel Prize in Physics for contributions to the development of laser-based precision spectroscopy, including the optical frequency comb technique.
In summary, ultrashort laser pulses are a relatively new technology that opens a range of applications that have the potential to exploit new light-matter phenomena that were not available before. At the current stage, there are a number of appealing applications but many of them can be further tweaked, like multiphoton microscopy by ts natural extension to coherent imaging by means of proper characterization and shaping of the ultrashort laser pulses at the sample plane of an imaging system.

2.5 Limitations and timeliness of this thesis.

The work on this Thesis started in 2003 and most part of the research was carried out along the years 2003 and 2007. However, professional career of the candidate delayed the preparation of this document, with the subsequent delay on thesis presentation. During 2005 I was in an exchange at the Massachusetts General Hospital on confocal microscopy

for skin cancer detection that is not reported in this document, and in 2008 I started developing my career in medical technologies at Hospital Clinic de Barcelona and created a spin-off company dedicated to imaging biomarkers for improved management of newborns. Particularly, a technology that substitutes an amniocentesis procedure by a non-invasive ultrasound scan in the last term of the pregnancy. This allows assessing fetal lung and have an estimate on the risk that the newborn develop respiratory distress syndrome, which is one of the main causes of newborn morbility and morbidity.

During these years, the candidate has continued some collaboration with Prof. Loza-Alvarez group on Polarization Second Harmonic Imaging.

The state-of-the-art has partially evolved but the contributions of the present work are still relevant and useful. Continuation of MEFISTO techniques has not been possible within the group but other groups have further studied the technique and develop measurement methodologies like MIFA, which is briefly mentioned along the thesis and briefly explained in chapter 4. CFROG technique has been used for measuringone of the shortest pulses and was recently published in Nature Photonics as mentioned in conclusions.

References

J Armstrong, “Measurement of picosecond laser pulse widths,” *Applied Physics Letters* **10** pp. 16-18 (1967).

W Denk, JH Strickler WW Webb, “Two-photon laser scanning fluorescence microscopy,” *Science* **248** pp.73-76.

J-C Diels, EW Van Stryland, and D Gold, “Investigation of the parameters affecting subpicosecond pulse duration of passively mode-locked dye laser,” in *Proceedings, First International Conference on Picosecond Phenomena*, *Springer-Verlag, New York,* pp. 117–120 (1978a).

J-C Diels, EW Van Stryland, and G Benedict, “Generation and measurement of 200 femtosecond optical pulses,” *Opt. Commun.* **25** pp. 93-95 (1978b).

M Maier, W Kaiser and J Giordmaine, “Intense Light Bursts in the Stimulated Raman Effect,” *Phys. Rev. Lett.* **17** pp. 1275-1277 (1966).

HP Weber, "Method for Pulsewidth Measurement of Ultrashort Light Pulses Generated by Phase-Locked Lasers Using Nonlinear Optics," *J. Appl. Phys.* **38** pp. 2231-2234 (1967).

CHAPTER 3

Ultrashort pulse measurements in the time domain: State-of-the-art (part 1).

3 Ultrashort pulse measurements in the time domain: State-of-the-art (part 1).

3.1 Introduction to time domain techniques.

Ultrashort pulses are one hundred thousand times faster than current oscilloscopes, one thousand times faster than photodiodes, and ten times faster than the fastest streak cameras (which are single shot, or can record a limited number of frames at such rate). Furthermore, at the time of this thesis has been submitted subfemtosecond pulses have been already available for a few years. Therefore, strategies, means and methodologies are mandatory to characterize the fastest event in a general manner and with minimal equipment. As mentioned above, it was soon realized that the only event remotely fast enough to measure an ultrashort pulse was the pulse itself. This gave birth to the now standard method of measurement: the intensity autocorrelation (Maier, 1966; Weber, 1967; Armstrong, 1967).

3.2 Pulse characterization in the time domain.

3.2.1 Autocorrelation.

One of the first methods ever employed to estimate pulse duration of an ultrashort pulse was the Second Harmonic Generation (SHG) Intensity Autocorrelation (IA). This is based on producing a quadratic interaction of a pulse with its delayed replica in a nonlinear medium. The experimental set up is based on an interferometer (Michelson) as shown in Figure 3.1.

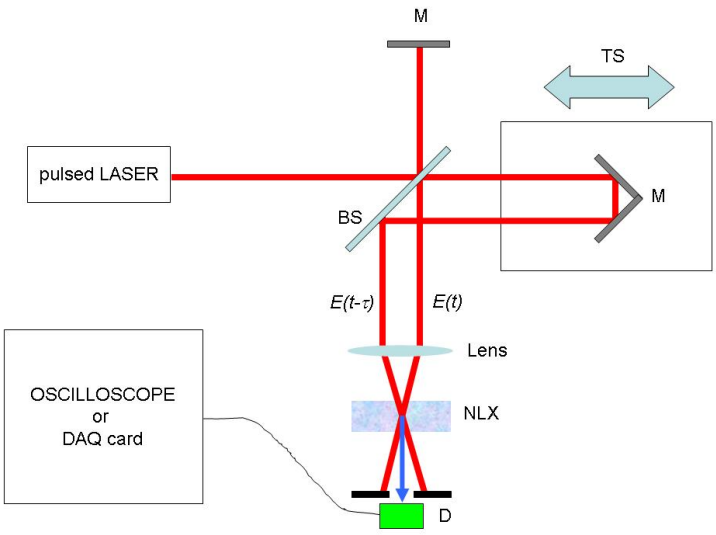

Fig. 3.1 Device to generate an autocorrelation between ultrashort pulses. This consists of a Michelson interferometer where two replicas of the same pulse travel different optical paths before being frequency doubled. Mirror (M), Corner Cube Mirror (CCM) and a beam-splitter (BS).

Figure 3.1 illustrates a typical device to generate an autocorrelation between ultrashort pulses. This consists of a Michelson interferometer where two replicas of the same pulse travel different optical paths before being frequency doubled. The interferometer splits the pulse into two copies. Each copy travels down a separate arm. A translation stage located in one of the arms of the interferometer creates a net difference of the optical path between the two replicated pulses. This difference in the optical path is also a difference in time delay, τ. A signal generator or a computer can then be used to control a programmable translation stage to obtain different delays. In the fixed arm we have:

$$\varepsilon(t)\exp\left(j2\pi f_0 t\right) \tag{3.1}$$

whereas in the other arm, the pulse has a net delay τ:

$$\varepsilon(t-\tau)\exp\left(j2\pi f_0 (t-\tau)\right) \tag{3.2}$$

where $\varepsilon(t)$ is the base band envelope of the complex electric field in time, and f_0 is the central optical frequency of the pulse.

By focusing the two separated beams into a nonlinear medium, it is then possible to generate a signal that carries the correlation information:

$$\varepsilon(t)\varepsilon(t-\tau)\exp\left(j2\pi f_0(2t-\tau)\right) \tag{3.3}$$

This signal is commonly generated at doubled frequency because it exploits the second order nonlinearity of the medium. Detection of this signal requires the integration of its intensity over time t of at least over one pulse. In general, detection results in the actual averaging over several pulses. This causes a delay difference τ between the two identical pulses. By moving the translation stage (TS) a set of different τ delays can be obtained. The time delayed SH signal (blue arrow) generated from the nonlinear crystal (NLX) is then detected. The obtained autocorrelation can then be acquired (for example, using a DAQ data acquisition device) as shown in Figure 3.1.

By doing so, we obtain SHG intensity autocorrelation, $R_I(\tau)$, which ideally corresponds to the strict mathematical definition:

$$R_I(\tau) = E\left\{I(t)I(t-\tau)\right\} \tag{3.4}$$

where $E\{\cdot\}$ is the expected value operator, τ is the delay between the two identical pulses and $I(t)$ is the instantaneous intensity pulse shape.

Measuring the pulses in this way has some advantages and disadvantages:

1) it allows for a straight forward interpretation of some qualitative smooth features of the pulse such as an approximated pulse width of the temporal intensity (as it is explained in the next paragraph), which can be used as guidance when carrying some pulse compression experiments;

2) it can be performed at video rate speeds or higher because it only requires collection of small amount of points.

3) however, the amount of information that it carries is limited because the pulse shape (Gaussian, $sech^2$, etc.,) has to be assumed and detailed knowledge about the pulse requires more sophisticated solutions (which will be explained below) .

Because nonlinear interactions (multiphoton processes) occur at high intensities, which means that below certain intensity threshold multiphoton processes can be neglected, is then reasonable that we establish the Full Width to the Half Maximum (FWHM) of the intensity profile to roughly approximate pulse duration.
Note that this FWHM of the intensity autocorrelation is equal the actual autocorrelation of two pulses with a defined intensity profile. Therefore, the temporal FWHM of the measured pulse is estimated by multiplying the FWHM of the IA by a scaling factor:

$$FWHM_{I(t)} = \frac{FWHM_{R_{I(t)}}}{\alpha} \tag{3.5}$$

where $\alpha = \sqrt{2} \cong 1.414$ for a Gaussian pulse or α = *cosh*(1) = 1.543 for a squared hyperbolic secant, $sech^2(t)$. Further coefficients can be obtained for different pulses depending on the experimental conditions.

3.2.2 Interferometric Autocorrelation.

Probably, a more natural type of measurement in the time-domain is the Interferometric AutoCorrelation (IAC). This method firstly proposed by Jean Claude Diels and Eric Van Stryland in the 70's was named Fringe Resolved Second Harmonic Generation (Diels, 1978a,b) (FRSHG). It contains a large amount of phase information and its experimental setup is simpler as it consists of an autocorrelator, SHG medium and a detector. Unfortunately, the additional phase information available in the IAC is mixed in a complex manner and training is necessary to visually extract some pulse information.
This means that both beams are overlapped as can be seen in Figure 3.2(a). This collinear arrangement causes that the detected quadratic signal includes interference among different terms. This can be mathematically written as:

$$R_{IA}(\tau) = E\left\{\left|\left(\varepsilon(t) + \varepsilon(t-\tau)\exp\left(-j2\pi f_0\tau\right)\right)^2\right|^2\right\} \tag{3.6}$$

The complex phasor depending on τ, $\exp(-j2\pi f_0\tau)$, is responsible for the appearance of the interferometric fringes as can be further seen in the following expressions:

$$R_{IA}(\tau) = E\left\{\left|\varepsilon^2(t) + \varepsilon^2(t-\tau)\exp\left(-j4\pi f_0\tau\right) + 2\varepsilon(t)\varepsilon(t-\tau)\exp\left(-j2\pi f_0\tau\right)\right|^2\right\} \tag{3.7}$$

These interferometric fringes, as shown in Figure 3.2, are the main difference between the IAC and the IA. From the experimental viewpoint, an IAC, is more practical because it is performed under collinear geometry. Figure 3.2 illustrates how this interference does not occur when non-collinear geometry is employed (Fig. 3.2(b)) and Intensity Autocorrelation is then obtained.

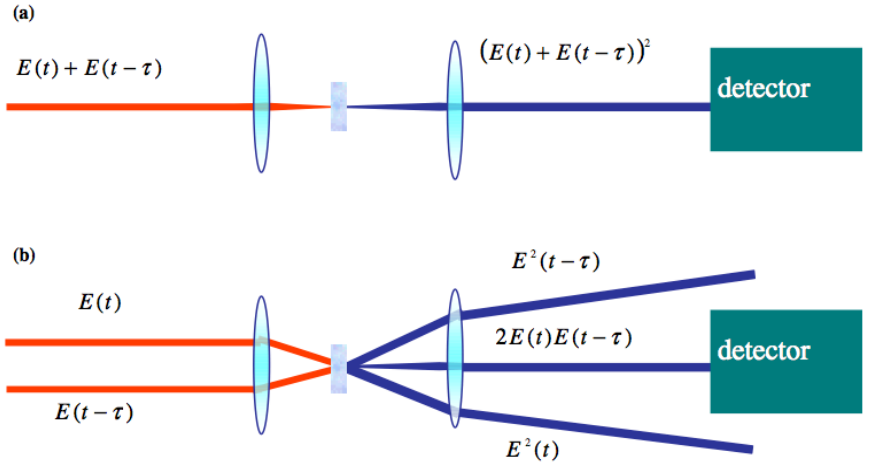

Fig. 3.2 (a) Collinear and (b) Non-collinear schemes to perform ultrashort pulse measurements.

The IAC can be rewritten as:

$$R_{IAC}(\tau) = E\left\{\begin{array}{c} I^2(t) + I^2(t-\tau) + \\ +4I(t)I(t-\tau) + \\ +4\big(I(t)+I(t-\tau)\big)\mathrm{Re}\Big[\varepsilon(t)\varepsilon^*(t-\tau)\Big]\cos\big(2\pi f_0\tau\big) + \\ +2\mathrm{Re}\Big[\varepsilon^2(t)\big(\varepsilon^*\big)^2(t-\tau)\Big]\cos\big(4\pi f_0\tau\big) \end{array}\right\} \qquad (3.8)$$

The first two terms of this equation correspond to the background, $E\left\{I^2(t)+I^2(t-\tau)\right\} = 2E\left\{I^2(t)\right\}$, which are the SHG Intensities of the pulse and its delayed replica without interfering. The third term is equivalent to the Intensity Autocorrelation $E\left\{I(t)I(t-\tau)\right\}$. It is worth to mention that these first three terms are not modulated in time delay, τ. In contrast, the fourth (complex interference) term is modulated at the central fundamental frequency f_0 in time delay, τ and the fifth term represents the Intensity Autocorrelation but modulated at the SHG frequency $2f_0$ in time delay, τ.

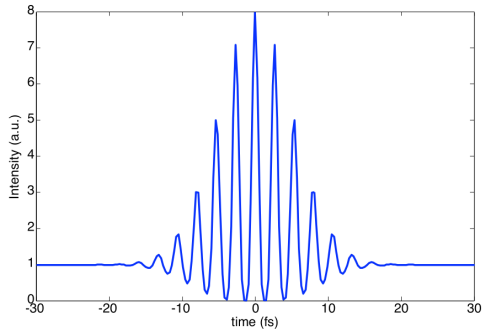

Fig. 3.3 Simulated Interferometric Autocorrelation of a transform limited pulse with Gaussian profile with FWHM=8 *fs*.

This notation allows extracting some important information about the collinear measurement such as an estimate of the quality of the measurement and any systematic errors performed during measurement. This can be done by noticing that at $R_{IA}(\tau)\big|_{\tau=0} = R_{IA}(0)$, which corresponds to the maximum value of the SHG Interferometric Autocorrelation, we obtain:

$$R_{IA}(0) = E\left\{\begin{array}{c} 2I^2(t) + \\ +4I^2(t) + \\ +8I^2(t) + \\ +2I^2(t) \end{array}\right\} = 16E\left\{I^2(t)\right\} \tag{3.9}$$

In addition to that, the background value can be calculated assuming that for large delays, there is no temporal overlap between the two pulses, $I(t)I(t-\tau) \cong 0$, or $\tau \to \infty$:

$$R_{IA}(\tau \to \infty) = E\left\{\begin{array}{c} I^2(t) + I^2(t-\tau) + \\ +0 + \\ +0 + \\ +0 \end{array}\right\} = 2E\left\{I^2(t)\right\} \tag{3.10}$$

Therefore, from Eq. 3.9 and 3.10 it is possible to the established maximum to background ratio must be 8:1 for an ideal measurement. Importantly, this simple rationing might help to assess which is the source of the experimental error if any. Ensuring the obtained result should be one of the main concerns when measuring ultrashort laser pulses; otherwise, the obtained retrieval might be erroneous.

Another convenient feature of the IAC is the fact that it is possible to obtain the IA. This is because the IA term is contained at the DC spectra of time delay, τ. Therefore, classical Low Band Pass Filtering (LBPF) is enough to obtain the autocorrelation plus a constant term (background). This LBPF can be either performed by a slow detector, by fast scanning the time delay, or by digital processing techniques once the trace has been electronically acquired. The new ratio for the collinear IA is the 3:1 (as can be seen from numerical simulations shown in Fig. 3.4 or deduced from Equation 3.10. in an analogous manner to the Interferometric Autocorrelation) by simply neglecting the high frequency terms (those modulated by cosine function) from Equation 3.8:

$$R_{IA}(\tau) = E\left\{\begin{array}{c} I^2(t) + I^2(t-\tau) + \\ +4I(t)I(t-\tau) \end{array}\right\} \tag{3.11}$$

and applying the same procedure shown above:

$$R_{IA}(\tau) = E\left\{\begin{matrix}2I^2(t)+\\+4I^2(t)\end{matrix}\right\} = 6E\left\{I^2(t)\right\} \qquad (3.\ 12)$$

And the background is calculated by

$$R_{IA}(\tau \to \infty) = E\left\{\begin{matrix}I^2(t)+I^2(t-\tau)\\+0\end{matrix}\right\} = 2E\left\{I^2(t)\right\} \qquad (3.\ 13)$$

which establishes the ratio 3:1 from numerical simulation assuming ideal experimental conditions, as shown in Figs 3.4 (c)-(f)-(i), and can be checked for validation of an experimental measurement.

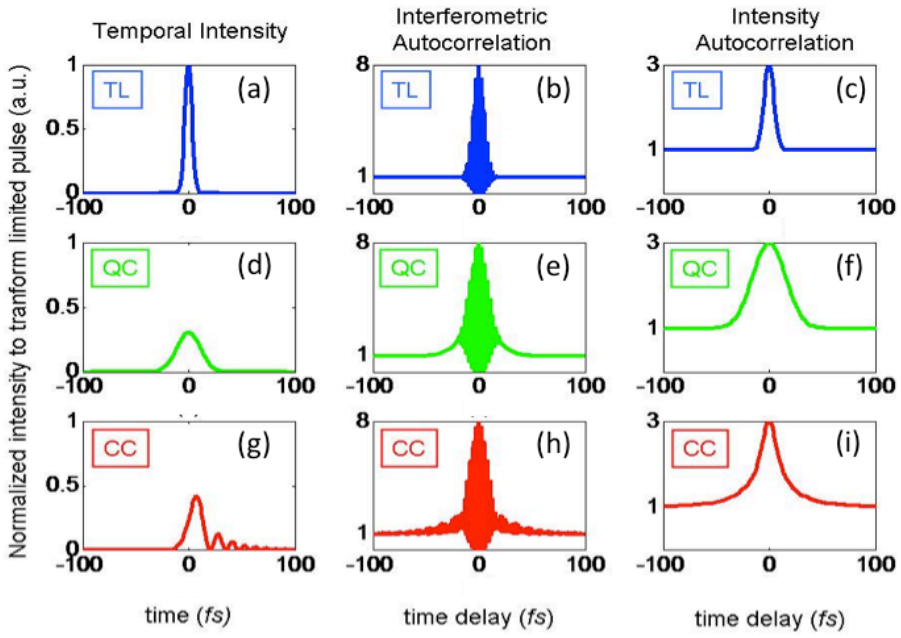

Fig. 3.4 Comparisson between (b), (e) and (h) Interferometric autocorrelation (1:8 ratio as seen in the axis) and (c), (f) and (i) Intensity autocorrelation (1:3 ratio as seen in the axis) for (a) Transform Limited (TL), (d) Quadratically Chirped (QC) and (g) Cubically Chirped (CC) pulses, respectively.

IAC, being a collinear technique, is sensitive to phase changes. However, these IAC are not adequate for a fully characterisation of ultrashort pulses. This is because different pulses can in fact produce very similar IAC and SHG spectrum[6]. Based on an IAC, there have been several

attempts to find a general method for a full ultrashort pulse measurement. These will be briefly reviewed in what follows.

3.2.3 MOSAIC.

MOdified-Spectrum AutoInterferometric Correlation (Hirayama, 2002; Bender, 2007, 2008), or MOSAIC, is a modification to the IAC method that makes it sensitive to temporal chirp. This technique is oriented for monitoring mode-locked laser pulses while performing real-time dispersion control to minimize the temporal phase distortions.

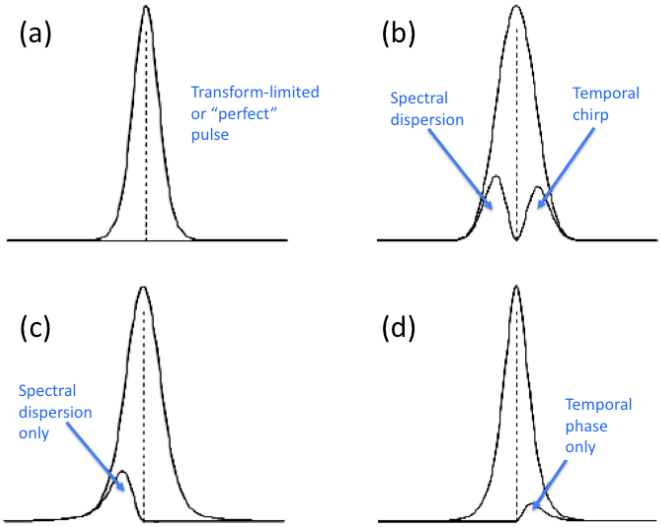

Fig. 3.5 Simulation of H-MOSAIC for a pulse having a symmetric spectrum with (a) no dispersión, (b) GVD, (c) TOD and (d) an asymmetric spectrum with no dispersión. The dashed line indicates zero delay. (figure acknowledged from ref. 9 Bender 2008)

MOSAIC is based in a simple post-processing technique. This requires modifying the IAC spectrum as follows: the $\pm f_0$ terms are eliminated, the $\pm 2f_0$ terms are amplified by a factor of 2, and the intensity autocorrelation term is unchanged. This spectral modification gives the time-domain MOSAIC signal:

$$I_{MOSAIC}(\tau) = 1 + 2E\left\{ I(t)I(t-\tau) + \mathrm{Re}\left[\varepsilon^2(t)\left(\varepsilon^*\right)^2(t-\tau)\exp\left(j4\pi f_0\tau\right)\right]\right\} \quad (3.14)$$

This technique allows obtaining a qualitative estimation of the pulse chirp at video-rates by simply displaying it into an oscilloscope; however, expertise is required. By adding the fundamental spectrum to the data set, it was further developed Hybrid-MOSAIC which allowed more intuitive representation of the amount of temporal chirp and spectral dispersion of the pulses and further development enabled ultrashort pulse measurements.

3.2.4 IRIS.

Prior to MOSAIC technique, an Iterative Reconstruction from Interferometric Signals (IRIS) technique was proposed at 1989 as an algorithm to retrieve an ultrashort pulse by measuring the Interferogram and the IAC (Naganuma, 1989). However, it has been shown to be susceptible to giving erroneous results under experimental conditions (Chung, 2001). Similarly in 1987, a computer assisted spectrum-resolved SHG autocorrelator for monitoring phase characteristics was also proposed (Watanabe, 1987).

3.2.5 PICASO.

Yet, another iterative algorithm appeared at the very end of the millennium, in 1999, to take time domain pulse retrieval one step beyond by measuring an intensity cross correlation from an unbalanced Michelson interferometer together with the pulse spectrum to feed an iterative algorithm that retrieves the complex pulse amplitude (Nicholson, 1999, 2000, 2002) named as Phase and Intensity from Correlation And Spectrum Only (PICASO). Similarly to other methodologies, they approach the problem by introducing an linear element with known dispersive properties in one of the arms of the unbalanced Michelson interferometer to generate an asymmetric cross correlation and start pulse retrieval guessing an initial spectral phase.

They model the measured cross correlation by guessing the electric field in both arms of the unbalanced Michelson interferometer as follows:

$$A_1(t) = F^{-1}\left\{\sqrt{S(\omega)}\exp\left(j\phi(\omega)\right)\right\} \tag{3.15}$$

where $A_1(t)$ is the estimated temporal electric field in the input pulse, $S(\omega)$ is the measured intensity sectrum, $\phi(\omega)$ is the guessed phase, $F^{-1}\{\cdot\}$ is the inverse Fourier Transform. Likewise, the output from the unbalanced arm, $A_2(t)$, is expressed as follows :

$$A_2(t) = F^{-1}\left\{\sqrt{S(\omega)}\exp\left(j\phi(\omega) - j\Psi(\omega)\right)\right\} \tag{3.16}$$

where $\Psi(\omega)$ models the known dispersive properties of the linear element. From this, the estimated pulse is computed as:

$$I_r(\tau) = \int\left|A_1(t)\right|^2\left|A_2(t-\tau)\right|^2 dt \tag{3.17}$$

The iterative algorithm is then framed in the context of a multidimensional minimization algorithm. In order to find the optimal solution, the authors propose the following merit function Δ:

$$\Delta^2 = \frac{1}{N}\sum_{i=1}^{N}\left(I_m(\tau_i) - I_r(\tau_i)\right)^2 \tag{3.18}$$

where N is the number of spectral sampling points and $I_m(\tau)$ is the measured intensity cross correlation. Of the many search algorithms available they chose a simplex method (Press, 1992) because of its simplicity and global search capabilities. The downhill simplex method works by constructing an (N+1)-sided volume, a simplex, in the N-dimensional space of spectral phases, where N is the number of sample points. The error Δ is calculated for each of the simplex's vertices, and then, they transform the simplex by moving vertices that have a high Δ, usually by using a reflection operation. The procedure is iterated until a predefined error is reached or the error converges. Main advantage of this approach is that it overcomes the limitation of time directions thanks to the use of an unbalanced interferometer that generates an asymmetric measurement. Main disadvantage is related to the practical aspect that different pulses might require different linear elements with known dispersive properties, $\Psi(\omega)$.

Further research on this idea was evolved towards an unbalanced third-order cross-correlation setup because the original scheme had some problems when retrieving asymmetric pulses (Nicholson, 2000) that are overcome by this approach. Although PICASO is perhaps the most successful of all IAC techniques described here it is however, as with all of the IAC techniques, lacking advanced error checking ability and requires pulse specific optical arrangements to guarantee the computed retrieval, and therefore, lacks of generality.

3.3 Conclusions.

Time domain techniques were the first attempt to characterise ultrashort laser pulses. They are an elegant and direct solution to a major problem of current physics that is lasting for almost half a century. They provided the first neat concept that we still work on: we require the shortest pulse to characterise the shortest pulse as this is the fastest event that we have in the lab. However, deeper and thorough study on ultrashort laser pulses soon required better and more accurate techniques in order to keep advancing.

From this sound basis, better and more refined techniques were later developed, and general solutions were found as is explained in the next chapter, however, there is still a need to develop flexible, fast and robust solutions to this technological bottleneck.

References

J Armstrong, “Measurement of picosecond laser pulse widths,” *Applied Physics Letters* **10** pp. 16-18 (1967).

DA Bender and M Sheik-Bahae,” Modified Spectrum Auto-Interferometric Correlation for Single Shot Pulse Characterization,” *Opt. Lett.* **32** pp. 2822-2824 (2007).

DA Bender, JW Nicholson, and M Sheik-Bahae, "Ultrashort laser pulse characterization using modified spectrum auto-interferometric correlation (MOSAIC)," *Opt. Express* **16** pp. 11782-11794 (2008).

JH Chung and AM Weiner, "Ambiguity of ultrashort pulse shapes retrieved from the intensity autocorrelation and the power spectrum," *IEEE J. Selec. Top. Quantum Electron.* **7** pp. 656-666 (2001).

J-C Diels, EW Van Stryland, and D Gold, “Investigation of the parameters affecting subpicosecond pulse duration of passively mode-locked dye laser,” in *Proceedings, First International Conference on Picosecond Phenomena Springer-Verlag, New York*, pp. 117–120, (1978a).

J-C Diels, EW Van Stryland, and G Benedict, “Generation and measurement of 200 femtosecond optical pulses,” *Opt. Commun.* **25**, pp. 93-95 (1978b).

T Hirayama and M Sheik-Bahae, “Real-time chirp diagnostic for ultrashort laser pulses,” *Opt. Lett.* **27** pp. 860-862 (2002).

M Maier, W Kaiser and J. Giordmaine, “Intense Light Bursts in the Stimulated Raman Effect,” *Phys. Rev. Lett.* **17** pp. 1275-1277 (1966).

K Naganuma, K Mogi, and J Yamada, “General method for ultrashort light pulse chirp measurement,” *IEEE J. Quantum Electron.* **25** pp. 1225–1233 (1989).

JW Nicholson, J Jasapara, W Rudolph, FG Omenetto, and AJ Taylor, “Full-field characterization of femtosecond pulses by spectrum and cross-correlation measurements,” *Opt. Lett.* **24** p. 1774 (1999).

JW Nicholson, M Mero, J Jasapara, and W Rudolph, "Unbalanced third-order correlations for full characterization of femtosecond pulses," *Opt. Lett.* **25** pp. 1801-1803 (2000).

JW Nicholson and W Rudolph, "Noise sensitivity and accuracy of femtosecond pulse retrieval by phase and intensity from correlation and spectrum only (PICASO)," *J. Opt. Soc. Am. B* **19** pp. 330-339 (2002).

WH Press, SA Teukolsky, WT Vetterling, and BP Flannery, "Numerical Recipes in C: The Art of Scientific Computing," *Third Edition of New York: Cambridge University Press*, pp. 502-510 (1992).

A Watanabe, H Saito, Y Ishida, and T Yajima, "Computer-Assisted Spectrum-Resolved SHG Autocorrelator for Monitoring Phase Characteristics of Femtosecond Pulses," *Opt. Commun.* **63** pp. 320-324 (1987).

HP Weber, "Method for Pulsewidth Measurement of Ultrashort Light Pulses Generated by Phase-Locked Lasers Using Nonlinear Optics," *J. Appl. Phys.* **38** pp. 2231-2234 (1967).

CHAPTER 4

Methods for the complete measurement of ultrashort laser pulses: State-of-the-art (part 2).

4 Methods for the complete measurement of ultrashort laser pulses: State-of-the-art (part 2).

4.1 Introduction to complete measurement.

In the prior chapter we have outlined methods for estimating some pulse characteristics by means of techniques based on a temporal analysis. Although extracting some features of the temporal intensity profile is an important step, in order to accurately measure pulses it is necessary to know the complex electric field (modulus and phase) of the unknown pulse. If these two parameters are established (aside from the uncertainty of the carrier envelope offset phase which is important only for near single-cycle pulses), it is said that a full or complete measurement has been carried out.

The main limitation of methods based on autocorrelations is that they are one-dimensional data sets and do not allow reliable neither general method to fully characterise ultrashort pulses. Barakat (Barakat, 1984) mathematically showed in 1984 that although in one dimension multiplicity of solutions to the phase reconstruction problem represents a serious problem, in two or more dimensions multiplicity would be pathologically rare.

Therefore, one possible solution to the phase reconstruction problem was to transform it into a complex two-dimensional phase retrieval problem by using a joint time-frequency representation. Due to this idea, a whole line of methods appeared based in a range of joint time-frequency representations, which were named spectrograms and sonograms.

A well-known example of joint time-frequency representation is the musical score, which shows in Figure 4.1 the frequencies present in an acoustic waveform during a given time interval, and is thus a plot of the waveform's frequency vs. time. Additional marks at the top - pianissimo or fortissimo - indicate the intensity vs. time.

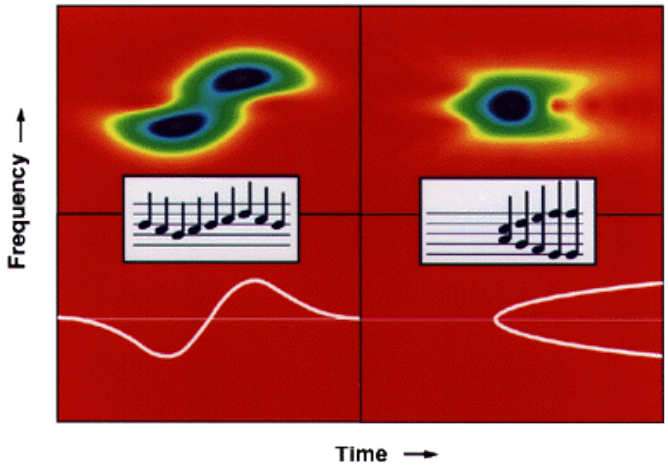

Fig. 4.1 Spectrograms (or sonograms), frequencies vs. time, and equivalent musical scores for two different pulses (one better described in the time domain and the other better described in the frequency domain). Note that the spectrogram and sonogram graphically follow the pulse frequency vs. time (left) or the group delay vs. frequency (right). (figure acknowledge to www.physics.gatech.edu/gcuo/opn/opn.html)

Two-dimensional measurements, within a joint time-frequency domain, were actually introduced at the very beginning of the 70's with an idea by Brian Treacy (Treacy, 1971). Unfortunately, this work was not appreciated at this time because the final step of pulse retrieval from these time-frequency images was not taken (Trebino, 1997). It was not until 1993, when Rick Trebino proposed Frequency Resolved Optical Gating (Trebino, 1993). This was the first method to completely characterise an ultrashort pulse in a wide range of situations without any *a priori* knowledge of the pulse.

After FROG algorithm solved the problem and showed a general manner to approach the measurement of ultrashort laser pulses in a robust and effective manner due to acquisition of a huge amount of data, there were immediately requirements for further improvements. Such improvements were mostly centred upon practical feasibility and speed in the retrieval.

Interferometric techniques (Iaconis, 1998a, 1998b) were born to address this latter problem: speed in the retrieval. Interferometric techniques offer

direct phase measurement without the need for retrieval algorithms or the collection of large data sets. As a consequence, pulse characterization can be carried out in real time (Shuman, 1999). Interferometric techniques, however, do not have a stringent error-checking capability; they normally rely on pulse-specific optical arrangements that might compromise practical feasibility.
In what follows, a more detailed description of different methods for complete measurement will be provided, and has been divided in four sub-sections: Time frequency, with especial emphasis to FROG; Other FROG implementations; Interferometric Techniques; and Recent techniques.

4.2 Methods for complete measurement.

4.2.1 Time-frequency Methods.

4.2.1.1 Introduction.

Time-frequency techniques attempt to fully characterize ultrashort pulses by processing the information from a measured image. This image is carried out in a joint time-frequency space. The main advantage of taking a 2D representation of an ultrashort pulse is that it possesses 1) several mechanisms to avoid multiplicity of solutions as shown by Barakat (Barakat, 1984) and 2) checking capabilities to ensure the obtained result through marginal analysis.
There exist a number of representations in a joint time-frequency domain for ultrashort laser pulses. In this part we will focus only in those 2D image representations that can be directly measured: sonograms and spectrograms. Although for other disciplines spectrograms and sonograms are equivalent techniques (i.e. sonograms are spectrograms of sound waves), in the context of ultrashort pulse measurement, they are

not (Walmsley, 1996). A few schemes will be introduced in this section to illustrate this.

4.2.1.2. Sonograms.

Sonograms (Chilla, 1991) are defined as the intensity vs. frequency for different frequency slices of the pulse (See Fig.4.2). Slicing the pulse in frequency requires performing a gating in frequency domain as seen in the following expression:

$$S_0(\Omega,T) = \left|\int \varepsilon(\omega) h(\omega - \Omega) \exp\left(-j\omega T\right) d\omega\right|^2 \qquad (4.1)$$

and this is actually the quantity that Treacy measured. Although several others, as briefly commented below with precise referencing, Yuzo Ishida, Eric Ippen, Andrew Wiener and J. P. Likforman, made measurements of various time-frequency domain quantities in the 1980's, Treacy's method did not find wide application until Juan Chilla and Oscar Martinez (Chilla, 1991) showed in 1991 that it could be used to reconstruct the full intensity and phase of the pulse. They realized that it was possible, under certain circumstances, to measure the approximate group delay. This solved the pulse measurement problem for many pulses. This technique was labelled by them Frequency Domain Phase Measurement, or FDPM, and by Treacy the dynamic spectrogram. Experimentally it is simple to measure: a portion of the pulse spectrum is selected by a spectrometer and then the cross-correlation of the selected slice with the input pulse is taken.

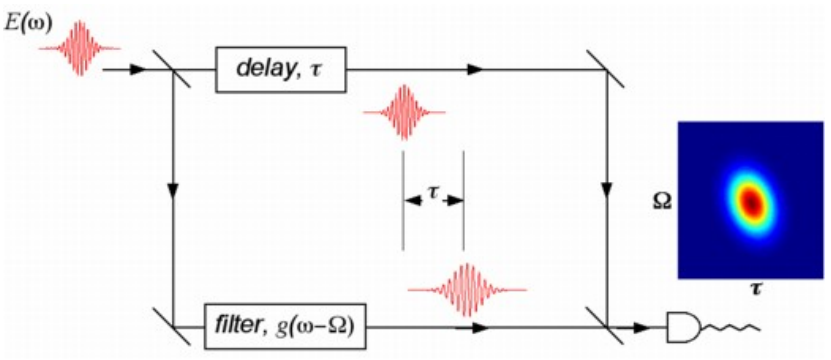

Fig. 4.2 Sonogram technique using a scanning Mach-Zehnder interferometer containing a scanning tuning Fabry-Perot etalon. On the right, example of possible measured image of the ultrashort pulse. (From Heriot Watt University, www.phy.hw.ac.uk/resrev/ufast/sonomzi.jpg).

The difficulty with the Chilla-Martinez recipe is that it requires the frequency gate to be extremely narrowband, making this filtering step quite inefficient. Only when the pulse spectral phase is well behaved (i.e. smooth), the gate can be made wide enough to allow through enough energy to detect SH signal and simultaneously narrow enough, so assumptions of algorithm to extract the phase work correctly. In this line, other researchers have since developed variations on Chilla-Martinez method (Chu, 1995; Rhee, 1996). This has been also experimentally shown in several works by performing complete pulse characterization in real time (Reid, 2002). Reid and Cormack reported a static single-shot configuration for measuring a sonogram trace of ultrashort optical pulses. The performance of the proposed instrument described by (Reid, 2002) yields complete and unambiguous pulse characterization.

Additionally, it sometimes occurs that, for a given frequency, a sonogram has two or more peaks in time, so that it is not possible to define uniquely a group delay. In this case the pulse cannot be reconstructed using a simple algorithm and more complex algorithms are required to overcome this limitation as reported and shown by Reid (Reid, 1999).

4.2.1.3 Spectrogram.

Ishida and co-workers were the first to make spectrograms of ultrashort laser pulses, but they did not retrieve pulses from them (Ishida, 1985; Watanabe, 1985, 1987). The underlying concept behind spectrograms is that gating occurs in time, rather than frequency as occurs for sonograms. This opened up a new range of possibilities to unwrap the pulse information hidden in the measured time-frequency image and presented alternative limitations to sonograms. Although this concept seems at first not to be straightforward, it actually is, as shown in Figure 4.1 by the musical score. A mathematically rigorous form of the traditional musical score is actually the "spectrogram" (Cohen, 1989) as defined for ultrashort pulse characterization :

$$S(\omega,\tau) = \left|\int \varepsilon(t) g(t-\tau) \exp\left(-j\omega t\right) dt\right|^2 \qquad (4.2)$$

where $g(t-\tau)$ is a variable-delay gate function. The spectrogram, analogously to the musical score, is the spectra at different temporal slices of the field.

Finally, Trebino and Kane (Trebino, 1993, 1997; Kane, 1993a, 1993b, 1998) introduced phase-retrieval techniques for obtaining the electric field from Eq. 4.2 and were the first to develop a rigorous method (Frequency Resolved Optical Gating) for pulse characterization.

4.2.1.4 FROG.

Frequency Resolved Optical Gating (FROG) is one of the most common and robust approaches to fully characterise ultrashort pulses. It has been successfully used to characterise pulses from the UV to the near-infrared (Trebino, 1997) with durations of only a few femtoseconds (Baltuska, 1998).

This development occurred when Rick Trebino and Daniel Kane realized that the problem of determining the pulse intensity and phase from a spectrogram was essentially equivalent to the two-dimensional "phase

retrieval" problem in image science and astronomy. Phase retrieval is the problem of finding a function knowing only the magnitude but not the phase of its Fourier transform. Phase retrieval for a function of one variable is impossible. For example, knowledge of a pulse spectrum does not fully determine the phase of the pulse as many different pulses have the same spectrum. However, twenty years ago, image scientists found that phase retrieval for a function of two variables is possible. Knowledge of only the magnitude of a two-dimensional Fourier transform of a function of two variables essentially uniquely determines of a function with finite extent. Interestingly, these results follow directly from the existence of the Fundamental Theorem of Algebra for polynomials of one variable and its non-existence for polynomials of two variables (Stark, 1987). The Fundamental Theorem of Algebra states that every non-zero single-variable polynomial, with complex coefficients, has exactly as many complex roots as its degree, if repeated roots are counted up to their multiplicity. In other words, for every complex polynomial p of degree n > 0 the equation p(z) = 0 has exactly 'n' complex solutions, counting multiplicities. Measurement of a spectrogram (or sonogram), which is the Fourier transform of a function of two variables, thus frames the ultrashort-pulse measurement problem in a form that allows a rigorous and general solution. This realization led to the introduction of iterative inversion algorithms (DeLong, 1994; Nicholson, 1999). The general prescription is that one seeks to find a test field $\varepsilon_{test}(t)$ that minimizes the difference between the measured spectrogram and the test spectrogram. An initial guess is refined through iteration by continually comparing the test and measured spectrograms and then using the difference between them to determine how to alter the test field.

The FROG technique can be implemented by exploiting several nonlinear effects such as: Polarization-Gate (PG-FROG), Self-Diffraction (SD-FROG), Transient-Grating (TG-FROG) and Second-Harmonic-Generation (SHG-FROG) (Trebino, 1997). Among all of them, SHG-FROG is the most popular because it can exploit the high second order

nonlinear coefficient rather than the, generally weaker, third order nonlinearities. SHG-FROG is also the preferred method for sub-100*fs* pulse characterization as it introduces very little material dispersion before the non-linear process takes place.

SHG-FROG

SHG-FROG trace consists of a frequency-resolved SHG intensity autocorrelation that provides the necessary frequency and time information to reconstruct the original intensity and phase of the pulse through an iterative algorithm. SHG-FROG is possibly the best-known representative all ultrashort pulse measurement techniques. The central idea is to measure temporal and spectral information simultaneously in some combined fashion, and then reconstruct the amplitude and phase profiles from the raw data by way of a suitable algorithm.

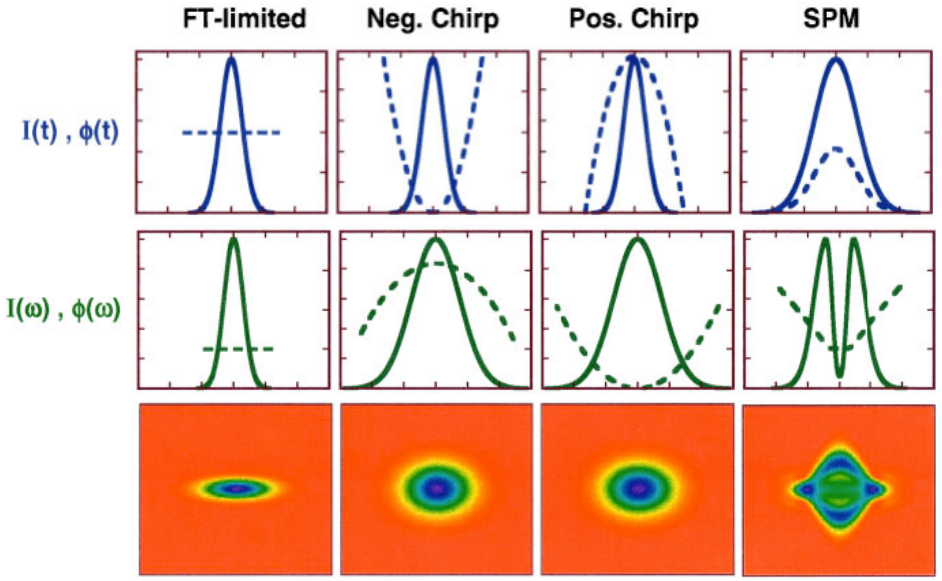

Fig. 4.3 Different examples of SHG-FROG measurements for different pulse dispersion showing a distinct SHG-FROG pattern except for the sign of the chirp for each type of dispersion. (figure acknowledged to reference Trebino 1997).

Experimentally, SHG-FROG is quite simple: the FROG spectrogram is just the spectrum of the autocorrelation. Since experimentalist already routinely measure pulse autocorrelations and spectra, they need only move their spectrometer to the output of their autocorrelator in order to make a SHG-FROG trace to characterise the pulses because it provides particular patterns for different types of chirps (except for time direction ambiguity), as shown in Figure 4.3. In addition, almost any nonlinear optical process can be used to generate a self-time gate, and a number have been demonstrated. Unfortunately, in general, all these approaches are limited for use within a non-collinear geometry (Fig. 4.1).

FROG algorithms

All FROG algorithms are fundamentally based under the same scheme as shown in Figure 4.4. Basically an initial pulse is guessed, this guess can be either a random pulse or a prior estimation from the Intensity spectrum and/or a measured autocorrelation. Then, a FROG trace is generated through steps (2 and 3) of Figure 4.4. This generated FROG trace is modified in the following manner: phase information is kept and modulus information is substituted by the measurement. The key step lies in number 6, in which different techniques have been utilized to retrieve the temporal profile of the pulse, because this step sets how the algorithm will actually go towards the right direction. In any iterative algorithm, the most important characteristics are two: (1) the algorithm in average minimizes the error; (2) the algorithm should not be trapped in any local minima. Second condition is difficult to ensure under all conditions, and in order to minimize this type of error is fundamental to design a proper global search strategy. Because even an exhaustive search in all the space can be compromised by sampling or become too time consuming without guarantee to be correct. There is also extensive literature regarding the first condition and there has been several algorithms to robustly ensure the convergence of FROG algorithm towards the measured FROG trace (Trebino, 1997; Kane, 1993a, 1998; DeLong 1994b, 1994c; Paye 1993;

Nicholson, 1999), among all, it has been suggested by Trebino and Kane that Principal Component Generalized Projection Algorithm (PCGPA) has a remarkable performance.

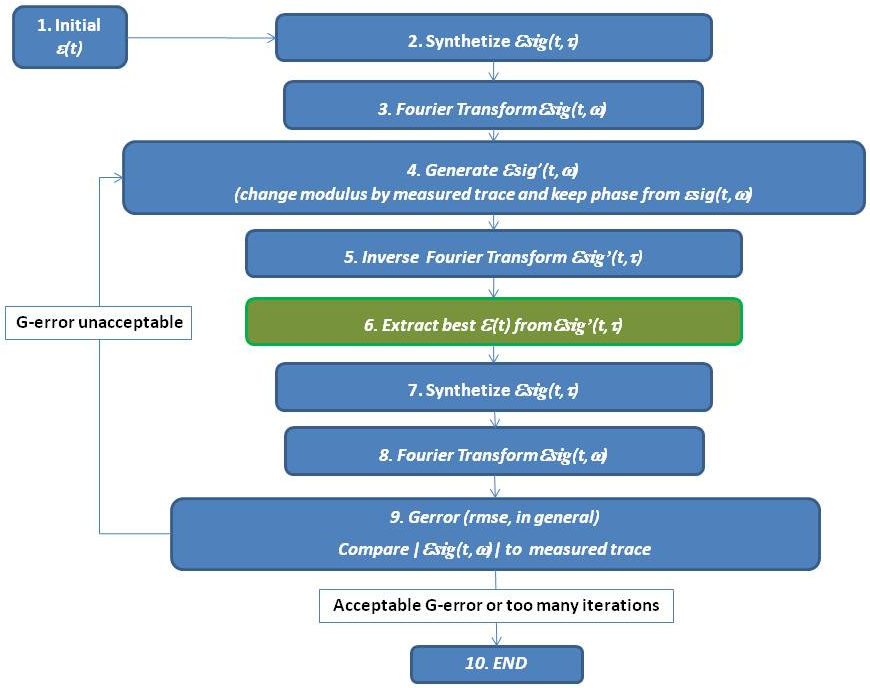

Figure 4.4 General FROG retrieval scheme.

The PCGPA handles the FROG trace as an outer product form matrix, O, as follows:

$$O = U \text{ x } W \text{ x } V^T \tag{4.3}$$

where U matrix contains the column probe vectors $\varepsilon(t)$, V^T the row gate vectors $\varepsilon(t,\tau)$, and W is a square diagonal matrix that contains the weight of each component. After this notation was made direct Principal Component analysis enables to extract the eigenvectors and the eigen-values of the FROG trace in a number of ways. Then PCGPA keeps the component with the largest weighting factor, which is the principal component, to compute the synthetic spectrogram $\varepsilon'_{sig}(\tau,\omega)$. Importantly, PCGPA ensures that for an ideal FROG trace, when both intensity and phase of the spectrogram $\varepsilon'_{sig}(\tau,\omega)$ are correct, the outer product form

matrix is a matrix of rank one. That is, it would have one and only one nonzero eigenvalue and one V^T-eigenvector and one U-eigenvector. Additional components will arise in experimental acquisitions due to experimental errors but this should be used only to establish the quality of the FROG trace measurement.

Furthermore, PCGPA is frequently used in phase retrieval problems unrelated to FROG. It is also commonly used in many other problems, from medical imaging (Magnetic Resonance Imaging) to the training of neural networks. Indeed it is one of the few algorithmic methods than can be proven to converge when reasonable conditions are met. Also, composite strategies have been strongly recommended to complement PCGPA when it stagnates like the use of Genetic Algorithms (Nicholson, 1999). Trebino and co-workers (Trebino, 1997) suggested the use of an independently measured spectrum as an additional constraint (DeLong, 1994c); however, this could cause instabilities under some circumstances (DeLong, 1994d).

A very important feature is that any FROG algorithm takes into account all the N by N data points of the spectrogram, which is a joint distribution of time-frequency, rather than N data points in the time domain and N data points in the frequency domain, produces a better estimate of the pulse, since there is redundancy of the signal. It has been shown that such collection of data, besides providing improved noise immunity (Wang, 2003) has built-in consistency checks via marginal analysis which allows the detection of different sources of error. Consequently, SHG-FROG techniques offer a complete set of tools to ensure a robust retrieval within a widespread range of cases.

One of the features often outlined by FROG's users is the fact that after the iterative algorithm has provided with a candidate pulse, the goodness of the estimate can be checked though the marginals. Marginals are actually the summation in any of the two axes of the retrieved FROG trace, therefore, we can check *temporal marginal* and *frequency*

marginal. The temporal marginal results from adding up all the spectral lines of the retrieved FROG trace and compare it with the Intensity Autocorrelation of the pulse. The frequency marginal is calculated by adding up all time delays of the retrieved FROG trace and compare it with the SHG spectrum of the pulse.

However, quite generally FROG techniques show the best results by analysis of more or less simple pulse shapes, such as the output pulses from lasers. More complex amplitude profiles remain problematic for all variations of FROG, in particular when there are zeros or well separated parts in the temporal or spectral domain (Keusters, 2003).
Measuring an SHG spectrogram does not avoid the problems of inversion mentioned above; however, if anything, they are worse: because the gate is the pulse itself, it can never be narrow enough to accurately obtain the frequency vs. time directly from the trace. In such cases, iterative FROG algorithms (Trebino, 2002; Kane, 1999) often do not converge and give meaningless and simply wrong output. Therefore, a reliable full field reconstruction of arbitrary pulse shapes could not be guaranteed by conventional FROG methods. Stagnation is also a persisting problem of conventional iterative FROG algorithms.

FROG is considered to be the gold standard for ultrashort pulse measurements up to date but it posses certain limitations. It was well know that SHG FROG trace does not allow establishing time direction because the same SHG FROG trace can be generated by $E(\omega)$ or $E^*(\omega)$. However, this trivial ambiguity can be overcame by using other nonlinear phenomena (like THG based FROG) or adding some known dispersion and measuring another trace.

As mentioned before, FROG algorithm tends to stagnate as pulse complexity increases. It has especially problems to identify between maxima or minima with points of inflection. Additionally, the good

estimate is mainly focused in the FWHM of the FROG trace that causes the wings to be poorly fitted because the total information is limited.
In this line, Seifert et al. performed a careful study on "Nontrivial ambiguities for blind FROG and the problem of uniqueness" (Seifert, 2004), which was an issue of major concern for certain applications. This recently developed into a new method named VAMPIRE (Seifert, 2004) to solve these limitations which is further explained below in this chapter (section 4.2.4.).

4.2.2 Other remarkable FROG schemes.

4.2.2.1 Introduction.

In this section, we briefly present several FROG schemes and algorithms that have been used and have helped to spread the technique abroad along the nineties and the beginning of the 2000's.

4.2.2.2 GRENOUILLE: simplified and single-shot FROG.

Grating Eliminated No-nonsense Observation of Ultrafast Incident Laser Light E-fields (GRENOUILLE) is actually a different and simpler SHG FROG arrangement that is able to obtain the FROG image in a single shot (O'Shea, 2001). GRENOUILLE is a logical extension of FROG and it means "FROG" in french. The optical arrangement consists in 6 elements: three cylindrical lenses, a Fresnel biprism, a SHG crystal and a CCD camera (see figure 4.5).

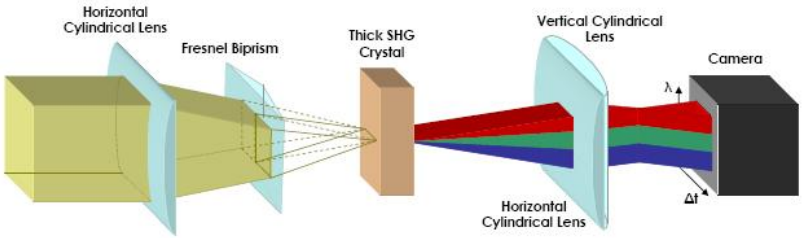

Figure 4.5 GRENOULLE experimental setup. (figure acknowledged to http://upload.wikimedia.org/wikipedia/en/b/bb/GRENOUILLE_long.JPG).

By assuming correct alignment, this set-up and some modifications in the original FROG algorithm, besides obtaining the complex electric field of the pulse, it also allows measuring spatial pulse-front tilt (Akturk, 2003a, 2003b) because linear wavefront deformation (pulse tilt) induces nonsymmetric FROG trace that can be handled by the retrieval FROG algorithm. This technique has exhibited to be robust and direct, however, it lacks of flexibility and its own compactness avoids to use it in a number of applications, like the focus of this thesis, to mesure an ultrashort laser pulse at the focus of a multiphoton microscope.

4.2.2.3 XFROG: Retrieval of two different pulses.

XFROG (DeLong, 1995; Kane 1997,Linden, 1998a, 1998b; Reid, 2000; Xu, 2000) uses two different pulses, one as gate and another one as a probe (reference pulse). Using sum (Linden 1998a) or difference-frequency mixing (Reid, 2000) of two pulses, we obtain a cross-correlation signal that is spectrally resolved. This results in the XFROG trace, one of the fundamental advantage of this approach is the capability to characterize weak ultrashort pulses from the mid-IR (Reid, 2000) and deep UV (Linden, 1998b) spectral regions. By using a reference pulse, which has been previously characterised, it is used as a constraint in the

algorithm to recover the unknown pulse. This variant of FROG has been demonstrated with the extremely complex pulse shapes of white-light continuum generated in microstructure fibres (Xu, 2000).

4.2.2.4 Blind FROG: Retrieval of two unknown pulses.

It was later shown that *a priori* knowledge of any of the pulses is not required to simultaneously retrieve the pulses (Kane, 2008) because PCGPA can cope with it due to the wealth of information contained in the XFROG trace and it works better for actual blind deconvolutions because both pulses are truly independent, as it is assumed in the theoretical framework of PCGPA.

4.2.3 Interferometric Techniques.

4.2.3.1 Introduction.

In the previous section we have presented FROG, which is considered up to date the gold standard of ultrashort pulse full-measurements. Another manner to circumvent the problem of retrieving the complete pulse characteristics is by taking a different approach based on spectral interferometry (SI). SI techniques were developed to enhance one of the main weak points of FROG: speed of retrieval. FROG algorithm is relatively robust and provides confidence to its users, however it requires large datasets to be acquired and executing an iterative retrieval algorithm. All this sequence of events is time consuming and is difficult to be carried out in real time. However, video rate FROG retrievals have been reported under specific setups as discussed below.
SI can be performed, in general, by putting the input pulse through some known splitters and dispersive filters. This produces at least one delayed pulse at specific distance and a broadly dispersed pulse. Then, by nonlinearly combining the pulses into an output pulse, we can measure

spectral interference fringes resulting of the different pulses at the detector. One of the key elements of the technique lies on the fact that it is possible to write an analytical expression of the output pulse as a function of the splitters and dispersive filters. In general, if the filters are properly chosen according to the spectral properties and dispersion of the input pulse, it is possible then to directly reconstruct the pulse field by an inversion algorithm applied to the detected output pulse.

There are two main advantages of this approach. Firstly, only a single measurement in one dimension needs to be acquired instead of the 2D images typical of spectrograms in the time-frequency domain. Secondly, pulse information can be extracted through a direct algorithm that is not iterative and therefore, it results in one of the fastest approach to characterise pulses (Walmsley, 2009).
One of the first IT was proposed by Diels, who reported an interferometric technique that uses an ultrafast diode and a Schottly nonlinear mixer to measure the interference intensity pattern between pairs of spectral components of the pulse (Prein, 1996). A similar technique known as Direct Optical Spectral Phase Measurement (DOSPM) uses a nonlinear crystal as a time gate to also trace interference beats (Chu, 1995). When compared to other time-frequency domain (i.e. FROG), these techniques are experimentally difficult which avoided them to be widely used. Nevertheless, all this changed in 1998 when Walmsley‘s group developed Spectral phase interferometry for direct electric-field reconstruction, SPIDER (Iaconis, 1998, 1999). SPIDER is currently the strongest alternative to FROG for complete measurement of an ultrashort laser pulse and is further discussed below.

4.2.3.2 SPIDER.

Spectral Phase Interferometry for Direct Electric-field Reconstruction (SPIDER) is an interferometric ultrashort pulse measurement technique in the frequency domain based on spectral shearing interferometry.

Spectral shearing interferometry is similar in concept to intensity autocorrelation except that, instead of gating a pulse with a time-delayed copy of itself, the pulse is interfered with a frequency-shifted or spectrally sheared copy of itself. The interferogram, measured with an integrating detector, is related to the input pulse spectrum by

$$S(f_c) = \begin{array}{c} |\varepsilon(f_c)|^2 + |\varepsilon(f_c+\Omega)|^2 + \\ +2|\varepsilon(f_c)||\varepsilon(f_c+\Omega)|\cos\left[\phi(f_c+\Omega)-\phi(f_c)+2\pi f_c\tau\right] \end{array} \tag{4.4}$$

where $\varepsilon(f_c)$ is the input pulse spectrum, Ω is the amount of spectral shear, τ is the temporal delay between the two replicas which needs to be adjusted for specific pulses and f_c is the base band frequency. The first two terms on the right-hand side of Eq. (4.4) are the individual spectra of the test pulse and its frequency-sheared replica, respectively. The third term provides the spectral phase in the form of the phase difference between spectral components separated by the shear Ω. One obtains the spectral phase for a set of discrete frequencies separated by Ω from the spectral phase difference by simply adding up the phase differences, which are deduced from prior knowledge on the pulse or experimental calibration. Initially, spectral amplitude was obtained from the square root of an independently recorded pulse spectrum. However, improvements provided ways to obtain the spectral intensity from the simple algebraic methods applied to the interferometric trace (Dorrer, 1999) to reduce experimental error and become self-callibrated.

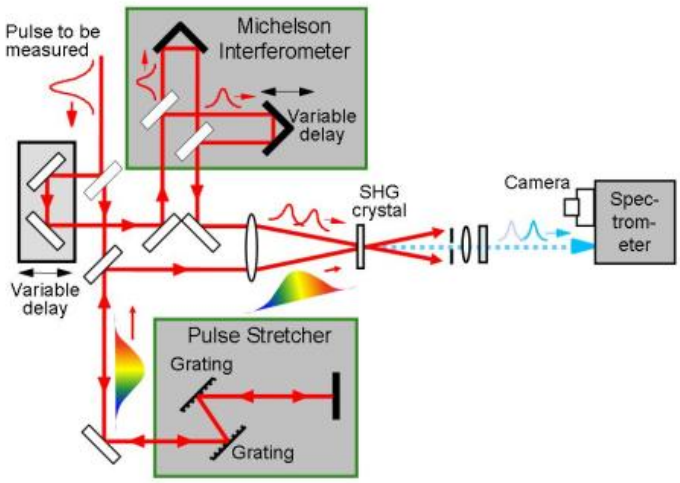

Fig. 4.6 SPIDER set-up and illustrative retrieval (ackowledged from www.swampoptics.com/tutorials_spider.htm).

Experimentally, as shown in Figure 4.6, the spectral shearing of the pulse is achieved by combining two properly conditioned beams within a nonlinear crystal such that the resulting sum or difference signal comprises a spectrally sheared pulse pair. The first beam consists of a pair of identical pulses, separated by a known time delay τ. The second beam consists of a highly chirped pulse. The amount of chirp added to this pulse is dependent upon two conditions. First, to ensure the pair of pulses in the first beam successfully interacts with the chirped pulse, the duration of the chirped pulse must be much longer than τ. Secondly, the chirp must be large enough to ensure that when the two beams mix each of the paired pulses mix with a different frequency in the chirped pulse. This procedure results in that each pulse emerging from the mixing crystal has a different centre frequency (sheared spectrum). By measuring the spectrum from the output of the nonlinear crystal, the SPIDER interferogram is acquired. To ensure the sampling rate is above Nyquist limit the value of τ must be chosen appropriately. Also, the amount of spectral shearing must be carefully controlled to ensure the Whittaker-Shannon interpolation theorem (Goodman, 1988) is satisfied. Importantly, if the shearing is too small or too large, phase measurement

will be incorrect and this difficults the generalization of the setup for any type of input pulse with completely unknown dispersion.

It was not until recently (Radunsky, 2006) that a simplified optical arrangement of SPIDER with more relaxed conditions was reported to overcome this limitations: Long Crystal – SPIDER (LX-SPIDER) as shown in Figure 4.7.

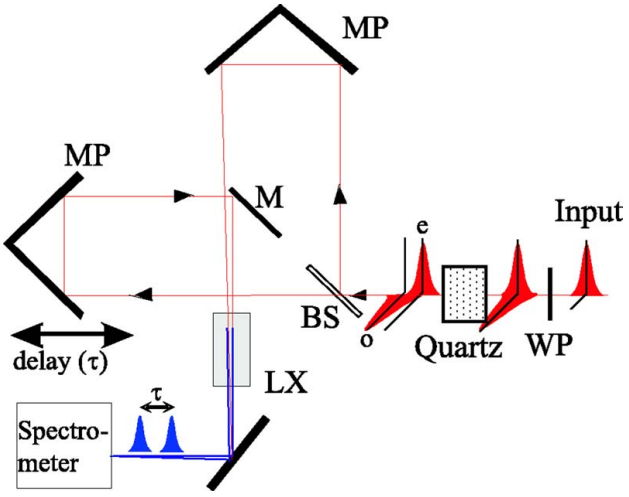

Figure 4.7 Scheme for Long Crystal – SPIDER. WP, half-wave plate; BS, beam splitter; M, mirror; MP, mirror pair; LX, crystal. (figure acknowledged from Radunsky 2006).

However, the arrangement still remains complex if compared with time-frequency techniques such as FROG. This importantly limits the range of applications.

Importantly, SPIDER has been successfully demonstrated with sub-6 fs pulses from Ti:sapphire lasers, compressed pulses from an amplifier system (Gallman, 1999, 2000; Schenkel 2003; Yamame, 2003) and optical parametric amplifiers (Dorrer, 1999a).

4.2.3.3 Retrieval algorithm of SPIDER.

To retrieve the phase information of the SPIDER interferogram, Eq. 4.4, Fourier filtering allows recovering the modulated phase signal of the cosine:
$\phi(f_c + \Omega) - \phi(f_c) + 2\pi f_c \tau$. The linear term can be removed by measuring a prior calibration interferogram that has no spectral shearing by simply blocking the chirped pulse.
By using concatenation (Zavelani-Rossi, 2001), the sampled spectrum phase at intervals Ω across the pulse spectrum can be calculated. Straightforward Fourier transform of the Spectrum and phase of the pulse allows computing the temporal intensity distribution of the pulse.

One of the major advantages of SPIDER is that it relies on directly measuring the pulses. Direct measurements are assumed to require low computational load to the processing units because no iterative algorithm is employed. Typically, acquisition speed is only limited by the readout speed of the CCD array used in the spectrograph. Acquisition and reconstruction rates of up to 20 Hz have been demonstrated (Shuman, 1999), which makes SPIDER an ideal online tool for aligning complex femtosecond laser systems. SPIDER can also be used in combination with pulse shapers (Baum, 2002).
Although SPIDER is an excellent technique there are a few fundamental disadvantages associated with it. The main disadvantage of SPIDER is its lack of major checking capability, in contrast to the Time-frequency in which marginal analysis might be utilized to seek for systematic errors. Consequently, SPIDER measurements are solely relying on the calibration of the optical arrangement, which is prone to errors. Dorrer et al. (Dorrer, 1999b) suggested few techniques for improving SPIDER calibration by measuring interference fringes at different pulse delays. Less data points also makes SPIDER more susceptible to noise. Anderson et al. studied SPIDER behaviour under noise (Anderson, 2000). They found that additive noise of an SNR=10dB the pulse shape could be recovered with an accuracy of 1.5%. Averaging of several

interferograms was suggested as a solution, at expenses of lower update speeds.
The second major disadvantage of SPIDER is the flexibility. Nyquist and Whittaker-Shannon sampling theorems are required and they have to be considered and altered for different pulses. This carries two problems: first, SPIDER requires some *a priori* knowledge on the pulse, which can be solved by using either an autocorrelation or FROG; second, if the pulse varies while measuring with SPIDER the amount of spectral shearing and pulse delay τ will require to be modified accordingly. Thus, the optical set-up will need to be re-callibrated.
As an overall, the SPIDER technique is based on interference, which is a delicate process that demands perfect alignment and this is quite difficult in different experimental circumstances. This is why SPIDER is currently demanding more complex algorithms. This has evolved into the utilization of wavelet transform that is more reliable for highly structured pulses at expenses of computational cost (Deng, 2005; Reolon, 2006; Bethge, 2007). A fast and robust algorithm should allow to be used by non-experts but this is still under development (Bethge, 2007).

4.2.4 Other techniques.

4.2.4.1 Introduction.

Although it is possible to measure a wide variety of ultrashort pulses all current techniques present certain limitations and there is no ideal or general method. Therefore, new techniques have been developed since the beginning of this thesis.

4.2.4.2 IFROG.

Developed by Günter Steinmeyer, Interferometric FROG (Stibenz, 2005) is based on a collinear FROG measurement. The full expression of a

collinear measurement is extensively developed in the subsequent chapter and the first set-up proposed by Steinmeyer can bee seen in Fig.4.8.

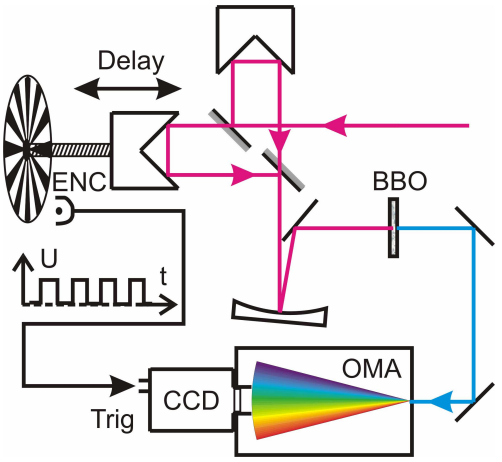

Figure 4.8 IFROG scheme (figure acknowledged from Stibenz 2005).

IFROG also utilizes the FROG algorithm but extracts information differently. First, it acquires a collinear measurement, which contains delay dependant fringes (as will be explained in detail in the following section), in a similar manner to what occurs between IA and IAC autocorrelations. In this line, IFROG demodulates the information coded around the fundamental-delay frequency to make the algorithm converge. This trace is not symmetric and this has some advantages for ensuring convergence and avoiding ambiguities. IFROG also uses the PCGPA in the step 6, presented above in section 4.2.2 and therefore is more computationally demanding than other direct measurements like SPIDER.

4.2.4.3. VAMPIRE.

Very Advanced Method of Phase and Intensity Retrieval of E-fields (Seifert, 2004; Hause, 2007), VAMPIRE, is a sophisticated optical arrangement and new algorithm for FROG to thoroughly retrieve the

phase information ultrashort pulses as mentioned in section 4.2.2. The existence of this technique follows from a work focused on studying the nontrivial ambiguities of typical FROG measurements.

Seifert et al.performed a careful study on "Nontrivial ambiguities for blind FROG and the problem of uniqueness" (Seifert, 2004), which was an issue of major concern for certain applications such as molecular dynamics studies. In order for the algorithm to fail or stagnate, mostly it is sufficient, that the FROG trace is close to a trace with exact or approximate ambiguities.

They conclude that a unique reconstruction of the pulses requires the knowledge of the pulse spectra and a non-centrosymmetric blind FROG trace. Furthermore, they showed that one necessary but not sufficient condition for the blind FROG uniqueness is to make sure that the spectral intensities of the two fields are distinguishable.

Therefore, a possible solution to the pulse retrieval ambiguities of the SHG FROG trace is to transform it into a non-centrosymmetric blind FROG trace. This method seeded by Seifert in 2004 was experimentally shown in 2007 to measure the phase structure of soliton molecules (Hause, 2007). They claim that VAMPIRE is the only experimental method up to date able to retrieve the exact information, as they needed for that purpose. However, this remains to be fully shown and they only compare it with FROG.

The proposed experimental set up to fulfil the requirements of a non-centrosymmetric blind FROG trace with distinguishable spectra and therefore unique solution is shown in Fig.4.9. However, the proposed setup is much more complex than typical SHG FROG arrangements.

VAMPIRE also provides a different procedure from commonly used iterative algorithms. VAMPIRE treats the spectrogram locally, not globally. This provides the means to check every single row of the trace for stagnating behavior: in every Gerchberg-Saxton loop, the error between the intermediate result and the measured data is calculated. This differs from FROG, which computes the whole trace at once, and not in a row-by-row fashion as VAMPIRE does.

After several iterations, rows with a low error are kept, while those with a higher error may be discarded. Discarding questionable data is might not be a big loss since spectrograms are overdetermined. Authors further claim that by this procedure, VAMPIRE is not only guaranteed to converge, but the convergence time is reduced drastically with respect to the commonly used PCGPA (Kane, 2008).

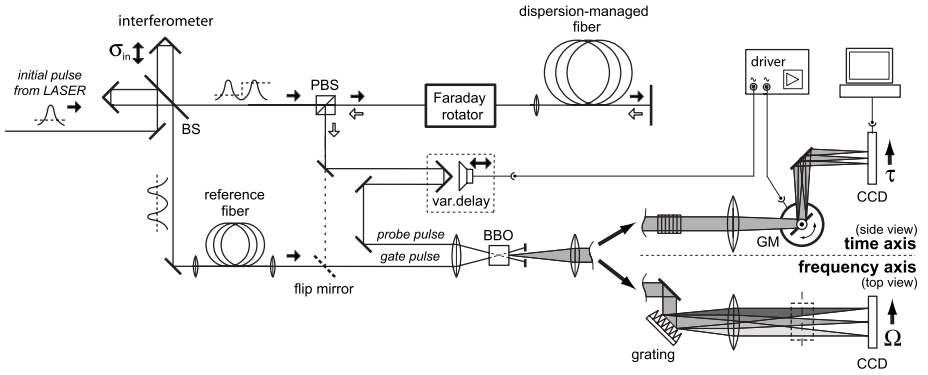

Figure 4.9 VAMPIRE scheme (figure acknowledged to Hause 2007).

This way the VAMPIRE spectrogram would contain two spectrally dispersed signals from the cross-correlations of the probe pulse with the two different components of the gate pulse so that the required non-centrosymmetric spectrogram is obtained (Seifert, 2004). In comparison to other pulse retrieval techniques, the asymmetry thus provided in the cross-correlation contains just that extra amount of information, which guarantees a unique relation between the cross-correlated pulses and the spectrogram.

4.2.4.4. MIIPS.

Multiphoton Intrapulse Interference Phase Scan (MIIPS) is analogous to the Wheatstone Bridge in electronics (which measures an unknown resistance by comparing it to known resistances), this recent method (Lozovoy, 2004; Xu, 2006) uses a calibrated phase function to directly measure the unknown phase distortions after iterative compensations.

A MIIPS-based device consists of two basic components: a pulse shaper (usually a liquid crystal based SLM), a spectrometer a nonlinear medium (like an SHG crystal) and a computer. The pulse shaper allows manipulation of the spectral phase and/or amplitude of the ultrashort pulses. The spectrometer records the spectrum of a nonlinear optical process such as second harmonic generation produced by the laser pulse. The well-known and calibrated spectral phase function is used in order to measure the unknown spectral phase distortions of the ultrashort laser pulses. Typically, the known superimposed function is a periodic sinusoidal function that is scanned across the bandwidth of the pulse.

MIIPS uses a pulse shaper that introduces a calibrated reference phase function to measure spectral phase distortions induced at the detector (see Fig. 4.10). The phase dependence of nonlinear optical processes such as second-harmonic generation (SHG) is used by the algorithm to directly measure the second derivative of the phase, this allows estimating the total phase which is introduced in the SLM and the algorithm reiterated until the error in the phase becomes irrelevant. As the reference phase is scanned, a MIIPS trace is obtained and the phase is calculated. This phase is used to compensate the pulse, via a pulse shaper, to achieve bandwidth-limited pulses.

The pulse shaper, which manipulates the spectral phase of the laser in the frequency domain, can use a programmable Spatial Light Modulator (SLM) capable of introducing arbitrary phase delay at specific spectral regions. In principle, pulse shapers can compensate any accurately measured spectral phase distortion. However, not all methods used to measure spectral phase are accurate enough, and communication between the pulse shaper and the pulse-characterization equipment is required.

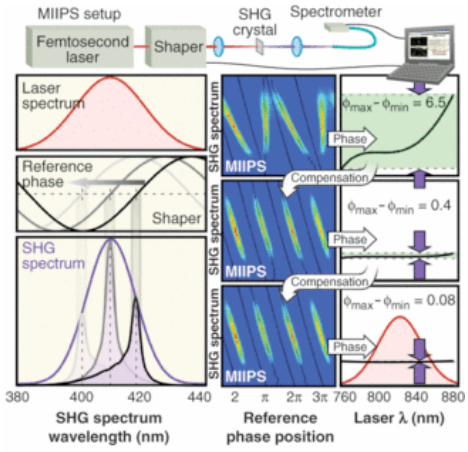

Figure 4.10 MIIPS scheme (figure acknowledged from www2.chemistry.msu.edu/faculty/dantus/UltrafastLaserOptics.html).

MIIPS is similar with FROG in that a frequency trace is collected (spectrogram) for the characterization of the ultrashort pulse. As explained above, a FROG trace is collected through scanning the ultrashort pulse across the temporal axis, and detecting the spectrum of the nonlinear process (Eq. 4.2). In MIIPS, instead of scanning on the temporal domain, a series of phase scan is applied on the phase domain of the pulse.

MIIPS takes advantage of the influence that phase modulation has on the probability of nonlinear optical processes at specific frequencies (Broers, 1992).This method has already proved to be useful for the demonstration of selective multiphoton microscopy by use of ultrashort shaped pulses (Pastrick, 2003).

It has been demonstrated not only with a thin SHG crystal, but also using surface-SHG from a silicon wafer, from KDP (potassium dihydrogen phosphate) powder located approximately 30 m from the laser (a demonstration of standoff pulse characterization), and from third-harmonic generation (THG). In all three cases, distortions below 0.1 rad are obtained across the bandwidth of the pulse without the expense and bandwidth restrictions of SHG crystals.

4.2.4.5 PRISM.

One of the last contributions reported for ultrashort pulse measurements is Phase resolved interferometric spectral modulation (PRISM; Wu, 2011) and it is based on the idea of using a phase only spatial light modulator to control the wavefront of light, which is incident on a target. Each phase element is dithered at a unique frequency. The scattered light from the target is demodulated for each modulation frequency and the phase values are extracted and used as the feedback signals to drive the phase elements such that they all interfere constructively at the target position. With a conventional 4f pulse shaper, the phase of different wavelength can be controlled. If one of the phase elements of the pulse shaper is changed from 0 to π, the pulse will become longer due to the nonconstructive interference between the out of phase wavelength and all the rest of the wavelengths at the temporal peak position. If the pulse interacts with a nonlinear medium and generates nonlinear signals, the signal strength will be lower than if all the wavelengths are in phase. If the phase of one of the wavelengths was originally φ out of phase with respect to all the rest of wavelength, adding $-\varphi$ to the out of phase wavelength with the pulse shaper can increase the nonlinear signal to the maximum value. By applying a continuous phase modulation and monitoring the nonlinear signal variation, we can determine the phase value of the out of phase element. The key difference between PRISM and many other ultrafast pulse measurement techniques is that PRISM requires no measurements of coherent nonlinear spectra like SHG. Even incoherent signals such as two-photon excited fluorescence emission can be used for PRISM. Such a property allows PRISM to be combined with multiphoton microscopy to directly use the nonlinear signal measured by a PMT to determine and compensate for spectral phase distortions inside samples.

4.3 Conclusions.

In this chapter, we have reviewed the two most important contributions for ultrashort pulse measurements: FROG and SPIDER. They are the flagship of two philosophies, time-frequency and interferometric techniques. However, these findings have been insufficient to transfer all the potential of ultrashort laser pulses beyond experienced physicists and engineers. For this reason, recent techniques have been proposed to solve particular ultrashort pulse measurement challenges: IFROG uses new terms in collinear geometry, which offers a simpler experimental setup and enables a wider range of applications and retrieves the phase information from an interferometric term; VAMPIRE solves all the ambiguities and produces experimental redundancy in the measured trace in a systematic manner that ensures accurate convergence of the trace at expenses of adding complexity to the experimental setup; and also MIIPS, which reduces the number of optical elements and uses an SLM to iteratively solve a customized spectrogram (similar to FROG) after pulse compensation until the pulse is transform limited.

All these efforts suggest that there is still a need for a general method which overcomes all the mentioned limitations, and most likely the solution lies in between time-frequency approaches and interferometric techniques, because the first family offers robust and self-callibrated solutions, whereas iterferometric techniques are fast but prone to errors.

Furthermore, the evident transdiciplinarity of the field results in new challenges where the light cannot be directly measured with some of these techniques, like multiphoton microscopy, in which light-matter interaction with living specimens offers a really exciting field for biophysicists and biomedical researchers.

In the next chapter we propose two tailored solutions for multiphoton microscopy, which aims to become a general methodology.

References

S Akturk, M Kimmel, P O'Shea, and R Trebino, "Measuring spatial chirp in ultrashort pulses using single-shot Frequency-Resolved Optical Gating," *Opt. Express* **11** pp. 68-78 (2003a).

S Akturk, M Kimmel, P O'Shea, and R Trebino, "Measuring pulse-front tilt in ultrashort pulses using GRENOUILLE," *Opt. Express* **11** pp. 491-501 (2003b).

ME Anderson, LEE de Araujo, EM Kosik, and IA Walmsley, "The effects of noise on ultrashort –optical-pulse measurement using SPIDER," *App. Phys. B-Lasers and Optics* **70** S85-S93 (2000).

A Baltuska, MS Pshenichnikov, and DA Wiersma, "Amplitude and phase characterization of 4.5-fs pulses by frequency-resolved optical gating," *Opt. Lett.* **23** pp. 1474-1476 (1998).

R Barakat and G Newsam, "Necessary conditions for a unique solution to two-dimensional phase recovery," *J. Math. Phys.* **25** pp. 3190-3193 (1984).

P Baum, S Lochbrunner, L Gallmann, G Steinmeyer, U Keller, and E Riedle. "Real-time characterization and optimal phase control of tunable visible pulses with a flexible compressor," *Appl. Phys. B* **74** S219–224 (2002).

J Bethge, C Grebing, and G Steinmeyer, "A fast Gabor wavelet transform for high-precision phase retrieval in spectral interferometry," *Opt. Express* **15** pp. 14313-14321 (2007).

B Broers, HB van Linden van den Heuvell, and LD Noordam, "Large interference effects of small chirp observed in two-photon absorption," *Opt. Commun.* **91** pp. 57-61 (1992).

JLA Chilla and OE Martinez, "Direct determination of the amplitude and the phase of femtosecond light pulses," *Opt. Lett.* **16** pp. 39-41 (1991).

KC Chu, JP Heritage, RS Grant, KX Liu, A Dienes, WE White, and A Sullivan, "Direct measurement of the spectral phase of femtosecond pulses," *Opt. Lett.* **20** pp. 904-906 (1995).

L Cohen, "Time-Frequency Distributions-A Review," Proc. IEEE **77** pp. 941-981 (1989); Time-Frequency Analysis (Prentice Hall, Englewood Cliffs, NJ, 1995).

KW DeLong, DN Fittinghoff, R Trebino, B Kohler and K Wilson, "Phase Retrieval in Frequency-Resolved Optical Gating Based on the Method of Generalized Projections," *Opt. Lett.* **19** pp. 2152-2154 (1994a).

KW DeLong and R Trebino, "Improved ultrashort-pulse-retrieval algorithm for frequency- resolved optical gating," *J. Opt. Soc. Am. A* **11** pp. 2429-2437 (1994b).

K.W. DeLong, D. N. Fittinghoff, R. Trebino, B. Kohler, and K. Wilson, "Pulse retrieval in frequency-resolved optical gating based on the method of generalized projections," *Opt. Lett.* **19** pp. 2152-2154 (1994c).

KW DeLong, R Trebino, J Hunter, and WE White, "Frequency-resolved optical gating with the use of second-harmonic generation," *J. Opt. Soc. Am. B* **11** pp. 2206- 2215 (1994d).

KW DeLong, R Trebino, WE White, "Simultaneous recovery of two ultrashort laser pulses from a single spectrogram," *J. Opt. Soc. Am. B* **12** pp. 2463-2466 (1995).

Y Deng, Z Wu, L Chai, C-Y Wang, K Yamane, R Morita, M Yamashita, and Z Zhang, "Wavelet-transform analysis of spectral shearing interferometry for phase reconstruction of femtosecond optical pulses," *Opt. Express* **13** pp. 2120-2126 (2005).

C Dorrer, B de Beauvoir, C Le Blanc, S Ranc, JP Rousseau, JP Chambaret, and F Salin, "Single-shot real-time characterization of chirped pulse amplification systems using spectral phase interferometry for direct electric-field reconstruction," *Opt. Lett.* **24** pp.1644–1646 (1999a).

C Dorrer, "Influence of the calibration of the detector on spectral interferometry," *J. Opt. Soc. Am. B* **16** pp. 1160-1168 (1999b).

C Dorrer, "Implementation of spectral phase interferometry for direct electric-field reconstruction with a simultaneously recorded reference interferogram," *Opt. Lett.* **24** pp. 1532-1534 (1999c).

L Gallmann, DH Sutter, N Matuschek, G Steinmeyer, U Keller, C Iaconis, and IA Walmsley, "Character- ization of sub-6-fs optical pulses with spectral phase interferometry for direct-field reconstruction," *Opt. Lett.* **24** pp. 1314–1316 (1999).

L Gallmann, DH Sutter, N Matuschek, G Steinmeyer, and U Keller, "Techniques for the characterization of sub-10-fs optical pulses: a comparison," *Appl. Phys. B* **70** pp. S67–S75 (2000).

J Goodman, *Introduction to Fourier Optics*. *New York: McGraw-Hill,* pp. 3-26 (1988).

A Hause, H Hartwig, B Seifert, H Stolz, M Böhm, and F Mitschke, "Phase structure of soliton molecules," *Phys. Rev. A* **75** pp. 063836/1-063836/7 (2007).

C Iaconis, V Wong, and IA Walmsley, "Direct interferometric techniques for characterizing ultrashortoptical pulses," *IEEE J. Sel. Top. Quantum Electron.* **4** pp. 285-294 (1998a).

C Iaconis and IA Walmsley, "Spectral phase interferometry for direct electric-field reconstruction of ultrashort optical pulses," *Opt. Lett.* **23** pp. 792-794 (1998b).

C Iaconis and IA Walmsley, "Self-referencing spectral interferometry for measuring ultrashort optical pulses," *IEEE J. Quantum Electron.* **35** pp. 501–509 (1999).

Y Ishida, K Naganuma, and T Yajima, "Self-phase modulation in hybridly mode-locked CW dye-lasers," *IEEE J. Quantum Electron*. **21** pp. 69-77 (1985).

DJ Kane and R Trebino, "Single-shot measurement of the intensity and phase of an arbitrary ultrashort pulse by using frequency-resolved optical gating," *Opt. Lett.* **18** pp. 823-825 (1993a).

DJ Kane and R Trebino, “Characterization of arbitrary femtosecond pulses using frequency-resolved optical gating,” *IEEE J. Quantum Electron.* **29** pp. 571-579 (1993b).

DJ Kane, G Rodriguez, AJ Taylor, and TS Clement, "Simultaneous measurement of two ultrashort laser pulses from a single spectrogram in a single shot," *J. Opt. Soc. Am. B* **14** pp. 935-943 (1997).

DJ Kane, “Real time measurement of ultrashort laser pulses using principal component generalized projections,” *IEEE J. Select. Topics Quantum Electron.* **4** pp. 278–284 (1998).

DJ Kane, “Recent progress toward real-time measurement of ultrashort laser pulses,” *IEEE J. Quantum Electron.* **35** pp. 421-431 (1999).
DJ Kane, ‘‘Principal components generalized projections: a review,” *J. Opt. Soc. Am. B* **25** pp. A120–A132 (2008).

D Keusters, H-S Tan, P O'Shea, E Zeek, R Trebino, and W. S. Warren, "Relative-phase ambiguities in measurements of ultrashort pulses with well-separated multiple frequency components," *J. Opt. Soc. Am. B* **20** pp. 2226-2237 (2003).

S Linden, H Giessen, and J Kuhl, “XFROG – A new method for amplitude and phase characterization of weak ultrashort pulses,” *Physica Status Solidi B-Basic Research* **206** pp. 119-124 (1998a).

S Linden , J Kuhl, and H Giessen, “Amplitude and phase characterization of weak blue ultrashort pulses by downconversion,” *Opt. Lett.* **24** pp. 569-571 (1998b).

VV Lozovoy, I Pastirk, and M Dantus, "Multiphoton intrapulse Ultrashort laser pulse spectral phase characterization and IV. interference. compensation," *Opt. Lett.* **29** pp. 775-777 (2004).

JW Nicholson, FG Omenetto, DJ Funk, and AJ Taylor, "Evolving FROGS: phase retrieval from frequency-resolved optical gating measurements by use of genetic algorithms," *Opt. Lett.* **24** pp. 490-492 (1999).

I Pastirk, J Dela Cruz, K Walowicz, V Lozovoy, and M Dantus, "Selective two-photon microscopy with shaped femtosecond pulses," *Opt. Express* **11** pp. 1695-1701 (2003).

J Paye, M Ramaswamy, JG Fujimoto, and EP Ippen, "Measurement of the amplitude and phase of ultrashort light pulses from spectrally resolved autocorrelation," *Opt. Lett.* **18** pp. 1946-1948 (1993).

S Prein, S Diddams and J-C Diels , "Complete characterization of femtosecond pulses using an all-electronic detector," *Opt. Comm*. **123** pp. 567 -573 (1996).

AS Radunsky, EM Kosik Williams, IA Walmsley, P Wasylczyk, W Wasilewski, AB U'Ren, and ME Anderson, "Simplified spectral phase interferometry for direct electric-field reconstruction by using a thick nonlinear crystal," *Opt. Lett.* **31** pp. 1008-1010 (2006).

DT Reid, "Algorithm for complete and rapid retrieval of ultrashort pulse amplitude and phase from a sonogram", *IEEE J. Quantum Electron*. **35** pp. 1584-1589 (1999).

DT Reid, P Loza-Alvarez, CTA Brown, T Beddard, and W Sibbett, "Amplitude and phase measurement of mid-infrared femtosecond pulses by using cross-correlation frequency-resolved optical gating," *Opt. Lett.* **25** pp. 1478-1480 (2000).

DT Reid and IG Cormack, "Single-shot sonogram: a real-time chirp monitor for ultrafast oscillators," *Opt. Lett.* **27** pp. 658-660 (2002).

J-K Rhee, TS Sosnowski, A-C Tien, and TB Norris, "Real-time dispersion analyzer of femtosecond laser pulses with use of a spectrally and temporally resolved upconversion technique," *J. Opt. Soc. Am. B* **13** pp. 1780-1785 (1996).

B Schenkel, J Biegert, U Keller, C Vozzi, M Nisoli, G Sansone, S Stagira, S De Silvestri, and O Svelto, “Generation of 3.8-fs pulses from adaptive compression of a cascaded hollow fiber supercontinuum,” Opt. Lett. **28** pp. 1987–1989 (2003).

B Seifert, H Stolz, and M Tasche, "Nontrivial ambiguities for blind frequency-resolved optical gating and the problem of uniqueness," *J. Opt. Soc. Am. B* **21** pp. 1089-1097 (2004).

T Shuman, IA Walmsley, L Waxer, M. Anderson, C Iaconis, and J Bromage, "Real-time SPIDER: ultrashort pulse characterization at 20 Hz," *Opt. Express* **5** pp. 134-143 (1999).

H Stark, “Image recovery: Theory and Application,” *Academic, Orlando, FL,* pp. 209- 212 (1987).

G Stibenz and G Steinmeyer, "Interferometric frequency-resolved optical gating," *Opt. Express* **13** pp. 2617-2626 (2005).

P O'Shea, M Kimmel, X Gu, and R Trebino, “Highly simplified ultrashort pulse measurement,” *Opt. Lett.* **26** pp. 932-934 (2001).

D Reolon, M Jacquot, I Verrier, G Brun, and C Veillas, "High resolution group refractive index measurement by broadband supercontinuum interferometry and wavelet-transform analysis," *Opt. Express* **14** pp. 12744-12750 (2006).

EB Treacy, "Measurement and Interpretation of Dynamic Spectrograms of Picosecond Light Pulses," *J. Appl. Phys.* **42** pp. 3848-3858 (1971).

R Trebino and DJ Kane, "Using Phase Retrieval to Measure the Intensity and Phase of Ultrashort Pulses - Frequency-Resolved Optical Gating," *J. Opt. Soc. Am. A* **10** pp. 1101-1111 (1993).

R Trebino, KW DeLong, DN Fittinghoff, JN Sweetser, MA Krumbügel, and BA Richman, “Measuring ultrashort laser pulses in the time-frequency domain using frequency-resolved optical gating,” *Rev. Sci. Instrum.* **68** pp. 3277-3295 (1997).

R Trebino, “Frequency-Resolved Optical Gating: The Measurement of Ultrashort Laser Pulses,” *Kluwer Academic Publishers, Boston*, pp. 101-179, (2002).

IA Walmsley and R Trebino, “Measuring fast pulses with slow detectors”, *Optics & Photonics News* **7** pp. 23-29 (1996).

IA Walmsley and C Dorrer, “Characterization of ultrashort electromagnetic pulses,” *Advances in Optics and Photonics* **1** pp. 308–437 (2009).

ZY Wang, E Zeek, R Trebino, and P Kvam, "Determining error bars in measurements of ultrashort laser pulses," *J. Opt. Soc. Am. B* **20** pp. 2400-2405 (2003).

A Watanabe, S Tanaka, H Kobayashi, Y Ishida, and T Yajima, “Microcomputer-based spectrum resolved second-harmonic generation correlator for fast measurement of ultrashort pulses,” *Rev.Sci. Instrum.* **56** pp. 2259-2262 (1985).

A Watanabe, H Saito, Y Ishida, and T Yajima, “A simple monitoring system for single subpicosecond laser pulses using an SH spatial autocorrelation method and a CCD image sensor,” *Opt. Commun.* **63** pp. 320 (1987).

T Wu, J Tang, B Hajj, and M Cui. “Phase resolved interferometric spectral modulation (PRISM) for ultrafast pulse measurement and compression,” *Opt. Express* **19** pp. 12961-12968.

B. Xu, J. M. Gunn, J. M. D. Cruz, V. V. Lozovoy, and M. Dantus, "Quantitative investigation of the multiphoton intrapulse interference phase scan method for simultaneous phase measurement and compensation of femtosecond laser pulses," *J. Opt. Soc. Am. B* **23** pp. 750-759 (2006).

L Xu, MW Kimmel, P O’Shea, R Trebino, JK Ranka, RS Windeler and AJ Stentz, ”Measuring the intensity and phase of an ultrabroadband continuum,” *Proc. Ultrafast Phenomena XII* (Charleston, SC) pp. 129–131 (2000).

K Yamane, Z Zhang, K Oka, R Morita, M Yamashita, and A Suguro, “Optical pulse compression to 3.4fs in the monocycle region by feedback phase compensation,” *Opt. Lett.* **28,** pp. 2258–2260 (2003).

M Zavelani-Rossi, G Cerullo, S De Silvestri, L Gallmann, N Matuschek, G Steinmeyer, U Keller, G Angelow, V Scheuer and T Tschudi, “Pulse compression over a 170 THz bandwidth in the visible by use of only chirped mirrors” *Opt. Lett.* **26** pp. 1155–1157 (2001).

CHAPTER 5

New methods for pulse measurements in collinear geometry

5 New methods for pulse measurement in collinear geometry.

5.1 Introduction.

Collinear geometry is often imposed in a number of cases where ultrashort pulse characterisation is required (Fittinghoff 1998, 1999). For example, in nonlinear microscopy pulse optimisation at the sample plane is required to minimise radiation and maximise the generated nonlinear signal on the biological sample (Amat-Roldan, 2004), helping to prolong the specimen's lifetime. To perform such optimisation, pulse measurement should be carried out at the sample plane of the microscope. Here, a collinear geometry is imposed since the full numerical aperture (NA) of the objective lens has to be fully filled. However, a complete measurement of an ultrashort pulse under collinear geometry has several difficulties and no robust methodology had been reported before this work, being Interferometric autocorrelation (IAC) techniques the standards at that time. IAC, is a collinear technique that is highly sensitive to phase changes. For example, The IAC has been used to measure the pulse width of sub-10-fs pulse passing through a microscope objective by assuming a Group Delay (GD) which is radius-dependent (Jasapara, 1999). However, as explained in the previous chapter (section 3.2) no quantitative information about this phase can be extracted from this type of measurements.

To fully characterise a pulse under high numerical aperture conditions, several attempts have been performed. Firstly, using a collinear geometry, and by way of type II SHG phasematching (Fittinghoff, 1998, 1999), a FROG trace had been measured. This technique requires the incorporation of $\lambda/2$ plates into one arm of the autocorrelator to cross polarize the beams so that no interference is introduced (and therefore, the interferometric fringes are eliminated). This technique however, may

be inappropriate when dealing with very short pulses (< 20 fs), as it adds extra dispersion by way of the λ/2 plates. More recently, this problem was solved by introducing a periscope for polarization rotation inside the autocorrelator (Gallmann, 2000). However, in both cases, residual interference was still present which had to be eliminated by Fourier filtering the trace. All these (λ/2 plates, periscope for polarization rotation and Fourier filtering) added complexity to the technique.

Our approach for fully characterising ultrashort pulse is based on a collinear interferometer (Michelson, Mach-Zender,…), a nonlinear medium and a spectrometer as seen in Fig.5.1.

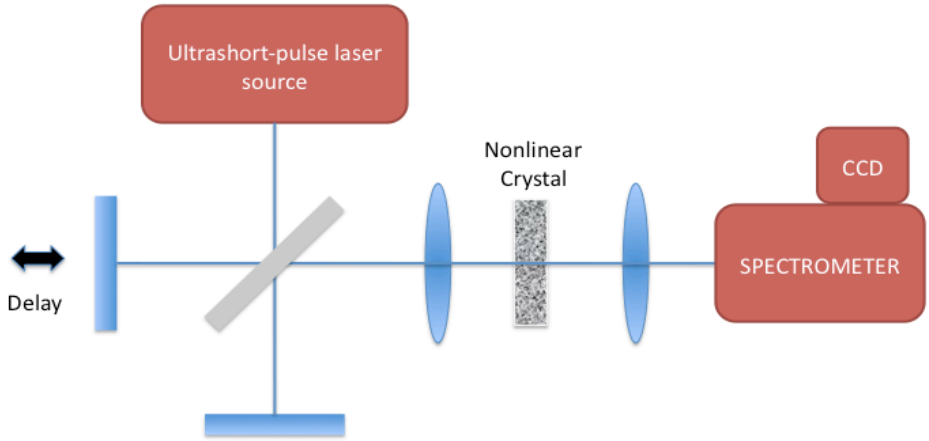

Fig. 5.1 Our collinear setup is based on a spectrally resolved collinear autocorrelator: collinear interferometer, nonlinear medium and a spectrometer.

By using this arrangement, it is possible to obtain a collinear (interferometric) spectrogram that contains the typical information of the known FROG spectrogram plus some other features that will be discussed later.

The full mathematical expression of the collinear spectrogram is presented bellow and subsequent sections of this chapter show its utility. Most importantly, this approach was the first general method to fully

characterize an ultrashort pulse at the focus of a multiphoton microscope (Amat-Roldan, 2004b) when this experiment was done in 2004.

5.2 Analysis of the collinear image.

The purpose of this section is to analytically show the wealth of information embedded into an SHG-based Collinear-FROG (CFROG) trace. In the subsequent sections, it will also bee shown how to classify the different pulse retrieval methods that can be simultaneously utilized/extracted with this type of collinear measurement.

We define the complex electric fields as

$$\hat{E}(t) = E(t)\exp\left(j2\pi f_0 t\right) \tag{5.1}$$

where *E(t)* is the slowly-varying amplitude and f_0 is the optical carrier frequency. The quadratic response of two pulses interacting in the nonlinear medium after the interferometer is given by

$$\left(\hat{E}(t) + \hat{E}(t-\tau)\right)^2, \tag{5.2}$$

Note that, when using the non-collinear geometry, it is experimentally possible to retain only the information of the required cross-term by:

$$\hat{E}(t)\hat{E}(t-\tau). \tag{5.3}$$

In this case, the SHG-FROG trace is an intensity autocorrelation that has been frequency-resolved and sampled within a delay-frequency grid. Thus, its general expression as a function of the input pulse $\hat{E}(t)$, is obtained using Eq. 5.3 as (Fittinghoff, 1998; Amat-Roldan, 2004; Tomlinson, 1984):

$$I_{FROG}^{SHG}(\tau, f) \propto \left| \int_{-\infty}^{\infty} \hat{E}(t)\hat{E}(t-\tau)\exp(-j2\pi f t)dt \right|^2 \tag{5.4}$$

This expression, however, does not apply for a collinear geometry. Thus, in order to obtain a general expression of the CFROG trace we need to use the most general expression based on Eq. 5.2:

$$I_{CFROG}^{SHG}(\tau, f) \propto \left| \int_{-\infty}^{\infty} \left(\hat{E}(t) + \hat{E}(t-\tau)\right)^2 \exp(-j2\pi f t)dt \right|^2 \tag{5.5}$$

It is clear from this expression that the CFROG trace resolves, in frequency, the whole quadratic response of the medium. By expanding the above expression it will be possible to establish the relations between the FROG trace and the collinear approach as explained below. The expanded collinear term, Eq. 4.2, can be grouped in three major terms: $\hat{E}^2(t)$, which represents the pulse interacting with itself; $\hat{E}^2(t-\tau)$, which represents the delayed pulse interacting with itself; and $\hat{E}(t)\hat{E}(t-\tau)$, the cross term, which represents the pulse interacting with the delayed pulse (FROG term). By Fourier analysis, Eq. 5.5 can be written as the addition of four terms occurring at different delay-frequencies:

$$I_{CFROG}^{SHG}(\tau,f) \propto \begin{array}{c} 2I^{SHG}(f) + \\ +2I^{SHG}(f)\cos\left(2\pi\left(2f_0+f\right)\tau\right) + \\ +4\,\mathrm{Re}\left\{\left(E^{SHG}(f)\right)^{*} E_{FROG}^{SHG}(\tau,f)\left(\exp(-j2\pi f_0\tau)+\exp\left(j2\pi\left(f_0+f\right)\tau\right)\right\}+ \\ +4I_{FROG}^{SHG}(\tau,f) \end{array}$$

(5.6)

in which

$$E^{SHG}(\tau,f) \propto \int E^2(t)\exp\left(-j2\pi ft\right)dt \qquad (5.7)$$

where $I^{SHG}(f) \propto \left|E^{SHG}(f)\right|^2$, and

$$E_{FROG}^{SHG}(\tau,f) \propto \int E(t)E(t-\tau)\exp\left(-j2\pi ft\right)dt \qquad (5.8)$$

where $I_{FROG}^{SHG}(f) \propto \left|E_{FROG}^{SHG}(f)\right|^2$.

The two first terms in Eq. 5.6 correspond to the intensity resulting from the linear interference between the SHG of the pulse and the delayed one. In particular, the first term, corresponding to the SHG intensity of both the delayed and non-delayed pulses, is related with the inherent background in an IA. The second term contains the exact same background information but modulated by $2f_0$ in the delay-frequencies and is the cross term of the interference between the two SHG pulses. The third term, modulated at f_0 is obtained from the interaction between the SHG field given by Eq. 5.3 and the SHG of the two individual pulses. Finally, the last term carries the SHG-FROG information that can be directly used for running retrieval FROG iterative algorithm.

5.3 CFROG: removing fringes.

5.3.1 Introduction.

Previous section shows the analytical structure of an SHG CFROG. Importantly, it demonstrates that the spectrogram utilized by the FROG algorithm is contained within the collinear measurement. In this section we present a general process to convert an SHG-based collinear FROG (SHG-CFROG) trace into a conventional non-collinear SHG-FROG trace and report some of the additional features of the collinear geometry approach. This allows the use of well established algorithms for pulse retrievals, while at the same time, eliminating the problems that the previous approaches had (Fittinghoff 1998, 1999).

From the previous section, we know that the full expression of a collinear measurement and is then straightforward to observe that the last term in Eq. 5.6 is exactly the same as the measured under non-collinear conditions, and thus needs to be unwrapped for our purposes. The technique to extract the SHG-FROG term from the others is by applying a simple Low Band Pass Filtering (LBPF). This allows keeping the DC terms, which are, SHG Background and FROG trace. Because FROG trace occurs only within some time-delay (τ) near zero delay($\tau \cong 0$) and SHG Background is independent from time-delay (τ) it is possible to obtain both separately by simple algebra. Next section employs a numerical example to fully illustrate this procedure.

5.3.2 Simulation.

Within this section we show by using a simulation tool that it is possible to unwrap the non-collinear term. By carrying out this analysis we have verified the integrity of the procedure helping to show important properties associated with the collinear approach. To do that, consider the pulse of Δt = 25 fs (measured at FWHM) showing an arbitrary shape and phase shown in Fig 5.2 (a).

With this pulse, it is then possible to calculate its IA (Fig. 5.2(b)) and the resulting CFROG trace (fig 5.2(c)) in which a delay sampling according to the Nyquist limit has been applied (Oppenheim, 1975). It is important to notice that to resolve the interferometric fringes the sampling must be at a delay step $\Delta\tau_N < 1/(2f_{max}) = 1/(4f_0)$. At this point, it is important to realise that a CFROG trace is an IA that has been frequency-resolved. Therefore, by integrating the spectrogram shown in Fig 5.2(c) in frequency it is possible to recover the autocorrelation shown in Fig. 5.2(b).

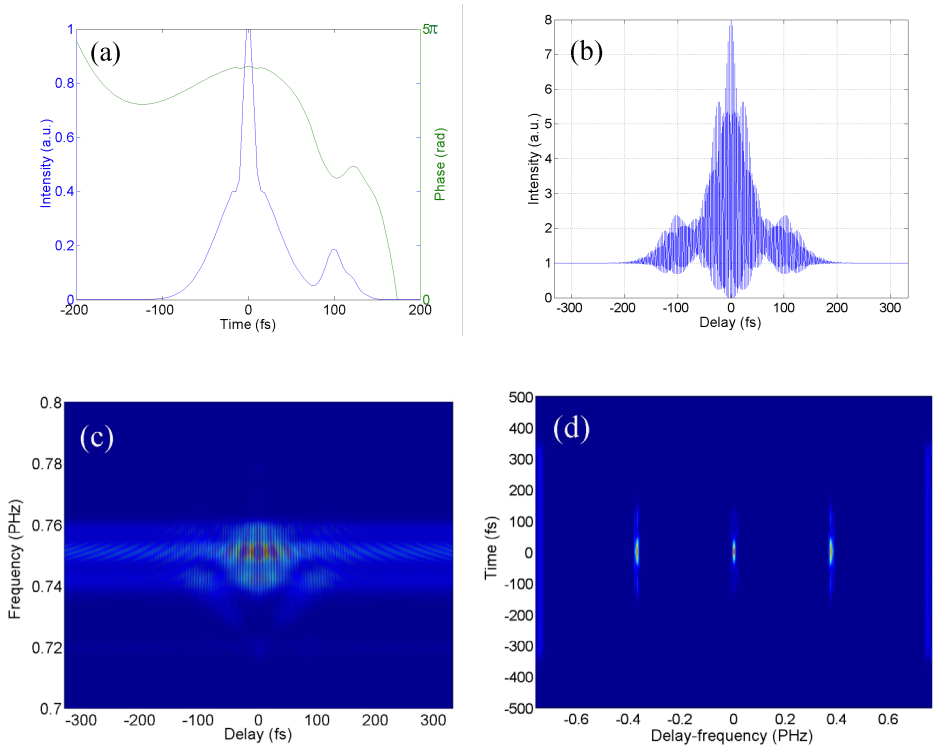

Fig. 5.2 Numerical results: (a) Multiple-pulse with cubic phase employed as input in our simulation tool (b) Interferometric Autocorrelation (c) CFROG trace (d) Fourier Transformed CFROG trace.

This allows the characteristic 8:1 ratio of an IAC to be verified during acquisition, providing a simple method to check the integrity of the measured trace in the laboratory. Importantly, this is not available with

non-collinear arrangements. Additionally, the delay axis can be self-calibrated by measuring the fringes. This enhances the detection of errors during the experimental measurement while, at the same time, helping add consistency to the acquired results. Fig. 5.2(d) shows the bidimensional Fourier transform of the acquired CFROG trace of Fig. 5.2(c), which is required to understand the procedure of unwrapping of non-collinear FROG term explained here below.

To unwrap the non-collinear FROG term we should notice that the second and third terms in Eq. 5.6, are modulated at frequencies f_0 and $2f_0$. These two terms can be removed by low pass band Fourier filtering. Fast Fourier transforming (FFT) a CFROG trace assumes periodicity in the applied direction. This is a condition that is impractical to carry out when experimentally acquiring the trace. As a consequence, an error will be introduced in the form of modulation components in the frequency direction. By using a two-dimentional Fourier Filter this error is greatly reduced. Fig. 5.2(d) reveals the two-dimensional Fourier Transform of the SHG-CFROG trace. It can be seen from this figure that a relaxed cut-off frequency for filtering can be applied without major loss of information since the interferometric terms f_0 and $2f_0$ are well separated from the DC. After filtering, the first term in Eq. (5.6), corresponding to the SHG spectrum, is the only non-desired term remaining in the CFROG trace. This overlaps with the DC term and can be easily removed by measuring it (for example by averaging from several samples at the edges of the delay axis) and then being subtracted from the trace. After all this process, the remaining DC term contains the same information as a non-collinear SHG-FROG trace and thus a conventional FROG retrieval algorithm can be employed. Fig. 5.3(a) and (b) show the filtered CFROG trace and the numerically generated non-collinear FROG trace, respectively. An excellent agreement between both traces can be observed. This is confirmed with an RMS G-Error between the two traces being $G = 2.7 \cdot 10^{-7}$. Finally, the need of a two-dimensional filtering is highlighted by comparing this result with that obtained when using a one-dimensional Fourier filtering. In this case, a much larger G-Error (G_{1D}), is obtained, having a value of $G_{1D} > 10^{-2}$.

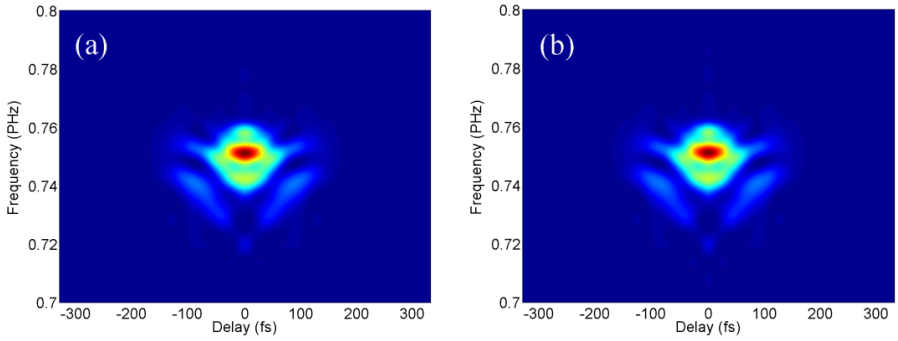

Fig. 5.3 Results: (a) filtered CFROG trace (b) FROG trace. $G=2.7\cdot10^{-7}$.

This simulation has shown that it is possible to obtain SHG-FROG traces under collinear geometry for complex pulses. This allows for full pulse characterization for a broader range of cases hence, extending the usefulness of the FROG technique. This includes not only pulse characterisation under high numerical apertures, but also the possibility of characterising very short pulses ($\Delta t < 20$ fs) using a type I SHG phasematching.

5.3.3 FAST-CFROG: Sampling strategy.

It should also be noted that when dealing with such short pulses, just a few points are required when sampling at the Nyquist limit and, as a consequence, it is possible to acquire the trace quickly. For example, obeying Nyquist, a Ti:sapphire laser at 800nm will require a delay step of $\Delta\tau < 0.66$ *fs*. For unchirped 10 *fs* pulses only about 80 data points are needed. However, for pulses that include a large number of optical cycles, i.e. 100-*fs*, over 800 data points would have to be acquired. This, therefore, generates a large and clumsy data set that is both difficult and time consuming to acquire and analyse.

The possibility to overcome the Nyquist limit will result in a faster measurement. To do this, we need to realize that we do not need to resolve the interferometric fringes as the algorithm only uses the DC

term. If however undersampling is carried out both the acquisition and data processing time can be significantly reduced without major loss in accuracy. In what follows we will describe a methodology to carry out this undersampling. We must first notice that the use of undersampling in the delay-frequency (or k-domain) causes frequencies above the Nyquist limit (B_N) to shift to lower frequencies (Oppenheim, 1975). For instance, a component $k > B_N$, will be shifted to a new frequency given by:

$$k' = k - nk'_{span} \qquad (5.9)$$

where n is an integer and $k' = 1/\Delta\tau$ is the total span of the k'-domain. In order to measure an undersampled CFROG trace capable of successful filtering we consider two constraints. The first constraint is to choose an appropriate delay step ($\Delta\tau$) to avoid frequency overlapping of the interferometric terms with the DC-FROG component. To achieve this, the shifted frequencies must be as far away as possible from the DC term ($k'=0$). From Eq. 5.6, it is possible to demonstrate that this optimal situation occurs when f_0 is shifted to $\pm k'_{span}/3$ and $2f_0$ to $\pm mk'_{span}/3$. Given this, the optimum delay step is:

$$\Delta\tau = \frac{n \pm \frac{1}{3}}{f_0} \qquad (5.10)$$

Even if the condition in Eq. 5.10 is satisfied, overlapping of the delay-spectral components can still occur for very large undersampling. To avoid this from happening, we need to ensure that the delay step in Eq. 5.10 is not too large, thus the following restriction needs to be imposed:

$$\Delta\tau < \frac{\tau_{IA}}{10} \qquad (5.11)$$

where τ_{IA} is defined as the full width at 15% of the maximum of the IA trace. This condition is equivalent to using more that 10 samples within the trace envelope. For simple well behaved bell-shaped pulses, this condition has been proven to work fine without loss of accuracy. However, to retain high frequency components within more complex pulses, a larger number of sampling points may be required.

The second constraint is used to define a sufficient delay span τ_{span} to give negligible error:

$$\tau_{span} = \frac{1}{\Delta k} \geq 2\tau_{IA} \qquad (5.12)$$

From Eq. (5.11-5.12), we obtain a criterion that recommends a minimum of 20 spectra.

In summary, using Eq. 5.10 with the restriction in Eq. 5.11 ensures that the distribution of the interferometric terms is sufficiently far away from DC term. In addition, Eq. 5.12 helps define a sufficient delay span for an accurate acquisition. Thus, a flexible and robust undersampling criterion is proposed to allow fast-CFROG retrieval.

The following section shows an experiment that answers two important issues: (1) does it work? and (2) which is the amount of error introduced by undersampling? can it be neglected?

5.3.4 Experimental results.

To further test this technique, we compared two experimentally acquired traces. One trace was obtained as a conventional non-collinear FROG trace while the other one was obtained by filtering an undersampled CFROG trace. Both traces were obtained from the same laser source during a single experiment.

The pulses from a Kerr-lens mode-locked Ti:sapphire laser with average power of 1.5W, a wavelength of 800nm and a repetition rate of 76 MHz were focused into an SHG type I BBO crystal through an autocorrelator. The SHG signal was sent to a spectrograph and detected by a CCD linear array. This arrangement enabled us to obtain a SHG-FROG trace and SHG-CFROG trace under very similar conditions. The delay step of the CFROG trace was fixed at $\Delta\tau = 1.76\ fs$, and it was estimated that $\tau_{IA} \approx 450$ fs (thus $\tau_{span} = 900$ fs). We first collected the data under a collinear geometry. Fig. 5.4 shows (a) the collinear measurement and (b)

the two-dimensional Fourier Transform of it. Also, in figure 3.4(c), we plot the IA obtained by integrating the CFROG trace showing that the characteristic 8:1 ratio can be checked even under undersampling conditions.

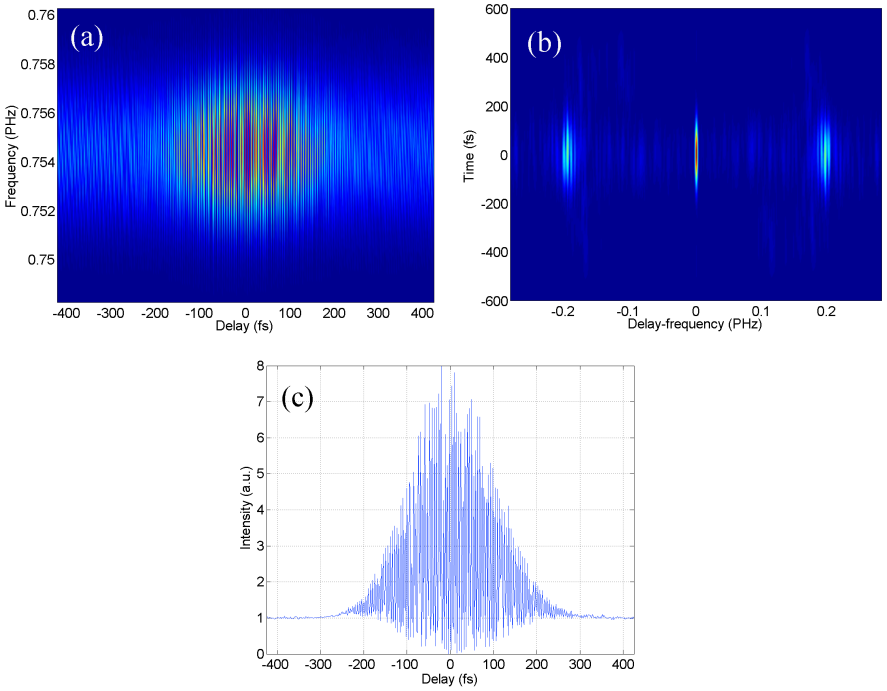

Fig. 5. 4 (a) Measured CFROG, (b) fourier transformed CFROG and (c) measured IA with a delay step of 1.76 fs and 512 samples.

We then proceeded to perform the background subtraction and Fourier filtering to the CFROG trace. The fully filtered CFROG trace can be seen in Fig. 5.5(a). Without stopping the laser, we changed to a non-collinear geometry. The resulting FROG trace is shown in Fig. 5.5(b).

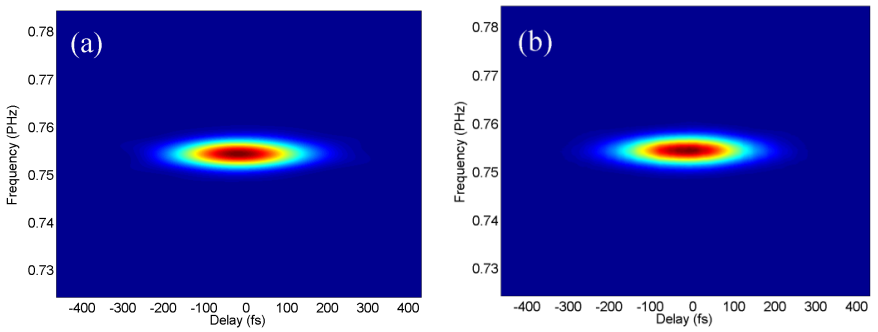

Fig. 5. 5 (a) filtered FAST-CFROG trace and (b) FROG trace. $G=3.9\cdot10^{-6}$.

We demonstrated the effectiveness of this technique by comparing both traces and computing the G error. For this reason, it was necessary to interpolate the FROG trace to obtain the same delay step of 1.76 *fs*. Excellent agreement is observed between the two traces (Fig. 5.5), where $G = 3.9\cdot10^{-6}$. To further check this result, time and frequency marginals for both traces have been calculated. Fig. 5.6 shows a comparison of such marginals where again very good agreement is obtained.

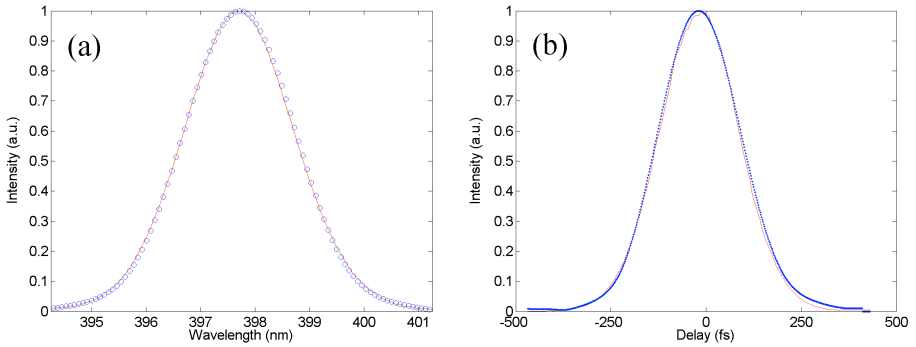

Fig. 5. 6 (a) Spectral marginal from the filtered CFROG trace (blue circles) and FROG trace (red line); (b) Intensity autocorrelation (delay marginal) from the filtered CFROG trace (blue dots) and the FROG trace (red line).

From figure 5.6, we can confirm that both traces are equivalent and that running the FROG retrieval algorithm with any of the traces shown in Fig. 5.5, will retrieve the same pulses.

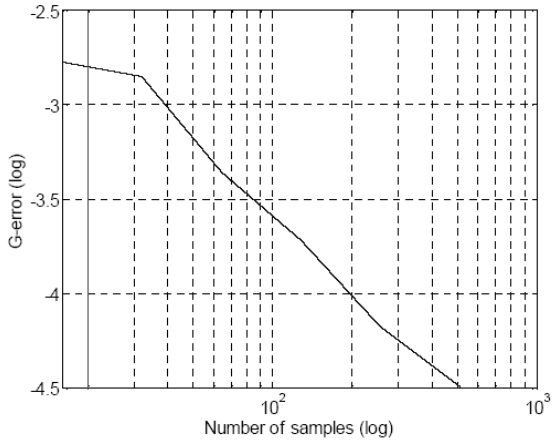

Figure 5.7 G-error as function of number of spectra (from 16 to 512) per trace.

In order to investigate the effect that undersampling has upon the experimentally acquired CFROG trace, we proceeded to resample our CFROG trace of Fig. 5.4(a) to a lower number of points (N). Thus traces of N = 256, 128, 64, 32 and 16 samples were generated from the original (N = 512 sampled) trace and the according G-error calculated as shown in Fig. 5.7. This is equivalent to increase the $\Delta\tau_I$ in powers of two for each case. Even for the highest sampling rate (N = 16), we obtained a relatively low error of $G = 1.6 \cdot 10^{-3}$. This sampling rate is below our sampling limit (Eq. 5.10 - 5.12), but as previously mentioned, for well-behaved pulses our criteria may be relaxed.

5.4 MEFISTO: direct pulse measurement.

5.4.1 Introduction.

Time-frequency techniques based on acquiring spectrograms generally allow for analysis that immediately detects systematic errors. They, however, rely on the acquisition of many data points as well as an iterative retrieval algorithms (Kane, 1998) to recover the pulse information. In contrast, interferometric techniques (Iaconis, 1998a, 1998b) offer direct phase measurement without the need for retrieval

algorithms or the collection of large data sets. As a consequence, pulse characterization can be carried out in real time (Shuman, 1999). Interferometric techniques, however, do not have a stringent error-checking capability and they normally rely on a pulse-specific optical arrangement. In this section, we describe MEFISTO (Measurement of Electric Field by Interferometric Spectra Trace Observation) as a new and important general methodology, based on Fourier analysis (Amat-Roldan 2004a, 2004b), which allows the phase of an unknown pulse to be analytically obtained. Furthermore, this novel method helps to bring together time-frequency and interferometric techniques while maintaining the robust error-checking capability of the time-frequency approaches and discarding some of their negative attributes. In addition MEFISTO requires only a simple collinear autocorrelator whose output is spectrally resolved as a function of delay as shown in Figure 5.1.

5.4.2 Theory of MEFISTO.

To understand MEFISTO, consider a pulse interacting collinearly within a nonlinear crystal, after passing through an autocorrelator. The second harmonic generated signal is then directed to a spectrograph to obtain an interferometric trace in terms of the time-delay τ and the frequency f. An experimental example of such a trace can be seen in Fig. 5.2(c). The resulting trace can be mathematically described as in Eq 5.6 of this chapter.
The main difference of MEFISTO with SHG-FROG is that all the cross-terms in are retained and, as we will show below, with the new information carried on these terms it will be possible to analytically obtain $E(t)$.

In order to do this, we first calculate the Fourier transform of Eq. 5.6 in the τ axis, $Y^{SHG}(f,\kappa) = F_{\tau}\left\{I^{SHG}(f,\tau)\right\}$. The resulting expression consist of 5 main spectral components (see Fig. 5.2(d)) at frequencies DC, $\pm f_0$

and $\pm 2f_0$. Since the interferometric trace (Fig. 5.2(c)) is symmetric and real, the negative spectral components are real and equal to the positive ones (see Fig. 5.2(d)). Therefore, to analyze the information enclosed in the transformed trace, we only need to focus on the positive frequency components. Each of these terms carry information of the pulse phase and intensity and their use will depend on the particular experimental conditions (Amat-Roldan, 2004).

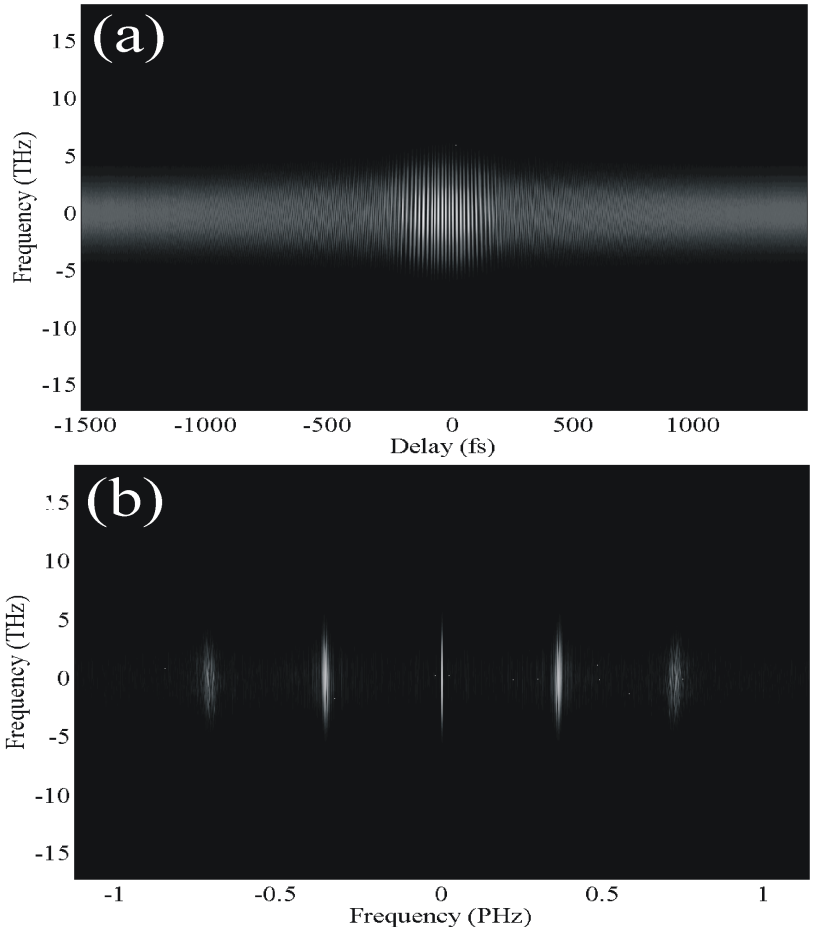

Figure 5. 8 a) Frequency resolved collinear autocorrelation. b) Same trace in the Fourier domain (For clarity, intensity scale is not linear).

Here, we focus on and analyze $Y^{SHG}(f,\kappa)$ at $\kappa \approx f_0$, the most interesting term of the spectral components for this section due to its asymmetry and

potential wealth of phase information which will be exploited by MEFISTO. In order to extract such information, we rewrite this spectral component as,

$$Y^{SHG}_{\kappa\approx f_0}(f,\kappa) = 2E^{SHG}(f)E^{*}(f+f_0-\kappa)E^{*}(\kappa-f_0)+\text{c.c.} \tag{5.13}$$

where $E^{SHG}(f)=\int df' E(f')E(f-f')$ and $E(f)=F_t\{E(t)\}$. Using equation (5.13), it is possible to determine $E(t)$ in an analytical way. To show this, we write the spectral component of the complex electric field in polar form, $E(f)=U(f)\exp\left(j\phi(f)\right)$. Then equation (5.13) can be written as

$$Y^{SHG}_{\kappa\approx f_0}(f,\kappa) = \begin{array}{c} 4U^{SHG}(f)U(f+f_0-\kappa)U(\kappa-f_0)\times \\ \cos\left(\phi^{SHG}(f)-\phi(f+f_0-\kappa)-\phi(\kappa-f_0)\right)\end{array} \tag{5.14}$$

Under typical lab conditions, the spectral amplitude of the fundamental pulses, $U(f)$, and of the corresponding second harmonic, $U^{SHG}(f)$ are known. Therefore, the only unknowns in equation (5.14) are the spectral phases of the fundamental and second harmonic pulses, $\phi(f)$ and $\phi^{SHG}(f)$. Once the phases are known, the pulses are completely characterized. This can be successfully achieved by taking two different slices in the transformed space of the interferometric trace, e.g., at $\kappa = f_0$ and $\kappa = f_0-\Delta f$. Then from (5.14) we obtain:

$$\phi^{SHG}(f)-\phi(f)-\phi(0)=\pm\cos^{-1}\left(\Omega(f,\kappa=f_0)\right) \tag{5.15}$$

and

$$\phi^{SHG}(f)-\phi(f+\Delta f)-\phi(-\Delta f)=\pm\cos^{-1}\left(\Omega(f,\kappa=f_0-\Delta f)\right) \tag{5.16}$$

where we have defined, $\Omega(f,\kappa)=\dfrac{Y^{SHG}(f,\kappa)}{4U^{SHG}(f)U(f+f_0-\kappa)U(\kappa-f_0)}$.

Note that all the functions in the parameter $\Omega(f,\kappa)$ can be experimentally obtained. Then, by subtracting equations (5.15) and (5.16) we get

$$\begin{array}{c}\Delta\phi(f)=\phi(f+\Delta f)-\phi(f)= \\ =\pm\cos^{-1}\left(\Omega(f,\kappa=f_0)\right)\mp\cos^{-1}\left(\Omega(f,\kappa=f_0-\Delta f)\right)+\phi(0)-\phi(-\Delta f)\end{array} \tag{5.17}$$

This is the critical equation. Similarly to spectral shearing interferometry we directly obtain the phase increment as a function of frequency. Therefore, the actual phase is just the addition along the frequency axis:

$$\phi(f) = \sum_{f=f_1}^{f_2} \Delta\phi(f) \qquad (5.18)$$

Where f_1 and f_2 are the lower and upper bounds of the considered bandwidth of the pulse respectively. This equation is the final result of the MEFISTO method and allows the determination of the phase of $E(f)$ taking an arbitrary origin $\phi(0)$ and varying f. However, in order to use equation (5.17) there are some aspects that are worth noting. Firstly, the term $\phi(0) - \phi(-\Delta f)$ in equations (5.17) is a constant that can be decided arbitrarily. This term adds a linear phase shift that is equivalent to determining the electric field origin in time. Second, in the theoretical development, a $\cos^{-1}\Omega$ function was used and as a consequence the sign of the phase shift is not determined. This results in two possible solutions, $E(f)$ and $E^*(f)$, which is the characteristic ambiguity that also appears in FROG measurements and it cannot be resolved using schemes based on quadratic nonlinearities. Additionally, for simplicity of the analysis, we have implicitly considered that the sampling step in the f and κ axis coincides ($\Delta\kappa = \Delta f$).

5.4.3 Simulation.

In this section a number of traces are numerically computed to evaluate some aspects of the performance of MEFISTO and provide evidence of its limitations and virtues. For this, a collinear trace is computed with a transform limited pulse and with a pulse with quadratic phase at different Signal-to-Noise Ratios (SNR). Although other experimental errors might be important, like small variations in the sampled delay of the trace, this can be experimentally solved with specific setups as reported in IFROG (Stibenz, 2005).

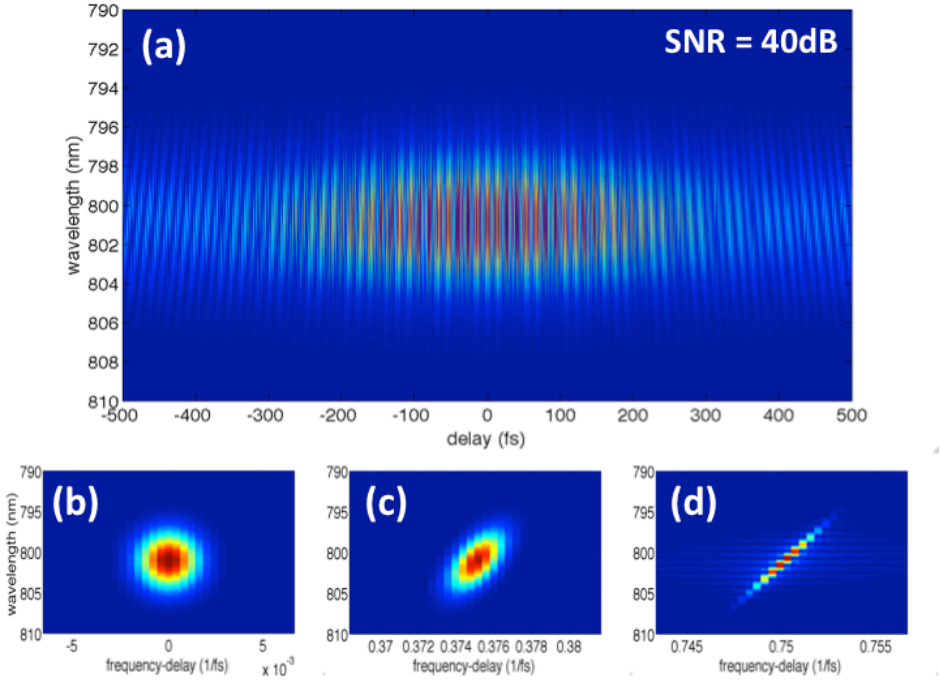

Figure 5.9. (a) Numerically simulated collinear trace generated with a transform-limited pulse with a pulse with of 94 fs acquired at SNR=40dB; (b) DC term, (c) fundamental term and (d) second-harmonic term of the delay-frequency of Eq.5.6.

Numerical traces are sampled in delay axis at $\Delta\tau = 0.6\,fs$ and a spectral resolution of 62.5 GHz (reciprocal to 16*ps*, which is about 0.133nm at 800nm. The delay span is equivalent to 2.46*ps* (reciprocal to 406.8 GHz); in this context, phase measurement will be limited by the delay span. Figure 5.9(a) shows the numerically simulated trace of the transform limited pulse, 5.9(b-d) show the DC term, the fundamental term and the second harmonic term, respectively. Figures 5.9(b-d) illustrate the different frequency resolution pointed out above 62.5 GHz for the spectrum (in the vertical axis) versus the 406.8 GHz of the frequency-delay (in the horizontal axis), in which the blocking effect of pixels is evident along the horizontal axis.

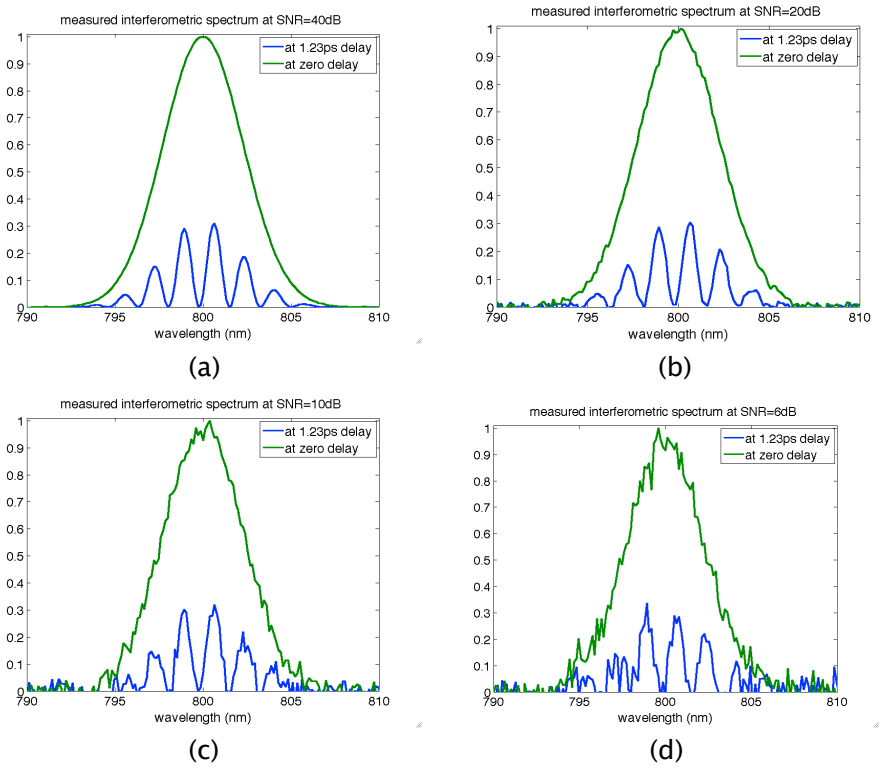

Figure 5.10. Numerically simulated spectrums form collinear trace generated with a transform-limited pulse at different SNRs: 40, 20, 10 and 10 dB for (a) to (d) respectively. Each figure contains two delays: at zero delay (green line) where SHG is maximum but highly inestable as small vibrations have strong variations and at 1.23ps (blue line) where SHG is generated by two pulses that are temporally separated. In spite of this, we still observe a strong delay dependant modulation for the SHG spectrum that shows the effects of collinear propagation.

Each trace is simulated 1,000 (one thousand) times at different signal-to-noise ratio (SNR) ratios of 6, 8, 10, 12, 14, 16 18, 20, 25, 30, 35 and 40 dB. This makes a total of 12,000 measurements to extract some exploratory conclusions.

MEFISTO measurement is performed by generating the trace, obtaining the SHG intensity spectrum from the trace and an independent measurement of the intesity of the fundamental spectrum. Figure 5.10 (a)-(d) shows the appearance of the numerically simulated spectra acquired when doing the experiment. When doing this, delays near zero

produce maximal SHG signal, but this point is highly unstable and small changes in air temperature or minimal vibrations produce destructive interference and the signal is almost gone by motions of few hundreds of nanometers. Alternatively, delay points far beyond the tails of the pulses, when interference is only produced by collinearity of both pulses, we find the SHG intensity spectrum modulated by a cosine function at a frequency proportional to the delay. These points are stable and experimentally interesting as they allow to check collinearity in a very direct manner.

Transform limited pulse

A collinear trace is numerically simulated with a gaussian pulse with a spectral FWHM of 14.4nm and transform-limited FWHM of 94 *fs* with flat spectral phase as shown in Fig. 5.9 (a) and the correspondig frequency-delay components after Fourier transforming the trace when measured at 40dB of SNR in Figs. 5.9(b-d); an example of the same trace at SNR=6dB is shown in Fig. 5.11.
Results of the simulation show that all pulses were measured at different SNRs an average phase error along the FWHM of the spectral pulse is 50mrad as shown in Fig. 5.12. Although average error is similar, 95% interval of confidence of the phase error is ten times larger at low SNR levels at ranges from 100 to 10mrad, whereas it ranges 50 to 60mrad at SNR of 40dB. This indicates that higher SNR improves repeatability of the measurement as expected.

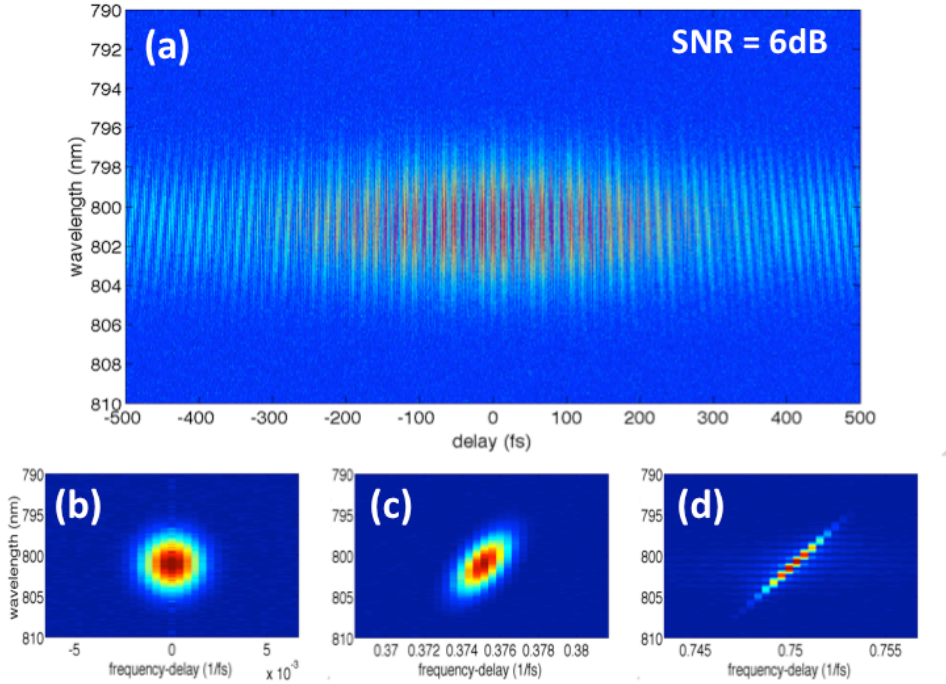

Figure 5.11. (a) Numerically simulated collinear trace generated with a transform-limited pulse with a pulse with of 94 fs acquired at SNR=6dB; (b) DC term, (c) fundamental term and (d) second-harmonic term of the delay-frequency of Eq.5.6.

It is important to notice that Fourier Transforming the trace is equivalent to average many data points of the acquired trace and, as observed in Fig.5.9(c) and 5.11(c) the fundamental term in delay-frequency is not visually affected. As the added noise is white gaussian it averages out along the trace and MEFISTO has shown nice performance under this type of experimental error.

Additionally, this phase measurement utilizes an independently measured fundamental spectrum of the pulse and it really makes a difference. Computing the fundamental from the trace is highly affected by noise and errors increase rapidly at different SNR. However, measurement of the fundamental spectrum is readily available and experimental calibration can be achieved by registering the independently measurement of the fundamental and the computed from the collinear

trace as explained in next section in Eq. 5.21. In conclusions, this differences can be overcome if proper experimental attention is paid and does not affects the fundamental basis of MEFISTO.

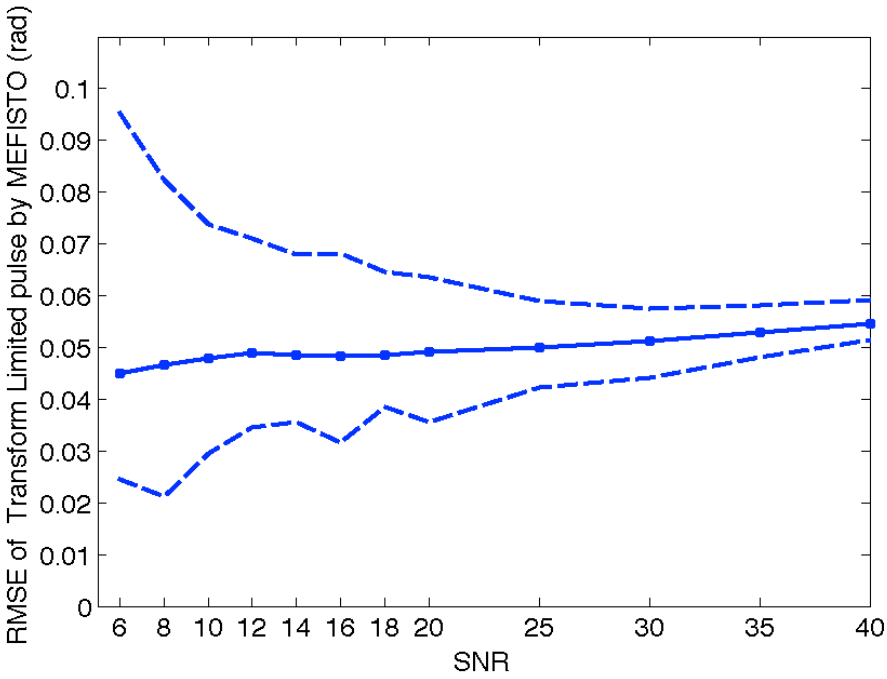

Figure 5.12 Error distribution at different SNRs. Solid line marks the median error and dashed lines mark the 95% confidence interval for the error.

Pulse with quadratic phase

Numerical simulation of a tranform-limited pulse supports specific aspects of the theoretical correctness of the MEFISTO approach. However, one of the main issues is whether it will behave well for large phase ranges, well beyond 2π where the effects of the arc cosine function may be a problem, and particularly under noisy situations. For this, the same gaussian pulse with a spectral FWHM of 14.4nm and transform-limited FWHM of 94 *fs* is now modified to account for a quadratic spectral phase of GDD=30,570 fs^2, which is equivalent to propagate the transform-limited pulse through a certain thickness as calculated below. Figure 5.12 shows the complex spectrum of the simulated pulse and

Figure 5.13 shows the comparison between the transform-limited pulse (green line) an the broadaned pulse (blue line).

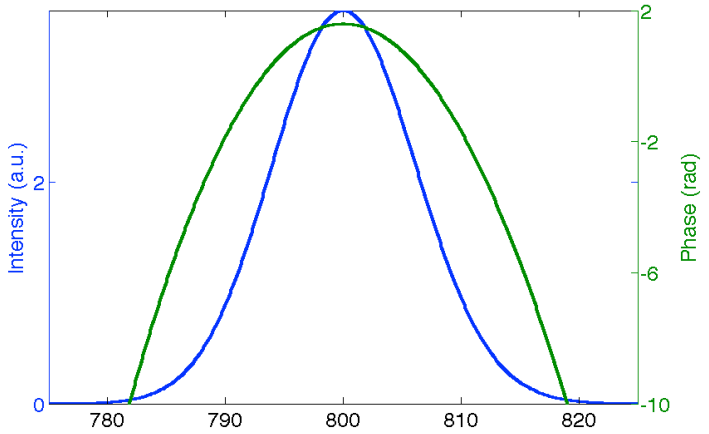

Figure 5.13 Spectral intensity (left axis) and phase (right axis) of the numerically simulated pulse.

According to Eq.1.18, the expected pulse broadening of a gaussian pulse that has propagated through dispersive media, a transform limited pulse of FWHM of 94 *fs* will be broaden to 250 *fs* after a GDD of 7,854 fs^2. As $GDD = z\,GVD$, where GVD is Group Velocity Delay of a specific dispersive material, and z is the thickness of material through which the pulse is propagated, it is possible to estimate the amount of thickness of glass or BK7 that the light has to travel in order to experience such dispersion. For example, for BK7, which has a GVD=50.6 fs^2/mm, a GDD of 7,854 fs^2 will be at z=155mm.

This numbers fit very well if we look to the numerical phase of the simulation, where $\partial^2\phi/\partial\omega^2 = 3{,}871.7\,fs^2$. From Eq. 1.16 and that GVD = $k'' = \partial^2 k/\partial\omega^2$, the second order term of the pulse phase is equal to $\frac{z}{2}\frac{\partial^2 k}{\partial\omega^2}(\omega-\omega_0)^2$ for t=0, the numerically estimated quadratic phase corresponds to a GDD = 7,743.5 fs^2, which is very similar to the gaussian approximation of Eq.1.18.

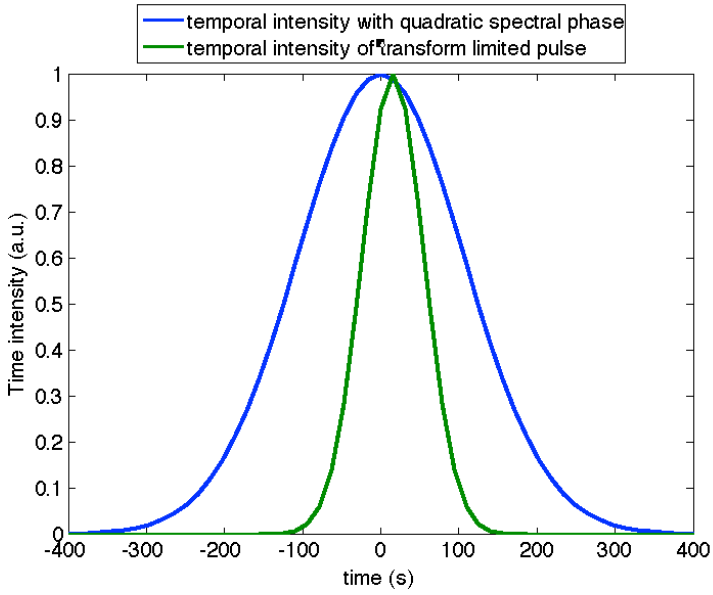

Figure 5.14. Temporal intensity of the transform-limited pulse (green line) and the broadened pulse (blue line).

Pulses with quadratic phase were automatically measured 1,000 (one thousand) times at the following SNRs in dBs: 6, 8, 10, 12, 14, 16 18, 20, 25, 30, 35 and 40. An automated and naive system to detect the change in phase direction, which we name phase-jump, produced by the arc cosine function of Eq. 5.17 was implemented in order to process in an unbiased manner all the 12,000 simulated traces. Constant and linear component of the phase was also automatically calculated and the original phase and the estimated by MEFISTO were compared.

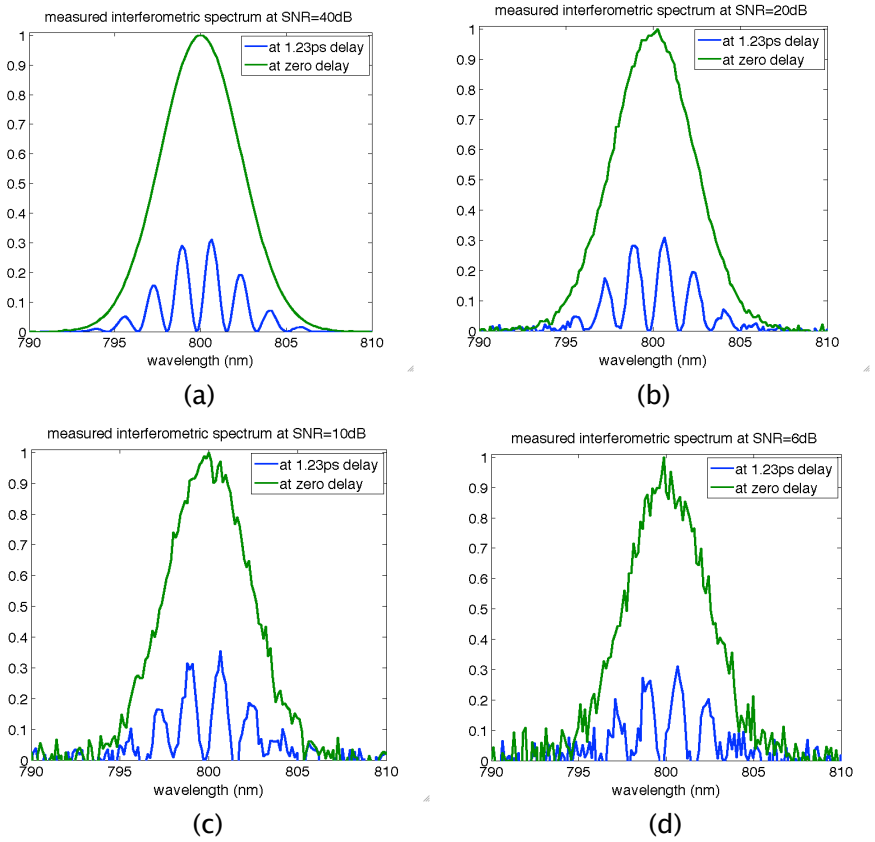

Figure 5.15. Numerically simulated spectrums form collinear trace generated with the pulse with quadratic phase (see Fig.5.13) at different SNRs: 40, 20, 10 and 10 dB for (a) to (d) respectively. Each figure contains two delays: at zero delay (green line) and at 1.23ps (blue line) where SHG is generated by two pulses that are temporally separated. In spite of this, we still observe a strong delay dependant modulation for the SHG spectrum that shows the effects of collinear propagation.

Fig. 5.16 shows the numerically simulated trace at SNR of 6 dB with the pulse shown in Fig. 5.13 and quadratic phase.

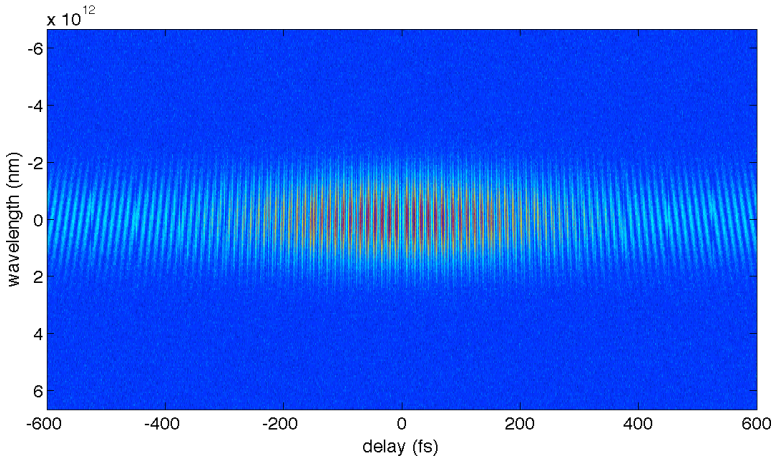

Figure 5.16. Simulated trace at SNR = 6dB and quadratic phase (pulse shown in Fig. 5.13).

Results of Fig. 5.17 show that successful MEFISTO measurement is related to the SNR of the trace. This is mostly related because noisy peaks might induce wrong phase-jumps and thus incorrect phase measurement. Reamarkably below 20dB the system seems to perform very similarly, in terms of successful measurement, that averages 10% of the traces. From 20dBs to 40dBs, successful measurement grows from 20% to almost 90% respectively.

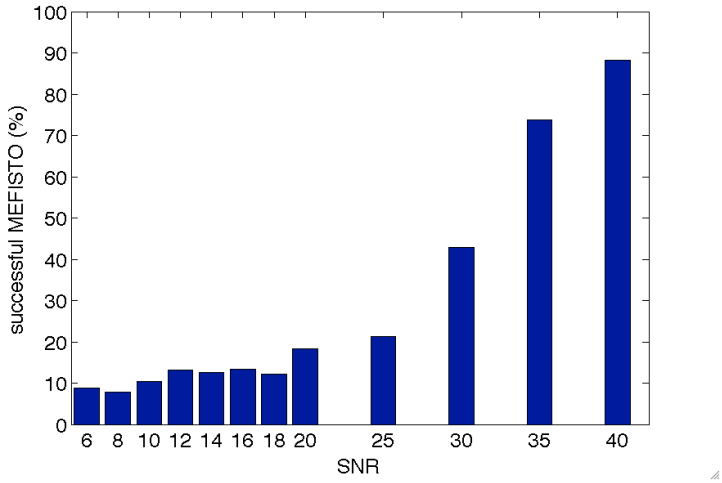

Figure 5.17. Percentage of successful MEFISTO measurement of the spectral phase out of 12,000 traces at different SNR (1000 per SNR).

However, Fig.5.18 shows the differences in terms of accuracy of the retrival. At SNR of 6dBs root mean squared error (rmse) averages almost 150mrad and the confidence interval achieves more than 350mrad, whereas at 18dBs, average rmse is below 100mrad and confidence interval is slightly below 300mrad. Remarkably, at 40dBs average rmse is below 50mrad and the confidence interval is slightly above 100mrad.

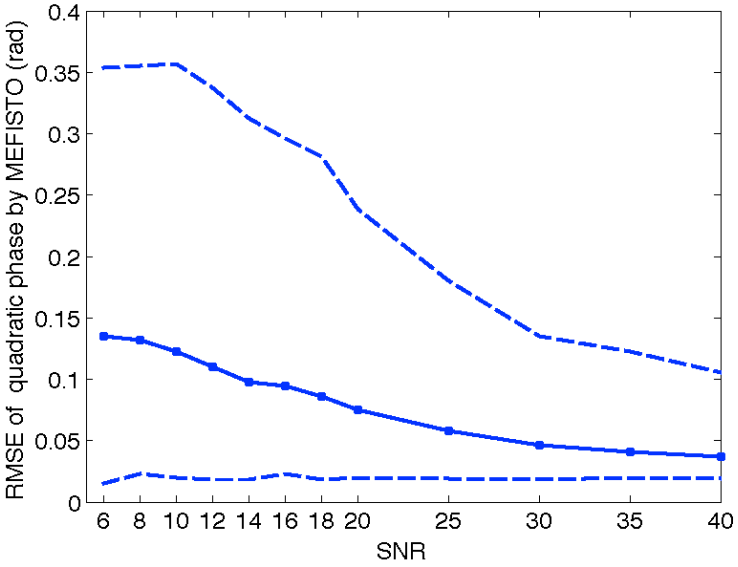

Figure 5.18. Error distribution of successful MEFISTO measurement of the spectral phase out of 12,000 traces at different SNR (1000 per SNR). Solid line marks the median error and dashed lines mark the 95% confidence interval for the error.

This results show that most critical aspects related to full automatization of MEFISTO are related to the identification of phase-jumps, the changes of phase direction, related to the use of arc cosine function of Eq. 5.17. This will be a further development for the technique to become feasible and automated for non-experts. It must be notice that this numerical simulations only use minor part of the collinear trace and compute the phase based on the information of two slices of the delay-frequency. Utilization of more slices will improve SNR and provide more information related to the phase-jumps, as continuous slices are frequency shifted and provide different parts of the phase information

with the phase-jumps at different positions. However, this requires an intensive work for development and validation.
Additional problems not evaluated here but present in the experimental section are (1) variability of the delay step (which distorts Fourier Transformation if not taken into acount) and (2) spectral calibration of the fundamental spectrum and the SHG collinear trace. However, this issues are overcome in this thesis by semi-automated means where gross correction is done automatically and fine tuning is achieved manually by checking the marginal errors, as normally done with other methodologies like FROG.
Next section, also includes other practical considerations for the utilization of the MEFISTO technique to match the units and space of the acquired data to the mathematical framework.

5.4.4 Practical considerations.

In this section I discuss important characteristics of MEFISTO that should be considered to ensure easier and successful pulse retrievals.

i) *Pulse Bandwidth.*

An important issue to consider is the maximum pulse bandwidth that MEFISTO can successfully characterize. This fundamental limit derives from the necessity to prevent overlap between the different components of the transformed trace as seen in Fig. 5.2(b). Specifically, the two slices at $\kappa = f_0$ and $\kappa = f_0 - \Delta f$ must not be affected by the tails of the $\kappa = 0$ component. In principle, this suggests that the available bandwidth could be equal to almost the bandwidth of optical carrier. However, in practice this might be affected by the particular pulse shape.

ii) *Frequency Resolution.*

In our analysis we have implicitly considered that the sampling step in the f and κ axis coincides ($\Delta\tau = \Delta f$). Initially, the frequency resolution is in fact given by the time-delay span τ_{span}, i.e., $\Delta\tau = 1/\tau_{span}$, which experimentally can differ from the spectrograph resolution. However, it is allowed to use interpolation techniques to fulfil $\Delta\tau = \Delta f$ in the case of a pulse with finite width (Oppenheim, 1975). Then, frequency resolution of the method can be extended to Δf without modifying the phase information.

iii) *Determining the fundamental spectrum and conversion efficiency parameter* χ.

In our theoretical development, we have considered all the spectral profiles to be normalized to unity at the central wavelength. An important factor that affects the determination of $\Omega(f,\kappa)$ is the effective conversion efficiency parameter χ. For pulse retrieval, the fundamental spectrum $U^2(f)$ is required and this can be directly obtained from the experimental interferometric trace. This is achieved as follows. First, the amplitude of the second harmonic pulse are obtained from the term at $\kappa = 2f_0$, resulting in

$$\sqrt{\chi}E_0^{SHG}U^{SHG}(f) = \sqrt{Y^{SHG}_{\kappa\approx 2f_0}(f,\kappa = 2f_0 + f)} \qquad (5.19)$$

By normalizing using $U_{SHG}(f=0)=1$, the spectral profile $U_{SHG}(f)$ and the factor $\sqrt{\chi}E_0^{SHG}$ needed to find χ_{eff} are obtained. Second, the term at $\tau = 0$ in the degenerate case results in

$$\begin{aligned} Y^{SHG}_{FROG}(f,\kappa = 0) &= 4\chi {E_0}^4 \int df' U^2(f')U^2(f - f') = \\ &= 4\chi {E_0}^4 U^2(f) \otimes U^2(f) \end{aligned} \qquad (5.20)$$

By using the inverse Fourier transform to deconvolve (5.20) we obtain:

$$\sqrt{\chi}{E_0}^2 U^2(f) = \frac{1}{2}F_t\left\{\sqrt{F_f^{-1}\left\{Y^{SHG}_{FROG}(f,\kappa = 0)\right\}}\right\} \qquad (5.21)$$

Here again, by normalising $U(f=0)=1$, the spectral profile of the fundamental pulse

$U(f)$ and the factor $\chi^{1/2} \cdot E_0^2$ needed to finally find χ is obtained. By not requiring an extra spectral measurement, all the data used for the pulse measurement is contained within a single set of data. This helps keep everything self-consistent and as a consequence reduces the risk of errors entering into the final results.

iii) *Spectral calibration.*

Method 1

By Fourier transforming the term modulated at the SH frequency-delay ($\kappa \cong 2f_0$) in Eq. 3.6 we can calculate the κ and f relationship. By estimating the SH frequency at each pixel of the spectrometer we can calibrate the spectrometer based on:

$$Y^{SHG}_{\kappa \approx 2f_0}(f,\kappa) = U_{SHG}(f)\delta(f + 2f_0 - \kappa) \tag{5.22}$$

This method allows calibrating the spectrometer and registering the fundamental spectrum extracted from the DC term. This is crucial for the correct phase estimation because MEFISTO is an interferometric technique and relies on accurate calibration of wavelength of fundamental and SH spectra.

Method 2

An experimental measurement, in general, requires two independent measurements: the two fundamental pulse spectra and the interferometric trace. The need for the exact determination of the f_0 and 2 f_0 places extreme demands and importance on the spectral calibration for this interferometric techniques. These demands can be relaxed significantly by evaluating equation (5.20), and using it to directly relate f_0 and 2 f_0 with one another:

By taking a convolution of the two measured fundamental spectra, an accurate spectral registration can be performed that relates the region of the fundamental spectrum with the region of the second harmonic spectrum, where the interferometric trace is obtained. This property allows the MEFISTO technique to be extremely robust against spectrometer miscalibration.

iv) *Symmetry considerations.*

We must take into account that the interferometic trace is symmetric with respect to the delay axis τ thus its Fourier transform must be real. This has two consequences. First, the upper term in the $\Omega(f,\kappa)$ functions is directly $Y^{SHG}(f,\kappa)$, where $\Omega(f,\kappa)$ now is written as

$$\Omega(f,\kappa) = \frac{Y^{SHG}(f,k)}{4\chi_{eff} U_{SHG}(f) U(f + f_0 - \kappa) U(\kappa - f_0)} \tag{5.23}$$

with $\chi_{eff} = \chi E_0^{SHG} E_0^2$. In an experimental situation, any imaginary component in $Y^{SHG}(f,\kappa)$ can be attributed to experimental errors. This is because the interferometric nature of this technique requires having a perfectly centered trace, exact delay steps, no laser instabilities, etc. In this situation, when the center of the delay axis is accurately known, the imaginary part can be omitted. This is the equivalent to the symmetrization process performed in the FROG technique. Retaining the absolute value is however preferred in most of the cases since experimental measurement are never performed under an ideal conditions and the delay origin is unknown. The second consequence of the trace being symmetric is that a positive and negative sign in front of equation (4.17) will give the as result $E(f)$ and $E^*(f)$. This is equivalent to the intrinsic ambiguity that appears in SHG-FROG measurements.

v) *Error checking capabilities.*

There are many different strategies that can be employed to check validity of the phase measurement performed by MEFISTO or any other technique based on a collinear measurement. In this part, we will number a few of them but the wealth of information contained in the collinear measurement allows for developing a manifold of new strategies.

Firstly, straight check can be made by making use of the intrinsic 8:1 ratio that inteferometric autocorrelation must have. By integrating the experimental data to obtain the time marginal immediately after acquisition, it is possible to check for the 8:1 ratio. If the ratio is not correct, the data can immediately be discarded and taken again.

Secondly, since IAC, fundamental and SHG spectra are included in a collinear measurement (see Eq. 5.6), these three signals can be computed from the retrieved pulse and compared to those from the experimental measurement as done in time domain techniques.

Thirdly, in an analogous manner, the FROG spectrogram, frequency and time marginals are also directly obtained from the collinear trace (see Eq. (5.6)). Thus, degree of validation can be at least as accurate as FROG.

5.5 Experimental results from MEFISTO measurements.

5.5.1 MEFISTO vs. CFROG.

To show the validity of the MEFISTO methodology, we experimentally obtain the spectral phase of pulses originating from a Kerr-lens mode-locked Ti:sapphire laser. The laser had a central wavelength of 800 nm and a repetition rate of 76 MHz. The laser beam was focused into a type I BBO crystal through a Michelson interferometer (autocorrelator). The SHG signal was sent to a spectrometer and detected by a CCD linear array. The obtained frequency resolved interferometric autocorrelation trace is the one shown in Fig 4.8(a). To resolve the interferometric

fringes we chose a delay step of $\Delta\tau$=0.44 fs, which followed Nyquist criteria. We chose a time-delay span τ_{span}=3 ps that resulted in a frequency step of Δf=0.33 ps^{-1} and a spectral resolution of $\Delta\lambda$ =0.17 nm. We then analytically extracted the spectral phase of our pulse using equations (5.17) and (5.18).

To demonstrate the effectiveness of MEFISTO, we used the same experimental data to analytically characterize the pulse and then compared them with a standard SHG-FROG retrieval. The SHG-FROG trace was obtained using the CFROG technique explained above in section 5.3. Marginal analysis was also carried out to ensure that errors were not present within the trace and to check the robustness of the retrieval. It should be emphasised that MEFISTO can use the same stringent marginal checks. The results are outlined in Fig. 5.19 where the spectral intensity and phase of the pulse obtained from both techniques are compared.

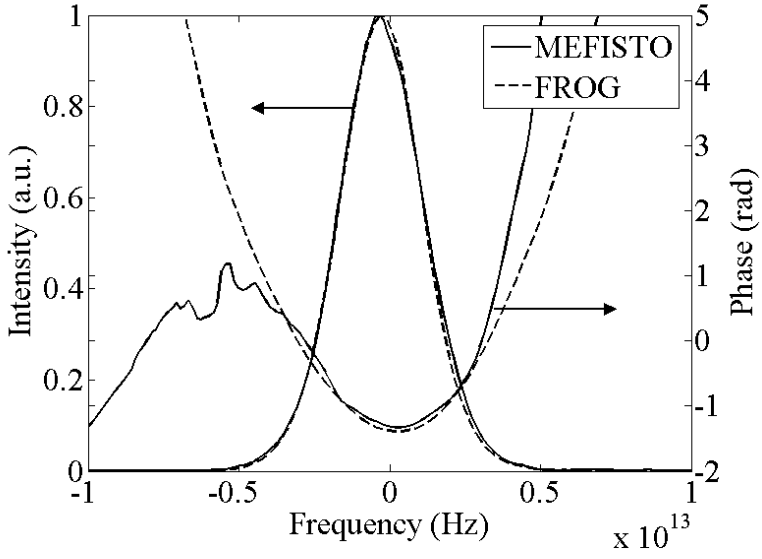

Figure 5.19 Spectra and phases of the pulse obtained using MEFISTO (solid lines) and a standard SHG-FROG procedure (dashed lines).

We can see that although the methodologies used to obtain the pulse characteristics were completely different, the intensity and phase are very similar. As a further evaluation, the calculated interferometric autocorrelations from both methods were compared with the experimental one, obtained by integrating the interferometric trace in the frequency axis. These results are shown in Fig. 5.20 showing good agreement.

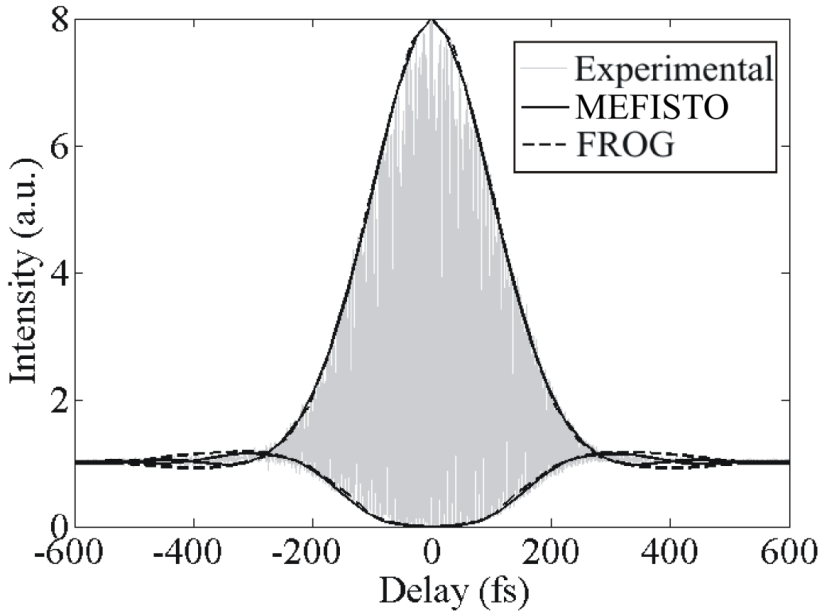

Figure 5.20 Numerical interferometric autocorrelations obtained from MEFISTO (solid line) and the SHG-FROG technique (dashed line) compared with experimental measurements (in light gray).

So far, MEFISTO has shown excellent agreement by recovering smooth or well-behaved pulses that contain small amount of chirp as they come out from a MIRA 900 after passing an $\Delta\lambda_{max} \approx \lambda_0$ optical isolator. Such pulses contain almost no structure and can be well approximated by a *sech* or gaussian function. In order to assess that the technique works for a more general cases, the results from a number of more complex pulses were explored: (1) sub-7*fs,* (2) stretched amplified pulses and (3) broadband chirped pulses from a single mode fiber.

5.5.2 Sub-7fs and stretched amplified pulses.

Firstly, we characterize sub-7*fs* pulses, whose collinear FROG trace was provided by the group of Günter Steinmeyer from the Max-Born Institute[14]. The trace was taken from a broadband Ti:sapphire oscillator system (Femtolasers Rainbow), delivering sub-7-*fs* pulses with 4 *nJ* pulse energy and characterized with three different techniques: SPIDER, IFROG and MEFISTO. Our group at ICFO, in Barcelona, worked on the characterization carried by MEFISTO without knowing any *a priori* characterization result and it was thus an excellent opportunity to objectively compare MEFISTO with other techniques which were computed by international experts at the Max-Born Institute.

These pulses were first characterized by Steimeyer's group (Stibenz, 2006) with the SPIDER method, yielding the 6.6-fs pulse shape of Fig. 5.17(a). As a cross-check, they also performed an interferometric autocorrelation of the same pulses, resulting in a 6.5 fs pulse duration under the somewhat simplistic assumption of a hyperbolic secant pulse shape. More stringently, however, the reconstructed interferometric autocorrelation from the measured SPIDER data showed an excellent agreement with the measured data, independently supporting the validity of the SPIDER retrieval. After this, Steinmeyer's group utilized its own developed iterative technique called IFROG, which is commented in Chapter 4. While iterative retrieval repeatedly imposes constraints on the electric field under reconstruction in both domains, the delay frequency domain and its Fourier counterpart, MEFISTO is based on a direct analytic dependence of the spectral phase as explained above. This allows for direct reconstruction of the spectral phase profile via concatenation of spectral phase differences in a similar manner to what is done in SPIDER.
The results of the iterative retrieval from IFROG are shown in Fig. 5.21(b), which have to be compared to the direct MEFISTO retrieval of Fig. 5.21 c). Most remarkably, the duration of the main pulse is reproduced within ±0.2 *fs* as about 6.7 *fs* by all the four methods

employed. Moreover, all methods predict strong satellite pulses at +10 and at +20 fs, even though their relative weight is not exactly reproduced. Reconstructed amplitudes in the spectral domain closely follow an independent measurement of the spectrum for both methods, too.

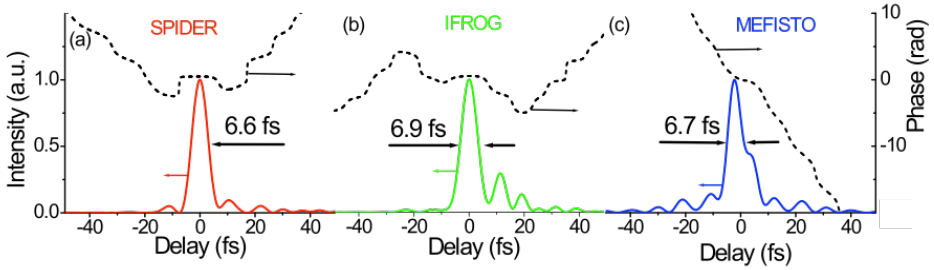

Fig. 5.21. Pulse shapes (solid lines) and temporal phases (dashed lines), as measured (a) with SPIDER, (b) by an iterative retrieval based on the IFROG data, and (c) from non-iterative retrieval following the MEFISTO method. The determined half widths of the pulses agree within <5%; the pulses exhibit satellites at nearly identical locations, i.e. +10 and +20fs, however, with varying relative weigths.

A second less elaborate test was done on amplified 30-fs Ti:sapphire pulses that were stretched to about 55 fs by a controlled amount of group delay dispersion (+400 fs^2).

The results of the second tests on the white-light continuum are shown in Fig. 5.22. Again, MEFISTO could reproduce the 55-fs pulse duration, see Fig. 5.22(a). The method was also capable of determining the 400 fs^2 group delay dispersion on these pulses, see Fig. 5.22(b).

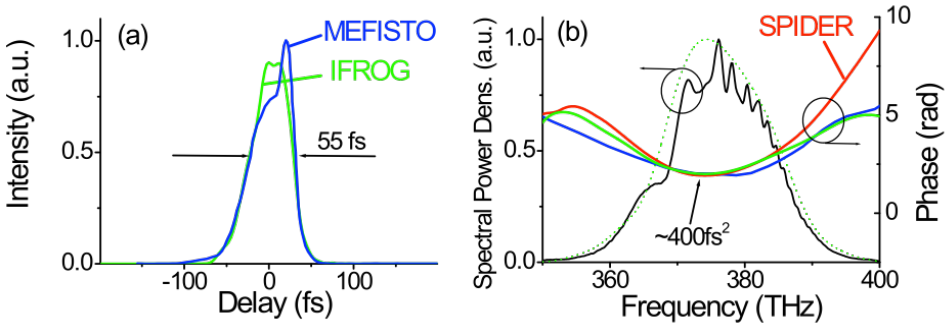

Fig. 5.22 Characterization of chirped pulses from a Ti:sapphire amplifier with MEFISTO, FROG, and SPIDER. (a) Comparison in the time domain; both retrieval methods result in nearly identical durations, despite some noticeable deviations in the retrieved pulse shapes. (b) Spectral domain. Measured spectral phases agree for most of the spectral range shown. Deviations are visible in the long-wavelength part of the reconstructions. The dotted line shows the reconstructed spectrum of the IFROG method in comparison to an independently measured one.

In summary, after comparing (MEFISTO, SPIDER and IFROG) using pulses of 2.5 optical cycle duration from an oscillator and chirped pulses from an amplified source, we find that MEFISTO is capable of determining the major pulse parameters even under the challenging pulse characterization scenarios we chose.

5.5.3 Pulses from a single mode fiber.

To further check MEFISTO, we experimentally obtained the spectral phase of an ultrashort pulse that was spectral broadened after passing through 10 cm of a single mode fiber. The laser pulses, before entering to the fibre, had a central wavelength of 800 nm and a repetition rate of 76 MHz and an average pulsewith of 240 *fs* as shown in the first measurement of this section in Fig. 5.19. Due to spectral broadening caused by self phase modulation (Tomlinson, 1984; Pinault, 1985) pulses, measured by an IAC directly outside the fibre showed a FWHM larger than 1ps. A numerical analysis previously performed in the group

(Gualda, 2005) showed that these pulses had a huge amount of quadratic dispersion. A simple pre-dispersion stage, consisting in a pair of prisms to introduce negative dispersion (Fork,1984), was employed to shorten pulse duration. Finally, characterised using MEFISTO in which the autocorrelator used a type I BBO crystal of 0.1 mm thickness to cope with the bandwidth.

Here, in Fig. 5.23, we show two different but representative MEFISTO measurements, one in which the pulse quadratic dispersion was compensated as much as possible using a pair of prisms (Fig.5.19) and another one, in Fig. 5.20, with an excessive amount of negative dispersion introduced by the pair of prisms which produces a longer pulse again.

Figure 5.23 shows the results of the compensated pulses by two prisms after self-phase modulation inside the optical fiber ant it achieves 37 *fs* FWHM. It is possible to observe that central part is mainly chirped by a cubic phase component, introduced by the whole setup.

Figure 5.24 shows a partially compensated pulse and strong residual quadratic phase modulation and it results in a temporally wider pulse and three satellites at 100, 150 and 200 *fs* from the main temporal peak.

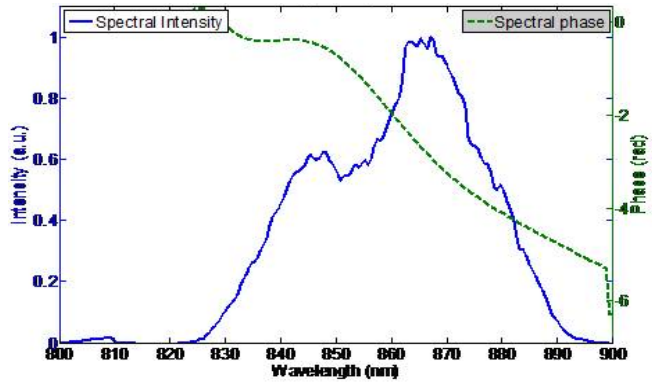

(a)

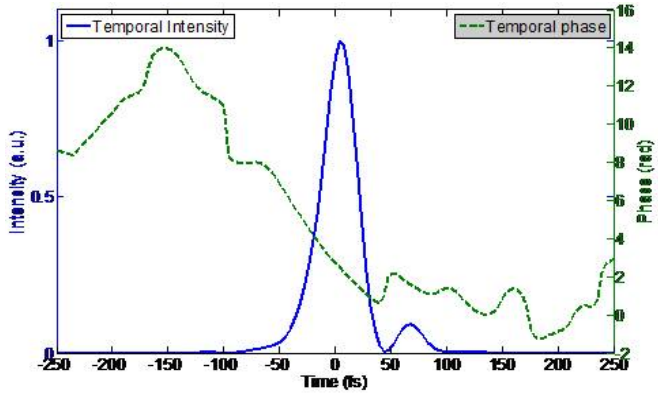

(b)

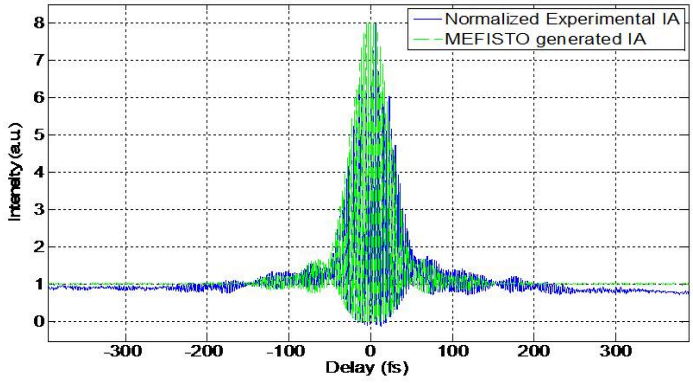

(c)

Fig. 5.23 (a) Measured complex spectrum from the collinear spectrogram by MEFISTO; (b) Temporal intensity and phase of the measured ultrashort pulse and (c) IAC is used to confirm the measured phase.

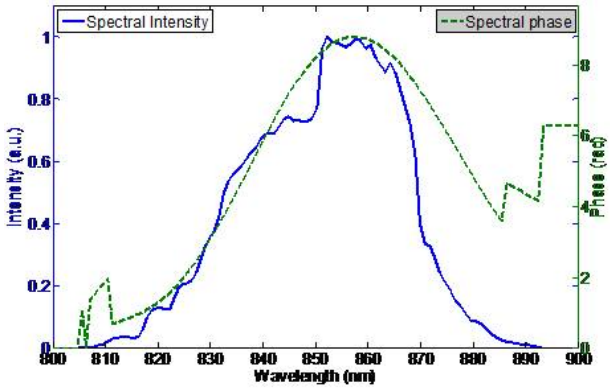

(a)

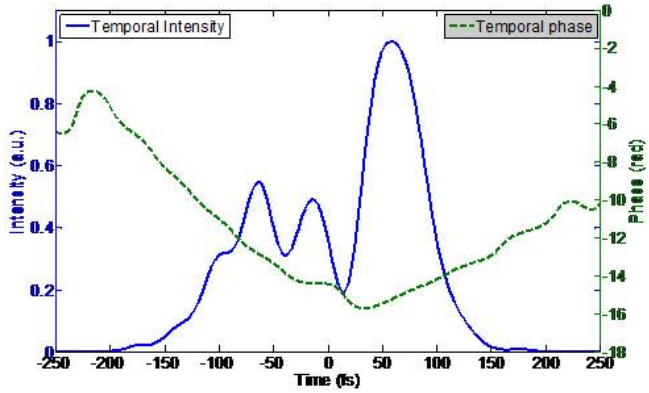

(b)

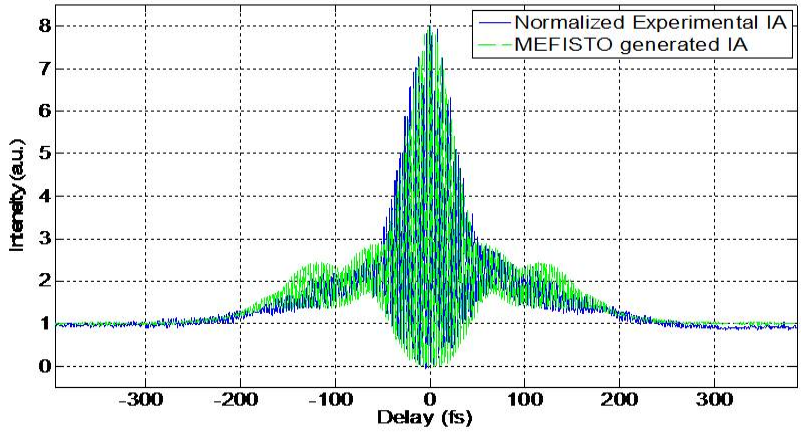

(c)

Fig. 5.24 (a) Measured complex spectrum from the collinear spectrogram by MEFISTO; (b) Temporal intensity and phase of the measured ultrashort pulse; and (c) IAC is used to confirm the measured phase.

5.6 Conclusions.

In conclusion, in this section we have outlined new procedures based on a simple collinear autocorrelator that allows the complex amplitude of ultrashort pulses to be deduced.
CFROG technique is a pre-processing technique that allows a conventional SHG-FROG retrieval algorithm to be utilized from a trace that has been measured under collinear conditions. This allows for more flexible, easier and multipurpose experimental conditions that reduce the overall experimental constraints of the FROG technique while at the same time helping to broaden the number applications in which FROG measurements can be utilized. e.g. nonlinear microscopy pulse optimisation. The preprocessing technique based on a filtering and background subtraction procedure has been analytically justified. The robustness of this approach has been fully tested using both numerical simulations and experimental data. In both cases, excellent agreement has been observed between the filtered CFROG trace and the non-collinear FROG trace giving G-Error as low as $G < 10^{-5}$. Furthermore, we have shown that, as the technique does not rely on resolving all the interferometric fringes, and thus it is possible to significantly reduce the acquisition time by undersampling the CFROG trace. FAST-CFROG is then presented to minimize the number of samples while ensuring little error is introduced into the trace.
We have focused upon SHG-FROG based measurements, but in a similar manner, this method can be extended to other FROG geometries. The result is a general method for full characterisation of ultrashort pulses under collinear conditions.

MEFISTO technique relies on Fourier analysis after obtaining a spectrally resolved interferometric autocorrelation trace (i.e. a CFROG trace). The MEFISTO methodology has the crucial advantage over SHG-FROG (and therefore over CFROG) in that it enables the simple extraction of pulse information without the need of an iterative retrieval algorithm. Furthermore, it still maintains the powerful error checking

capabilities that are associated with time-frequency techniques which other interferometric techniques do not posses. We have experimentally demonstrated the effectiveness of the new procedure by comparing results with the more traditional characterisation technique of SHG-FROG using an identical optical arrangement. This setup is extremely flexible and simple, allowing a large number of different applications to be carried out.

References

I Amat-Roldan, IG Cormack, EJ Gualda, D Artigas, and P Loza-Alvarez. "Ultrashort pulse characterisation with SHG collinear-FROG," *Opt. Express* **12** pp. 1169–1178 (2004a).

I Amat-Roldan, IG Cormack, P Loza-Alvarez, and D Artigas, "Starch-based second-harmonic-generated collinear frequency-resolved optical gating pulse characterization at the focal plane of a high-numerical aperture lens," *Opt. Lett.* **29** pp. 2282–2284 (2004b).

I Amat-Roldan, IG Cormack, P Loza-Alvarez, and D Artigas, "Nonlinear microscopy pulse optimization at the sample plane using Second Harmonic Generation from starch." *Proc. SPIE*, pp. 5463-09 (2004c).

DN Fittinghoff, JA Squier, CPJ Barty, JN Sweetser, R Trebino, and M Muller, "Collinear type II second harmonic-generation frequency-resolved optical gating for use with high-numerical-aperture objectives," *Opt. Lett.* **23** pp. 1046-1048 (1998).

DN Fittinghoff, AC Millard, JA Squier, and M Muller, "Frequency-resolved optical gating measurement of ultrashort pulses passing through a high numerical aperture objective," *IEEE J. Quantum Electron.* **35** pp. 479-486 (1999).

RL Fork and OE Martinez, "Negative dispersion using pairs of prisms," *Opt. Lett.* **9** pp. 150- (1984).

EJ Gualda, "Optimización de las prestaciones de enlaces ópticos submarinos de gran capacidad y larga distancia mediante el control de la dispersión", Tesis Doctoral, Universitat Politècnica de Catalunya (2005).

L Gallmann, G Steinmeyer, DH Sutter, N Matuschek, U Keller, "Collinear type II second-harmonic generation frequency-resolved optical gating for the characterization of sub-10-fs optical pulses," *Opt. Lett.* **25** pp. 269-271 (2000).

C Iaconis, V Wong, and IA Walmsley, “Direct interferometric techniques for characterizing ultrashort optical pulses,” *IEEE J. Sel. Top. Quantum Electron.* **4** pp. 285-294 (1998a).

C Iaconis and IA Walmsley, “Spectral phase interferometry for direct electric-field reconstruction of ultrashort optical pulses,” *Opt. Lett.* **23** pp. 792–794 (1998b).

J Jasapara and W Rudolph, "Characterization of sub-10-fs pulse focusing with high-numerical-aperture microscope objectives," *Opt. Lett.* **24** pp. 777-779 (1999).

DJ Kane, “Real-time measurement of ultrashort laser pulses using principal component generalized projections,” *IEEE J. Sel. Top. Quantum Electron.* **4** pp. 278 (1998).

AV Oppenheim and RW Schafer, Digital Signal Processing (Prentice-Hall, 1975).

SC Pinault and MJ Potasek, "Frequency broadening by self-phase modulation in optical fibers," *J. Opt. Soc. Am. B* **2** pp. 1318-1319 (1985).

T Shuman, IA Walmsley, L Waxer, M Anderson, C Iaconis, and J Bromage, "Real-time SPIDER: ultrashort pulse characterization at 20 Hz," *Opt. Express* **5** pp. 134-143 (1999).

G Stibenz and G Steinmeyer, “Interferometric frequency-resolved optical gating,” *Opt. Express* **13** pp. 2617-2626 (2005).

G Stibenz, I Amat-Roldán, IG Cormack, D Artigas, P Loza-Alvarez, and G Steinmeyer, "Comparison of Iterative and Non-Iterative Retrieval From Few-Cycle Interferometric FROG Traces," in Conference on Lasers and Electro-Optics/Quantum Electronics and Laser Science Conference and Photonic Applications Systems Technologies, (Optical Society of America, 2006).

WJ Tomlinson, RH Stolen, and CV Shank, "Compression of optical pulses chirped by self-phase modulation in fibers," *J. Opt. Soc. Am. B* **1** pp. 139-149 (1984).

CHAPTER 6

New analytical method for measurement of two unknown pulses in collinear geometry.

6 New analytical method for measurement of two unknown pulses in collinear geometry.

6.1 Introduction.

In the previous chapter we have experimentally demonstrated a new interferometric-based pulse characterisation technique called MEFISTO (Measuring the electric field by interferometric spectral trace observation, Amat-Roldan 2005). MEFISTO has allowed for the first time, the analytical characterization of an unknown ultrashort pulse from a time-frequency representation of a pulse.

MEFISTO, as SPIDER, allows the pulse information to be directly extracted from experimental data. However, unlike SPIDER, it is based on recording a time-frequency measurement of the pulse which makes it strongly related to FROG. This ambivalent nature makes it possible to share some of the advantages attributed to both methodologies. On one side, as in SPIDER, the extraction of the phase can be directly performed without the need of an iterative retrieval algorithm. On the other side, MEFISTO possesses extended error checking capabilities and simpler experimental arrangement as FROG allowing it to be used in a broader range of applications where collinear geometry is required (Amat-Roldan, 2004). Furthermore, as we show in this chapter, the time-frequency nature of the method makes possible, as in XFROG (DeLong, 1995; Reid, 2000), the simultaneous characterization of two unknown ultrashort pulses, a technique we refer to as blind-MEFISTO.

The aim of next section is to outline the theoretical background and discuss the retrieving analytical procedure in a more general case. Our main goal here is to present the generalized theory for Blind-MEFISTO and then go on to discuss the particular issues addressed when experimentally retrieving an ultrashort pulse. For this purpose, the chapter has been organized as follows: In section 6.2, we develop the general theory. This is followed by some experimental and practical

consideration. In section 6.4. a theoretical example of the blind-MEFISTO retrieval is presented. Finally, general conclusions are given.

6.2 Analysis of the image from two different pulses.

BLIND-MEFISTO is based on the Fourier analysis of a spectrally resolved interferometric correlation trace between two pulses (not necessarily equal). The experimental set up to obtain such correlation trace can be seen in Fig. 6.1.

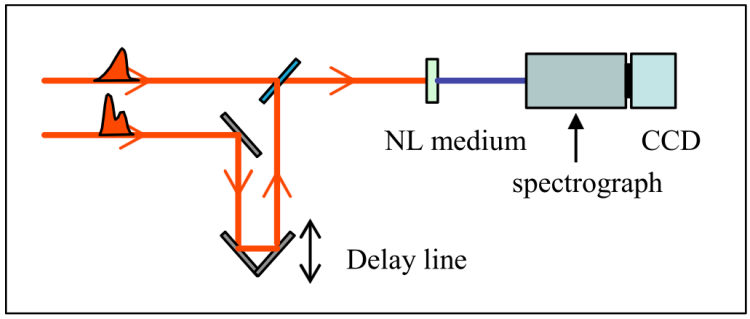

Fig. 6.1. Typical experimental set up needed to obtain a Frequency resolved interferometric correlation trace.

Two pulses interact collinearly within a nonlinear medium, one of them after passing through a delay arm. The second harmonic generated signal is then directed to a spectrograph to obtain the interferometric time-frequency trace in terms of the time-delay τ and the frequency f. An example of the resulting trace can be seen in Fig. 6.2(a). In a general case, this trace can be mathematically described as

$$I^{SHG}(f,\tau) = \chi \left| F_t\left\{ \left(E(t)exp\left(j2\pi f_1 t\right) + G(t-\tau)exp\left(j2\pi f_2 t\right)\right)^2 \right\} \right|^2 \tag{6.1}$$

where $E(t)$ and $G(t)$ are the slowly varying amplitude of the complex electric field centered at the frequencies f_1 and f_2. The Fourier transform with respect to the variable t is indicated by F_t and χ is related with the

conversion efficiency in the nonlinear process. Note that the two interfering *E(t)* and *G(t)* can be either different, what is referred to us as Blind-MEFISTO, or equal, which is the general case that for simplicity is solely named MEFISTO (the degenerate case). In Blind-MEFISTO, phase matching must be achieved for all the cross-terms in Eq. (6.1) and, as we will show, the new information carried on the interferometric terms will allow the simultaneous analytical determination of *E(t)* and *G(t)*. In general, this should restricts the use of Blind-MEFISTO to the case in which the central frequencies of *E(t)* and *G(t)* are equal ($f_1 = f_2 = f_0$).

We start our analysis by calculating the Fourier transform of equation (5.1) in the τ delay axis, i.e., $Y^{SHG}(f,\kappa) = F_\tau\left\{I^{SHG}(f,\tau)\right\}$. The resulting expression consist of five main spectral components (see Fig. 6.2(b)) at delay-frequencies $\kappa = \left\{0, \pm f_0, \pm 2f_0\right\}$. Since the interferometric trace (Fig. 6.2(a)) is real, the negative spectral components in Fig. 6.2(b) are the complex conjugate of the positive ones. We therefore only need to focus upon one of the components (either the positive or the negative) to analyze the information enclosed in the transformed trace. Each of these terms contain information of the pulse phase and intensity and their use will depend on the particular experimental conditions. To highlight the information enclosed in $Y^{SHG}(f,\kappa)$, we will separately focus on the mathematical expression for each component and analyze their possibilities.

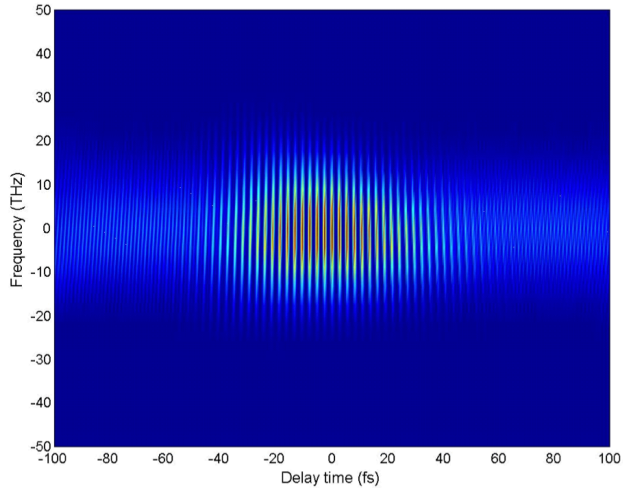

(a)

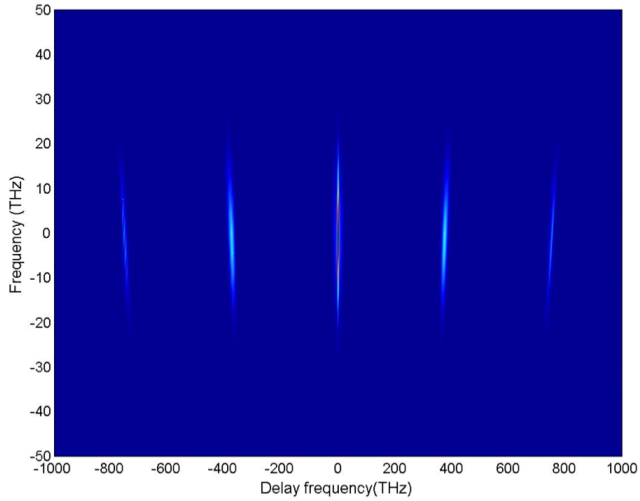

(b)

Fig. 6.2. (a) Frequency resolved interferometric correlation trace and (b) its Fourier transform in the delay-frequency axis, showing the different spectral components.

We start analyzing the component at $\kappa = 0$, which can be written as:

$$Y_{DC}^{SHG}(f,\kappa) = \chi\left(\left|E_{SHG}(f)\right|^2 + \left|G_{SHG}(f)\right|^2\right)\delta(\kappa) + \\ +4\chi\int_{-\infty}^{\infty} df' E(f')G(f-f')E^*(f'-\kappa)G^*(f-f'+\kappa) \tag{6.2}$$

where the second harmonic of the two unknown fields $E_{SHG}(f)$ and $G_{SHG}(f)$, are related with the fundamental pulse following $F_{SHG}(f) = \int_{-\infty}^{\infty} F(f')F(f-f')df'$, with f corresponding to the base-band frequency (Oppenheim, 1975). The second term in Eq. (6.2) includes the standard XFROG trace that has been used to characterize ultra short laser pulses (Reid, 2000; DeLong, 1995). It is worth noting that this term, with the use of adequate phase matching conditions, can be obtained even in the case where the spectra of the two pulses do not overlap ($f_1 \neq f_2$) allowing XFROG to be used to characterise pulses that have differing central frequencies. In a previous paper we outlined a filtering procedure capable to extract the FROG term from the $\kappa = 0$ component in the degenerate case ($E(t) = G(t)$). This technique named as CFROG (Amat-Roldan, 2004) can straightforwardly be extended to obtain the XFROG term. However, when retrieving the pulses, it again relies upon the use of retrieval algorithms since the integral on Eq. (6.2) does not allow the analytical determination of $E(t)$.

We continue our analysis by focusing upon the spectral component of $Y^{SHG}(f,\kappa)$ at $\kappa=2f_0$. This component can be written as

$$Y^{SHG}_{\kappa\approx 2f_0}(f,\kappa) = \chi \times E_{SHG}(f)G^{*}_{SHG}(f)\delta(f-\kappa+2f_0) \tag{6.3}$$

This expression corresponds to a straight line in the transformed trace (Fig. 6.2(b)) given by $\kappa = f + 2f_0$. This term can be used for different purposes. Firstly, in an experimental trace, the divergence from an ideal delta function gives a measure of the pulse jitter, as suggested by Stibenz and Steinmeyer (Stibenz, 2005), or in general, the quality of the measurement. In addition, any deviation from a linear dependency between κ (real frequency) and f (base band frequency) will indicate a spectrograph miss-calibration. This component can also determine $E(t)$ when the gating function, $G(t)$, is already known. It can therefore be used

as a further verification of the blind-MEFISTO retrieval by checking that the two pulses fulfill

$$E(t) = \sqrt{F_f^{-1}\left\{\frac{Y^{SHG}\left(f,\kappa = f + 2f_0\right)}{\chi \times F_t\left\{\left(G(t)\right)^2\right\}}\right\}} \tag{6.4}$$

Although the terms at $\kappa = 0$ and $\pm 2f_0$ are useful to obtain some pulse information, it is the component at $\kappa \approx f_0$ of $Y^{SHG}(f,\kappa)$ that allows the simultaneous analytical characterization of two unknown ultrashort pulses. The mathematical expression for this component can be written as:

$$\begin{aligned} Y^{SHG}_{\kappa \approx f_0}(f,\kappa) = {} & 2\chi \times E_{SHG}(f)E^*(f + f_0 - \kappa)G^*(\kappa - f_0) + \\ & 2\chi \times G^*_{SHG}(f)G(f + f_0 - \kappa)E(\kappa - f_0) \end{aligned} \tag{6.5}$$

This equation shows the main advantage of Fourier transforming the trace as was done in Fig. 6.2(b): All the convolutions that appear in the time domain have been transformed into products in the frequency domain. This isolates the individual pulse fields and makes it possible to resolve analytically. To show this, we firstly write all the involved complex magnitudes in polar form, i.e., $E(f) = E_0 U(f)\exp\left(j\phi(f)\right)$, $G(f) = G_0 V(f)\exp\left(j\gamma(f)\right)$, and equivalently for the harmonic pulses $E_{SHG}(f) = E_0^{SHG} U_{SHG}(f)\exp\left(j\phi_{SHG}(f)\right)$ and $G_{SHG}(f) = G_0^{SHG} V_{SHG}(f)\exp\left(j\gamma_{SHG}(f)\right)$.

Here, for convenience, all spectral profiles *U(f)* are normalized at the central base-band frequency (*U(f=0)=1*). Then, taking $Y^{SHG}(f,\kappa) = R(f,\kappa)\exp(i\theta(f,\kappa))$, Eq. 6.5 can be written as

$$\begin{aligned} & R(f,\kappa) = 2\chi_1 U_{SHG}(f)U(f + f_0 - \kappa)V(\kappa - f_0) \times \\ & \exp\left[\phi_{SHG}(f) - \phi(f + f_0 - \kappa) - \gamma(\kappa - f_0) - \theta(f,\kappa)\right] + \\ & 2\chi_2 V_{SHG}(f)V(f + f_0 - \kappa)U(\kappa - f_0) \times \\ & \exp\left[-\gamma_{SHG}(f) + \gamma(f + f_0 - \kappa) + \phi(\kappa - f_0) - \theta(f,\kappa)\right] \end{aligned} \tag{6.6}$$

Here we have defined two parameters $\chi_1 = \chi E_0^{SHG} E_0 G_0$ and $\chi_2 = \chi G_0^{SHG} E_0 G_0$, which can be understood as effective conversion efficiency parameters. In section 4.4, we will go on to describe a procedure to obtain χ_1 and χ_2 from the experimental trace. In what follows, and for clarity purposes, we will assume that these parameters are known. Under typical lab conditions the normalized spectra profiles, *U(f)*, *V(f)*, $U_{SHG}(f)$ and $V_{SHG}(f)$ can be directly measured. As $R(f,\kappa)$ and $\theta(f,\kappa)$ are obtained from the interferometric trace, therefore, the only unknowns in Eq. 6.6 corresponds to the phase of the fundamental and second harmonic pulse, i.e., $\phi(f)$, $\gamma(f)$, $\phi_{SHG}(f)$ and $\gamma_{SHG}(f)$. In order to fully characterize the pulses these unknowns must be calculated. This can be achieved by first taking two different slices in the transformed space of the interferometric trace, e.g., at $\kappa = f_0$ and $\kappa = f_0 - \Delta f$. Then, by taking the real and imaginary parts in Eq. 6.6, we can isolate the phase component at $\kappa = f_0$, obtaining

$$\phi_{SHG}(f) - \phi(f) - \gamma(0) = \pm\cos^{-1}\left[\Omega_1(f,\kappa = f_0)\right] + \theta(f,\kappa = f_0) \qquad 6.7(a)$$

$$\gamma_{SHG}(f) - \gamma(f) - \phi(0) = \pm\cos^{-1}\left[\Omega_2(f,\kappa = f_0)\right] - \theta(f,\kappa = f_0) \qquad 6.7(b)$$

and at $\kappa = f_0 - \Delta f$

$$\phi_{SHG}(f) - \phi(f + \Delta f) - \gamma(-\Delta f) = \pm\cos^{-1}\left[\Omega_1(f,\kappa = f_0 - \Delta f)\right] + \theta(f,\kappa = f_0 - \Delta f) \qquad 6.7(c)$$

$$\gamma_{SHG}(f) - \gamma(f + \Delta f) - \phi(-\Delta f) = \pm\cos^{-1}\left[\Omega_2(f,\kappa = f_0 - \Delta f)\right] - \theta(f,\kappa = f_0 - \Delta f) \qquad 6.7(d)$$

where we have defined two functions that relate the different pulse spectra and the trace as

$$\Omega_1(f,\kappa) =$$

$$= \frac{R^2(f,k) + 4\left[\chi_1^2 U_{SHG}^2(f) U^2(f + f_0 - \kappa) V^2(\kappa - f_0) - \chi_2^2 V_{SHG}^2(f) V^2(f + f_0 - \kappa) U^2(\kappa - f_0)\right]}{4\chi_1 R(f,\kappa) U_{SHG}(f) U(f + f_0 - \kappa) V(\kappa - f_0)}$$

and

$$\Omega_2(f,\kappa) =$$

$$= \frac{R^2(f,k) - 4\left[\chi_1^2 U_{SHG}^2(f)U^2(f+f_0-\kappa)V^2(\kappa-f_0) - \chi_2^2 V_{SHG}^2(f)V^2(f+f_0-\kappa)U^2(\kappa-f_0)\right]}{4\chi_2 R(f,\kappa)V_{SHG}(f)V(f+f_0-\kappa)U(\kappa-f_0)}$$

Then, by subtracting equations 6.7(a) and 6.7(c) we get

$$\Delta\phi_\kappa(f) = \phi(f+\Delta f) - \phi(f) = \pm\cos^{-1}\left[\Omega_1\left(f,\kappa=f_0\right)\right] \mp \cos^{-1}\left[\Omega_1\left(f,\kappa=f_0-\Delta f\right)\right] + \\ + \theta\left(f,\kappa=f_0\right) - \theta\left(f,\kappa=f_0-\Delta f\right) + \gamma(0) - \gamma\left(-\Delta f\right) \tag{6.8}$$

From this equation the phase for the spectral component $E(f)$, i.e., $\phi(f)$ can be determined by taking an arbitrary origin $\phi(0)$ and adding up $\Delta\phi_\kappa(f)$ as

$$\phi(f) = \phi(0) + \sum_{f'=\Delta f}^{f} \Delta\phi_\kappa(f'). \tag{6.9}$$

In a similar way, by subtracting equations 6.7(b) and 6.7(d), we obtain the equation necessary to determine the phase increment for *G(f)* in terms of the frequency as

$$\begin{aligned} &\Delta\gamma_\kappa(f) = \gamma(f+\Delta f) - \gamma(f) = \\ &= \pm\cos^{-1}\left[\Omega_2(f,\kappa=f_0)\right] \mp \cos^{-1}\left[\Omega_2(f,\kappa=f_0-\Delta f)\right] - \\ &-\theta(f,\kappa=f_0) + (f,\kappa=f_0-\Delta f) + \phi(0) - \phi(-\Delta f) \end{aligned} \tag{6.10}$$

and, as in the previous case, by taking an arbitrary origin $\gamma(0)$ find the spectral phase components as

$$\gamma(f) = \gamma(0) + \sum_{f'=\Delta f}^{f} \Delta\gamma_\kappa(f'). \tag{6.11}$$

Notice that the terms $\gamma(0) - \gamma(-\Delta f)$ and $\phi(0) - \phi(-\Delta f)$ in Eq. 6.8 and 6.10 are unknown constants. These terms add a linear spectral phase shift that only affects the electric field time origin and therefore they can be decided arbitrarily without affecting the shape of the temporal pulse envelope. Eq. 6.8 - 6.11 are the principal result of this work showing that to simultaneously characterize two different pulses in an analytical way is possible.

6.3 Experimental and practical considerations.

In this section we discuss important characteristics of MEFISTO that should be considered to ensure easier and successful pulse retrievals.

i) *Pulse Bandwidth*

An important issue to consider is the maximum pulse bandwidth that MEFISTO can successfully characterize. This fundamental limit derives from the necessity to prevent overlap between the different components of the transformed trace (see Fig. 6.2(b)). Specifically, the two slices at $\kappa = f_0$ and $\kappa = f_0 - \Delta f$ must not be affected by the tails of the $\kappa = 0$ component. In principle, this suggests that the available bandwidth could be equal to the optical carrier, i.e., $\Delta\lambda_{max} = \lambda_0$. However, in practice, this can be affected by the particular pulse shape.

ii) *Frequency Resolution*

In our analysis we have implicitly considered that the sampling step in the f and κ axis coincides ($\Delta\kappa = \Delta f$). Initially, the frequency resolution is in fact given by the time-delay span τ_{span}, i.e., $\Delta\kappa = 1/\tau_{span}$, which experimentally can differ from the spectrograph resolution. However, by using interpolating techniques to fulfil $\Delta\kappa = \Delta f$, the frequency resolution of the method can be extended to Δf.

iii) *Determining the conversion efficiency parameters* χ_1 *and* χ_2

In our theoretical development, we have considered all the spectral profiles to be normalized to unity at the central wavelength. The energy of each pulse is therefore associated with the spectral amplitudes E_0, E_0^{SHG}, G_0 and G_0^{SHG}. These terms, together with the nonlinear coefficient

χ are included in the conversion efficiency parameters χ_1 and χ_2. Here we will outline how these parameters can be calculated using the $\kappa = 0$ and $\kappa = 2f_0$ components of the transformed interferometric trace. To achieve this we must first define three separate equations, two that are derived from the $\kappa = 0$ term and one that is derived from the $\kappa = 2f_0 + f$ term. Firstly, using the same procedure outlined in Ref. 8, the two contributions to the $\kappa = 0$ term in Eq. 6.2 can be separated. The first part, involving the delta function, when $\kappa = 0$ gives

$$Y_0^{SHG}(f,\kappa = 0) = \chi\left(\left(E_0^{SHG}\right)^2 U_{SHG}{}^2 + \left(G_0^{SHG}\right)^2 V_{SHG}{}^2\right) \tag{6.12}$$

and the second part, involving the CFROG information, when $\kappa = 0$ and $f = 0$, yields,

$$Y_{CFROG}^{SHG}(0,0) = 4\chi E_0^2 G_0^2 \mathrm{P} \tag{6.13}$$

where $\mathrm{P} = \int_{-\infty}^{\infty} df' U^2(f') V^2(-f')$ can be experimentally determined from the experimental spectra $I_E(f) = U^2(f)$ and $I_G(f) = V^2(f)$. The third equation is obtained by looking at the component at $\kappa = 2f_0 + f$ and taking its modulus;

$$\left|Y_{\kappa=2f_0}^{SHG}(f,k = 2f_0 + f)\right| = \chi \times E_0^{SHG} G_0^{SHG} U_{SHG}(f) V_{SHG}(f) \tag{6.14}$$

After some algebra, equations (5.12 - 5.14) lead to

$$\chi_1^2 U_{SHG}^2(f) = \frac{Y_{CFRO}^{SHG}(0,0)}{8\mathrm{P}}\left[Y_\delta^{SHG}(f,0) \pm \sqrt{(Y_\delta^{SHG\,2}(f,0) - 4(Y_{\kappa=2f_0}^{SHG}(f,2f_0 + f)}\right] \tag{6.15}$$

$$\chi_2^2 V_{SHG}^2(f) = \frac{Y_{CFRO}^{SHG}(0,0)}{8\mathrm{P}}\left[Y_\delta^{SHG}(f,0)\,\mathrm{m}\sqrt{(Y_\delta^{SHG\,2}(f,0) - 4(Y_{\kappa=2f_0}^{SHG}(f,2f_0 + f)}\right] \tag{6.16}$$

where all terms on the right hand side are experimental parameters. The sign before the square root depends on the peak intensities of the two second harmonic pulses and must be chosen accordingly so that when, for example, $I_E^{SHG} > I_G^{SHG}$ then $\chi_1 > \chi_2$. By determining equations (6.15) and (6.16) we have shown how it is possible to evaluate the functions

$\Omega_1(f,\kappa)$ and $\Omega_2(f,\kappa)$ without the need of experimentally measuring the intensities of the second harmonic spectra $U_{SHG}(f)$ and $V_{SHG}(f)$.

iii) *Spectral calibration*

Method 1

By Fourier transforming the term modulated at the SH frequency-delay ($\kappa = 2f_0$), expression in Eq. 6.3, we can calculate the κ and f relationship to calibrate the pulse image. By estimating the Second Harmonic frequency at each pixel of the spectrometer we can calibrate the spectrometer based on:

$$Y^{SHG}_{\kappa \approx 2f_0}(f,\kappa) = U_{SHG}(f)\delta(f + 2f_0 - \kappa) \tag{6.17}$$

This method allows calibrating the spectrometer and registering the fundamental spectrum extracted from the DC term. This is crucial for the correct phase estimation because MEFISTO is an interferometric technique and relies on accurate calibration of wavelength of fundamental and SH spectra.

Method 2

An experimental measurement, in general, requires two independent measurements: the two fundamental pulse spectra and the interferometric trace. The need for the exact determination of the f_0 and $2f_0$ places extreme demands and importance on the spectral calibration for this interferometric techniques. These demands can be relaxed significantly by evaluating the second term of equation (6.2) at $\kappa = 0$, and using it to directly relate f_0 and $2f_0$ with one another.

By taking a convolution of the two measured fundamental spectra, an accurate spectral registration can be performed that relates the region of the fundamental spectrum with the region of the second harmonic

spectrum, where the interferometric trace is obtained. This property allows the MEFISTO technique to be extremely roboust against spectrometer miscalibration.

6.4 Blind-MEFISTO results

In this section we will numerically go through an analytical retrieval step by step in order to show details of how the method should be performed in an experimental case.

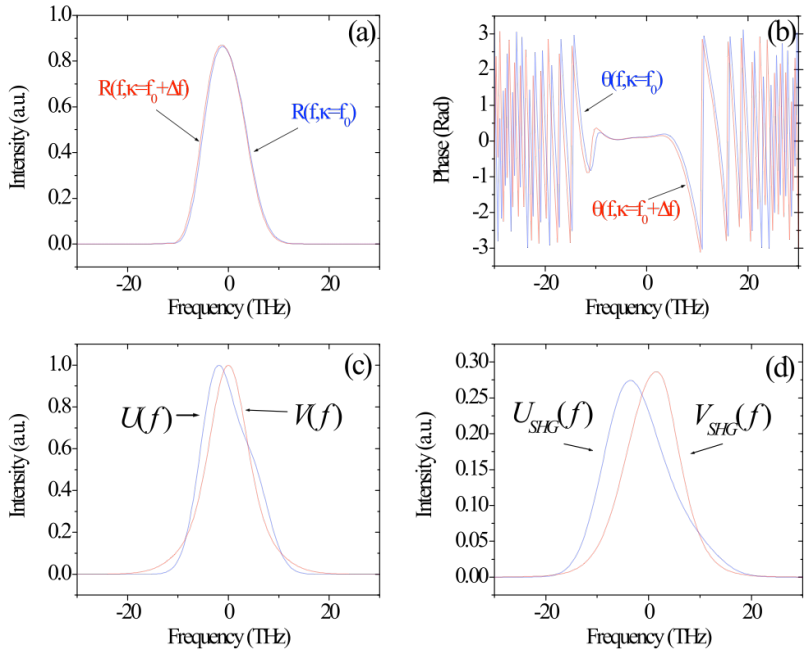

Fig. 6.3. Experimental data necessary to solve equations (8) and (10). In (a) we show the amplitude and in (b) the phase corresponding to the two slices at $\kappa=f_0$ and $\kappa=f_0+\Delta f$ obtained from the transformed trace in Fig. 6.2(b). We also show the spectra for the two fundamental pulses (c) and at the SHG frequency (d).

First, as commented we need to take the two slices (at $\kappa = f_0$ and $\kappa = f_0 + \Delta f$) of the Fourier transformed interferometric trace shown in Fig. 6.2(b).

The amplitude of the trace *R(f,κ)* and the phases θ*(f,κ)* are respectively shown in Fig. 6.3 (a) and (b) at $\kappa = f_0$ and $\kappa = f_0 - \Delta f$. In addition, to evaluate the $\Omega_1(f,\kappa)$ and $\Omega_2(f,\kappa)$ functions, the two fundamental pulses spectra are needed (Fig. 6.3(c)), which must be obtained experimentally. The two spectra of the second harmonic pulses (Fig. 6.3(d)) and the parameters χ_1 and χ_2 can be either obtained experimentally or directly from the interferometric trace using the method outlined in section 6.4 (Eq. 6.15-6.16).

In an experimental case $\Omega_1(f,\kappa)$ and $\Omega_2(f,\kappa)$ are therefore evaluated using solely experimental data. The resulting $\Omega_1(f,\kappa)$ and $\Omega_2(f,\kappa)$ function are shown, respectively, in Figures 6.4(a) and 6.4(b), at $\kappa = f_0$ and $\kappa = f_0 - \Delta f$.

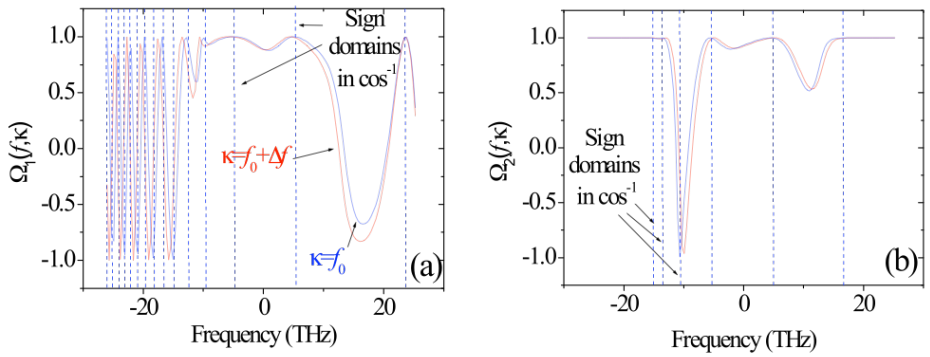

Fig. 6.4. (a) Function $\Omega_1(f,\kappa)$ and (b) $\Omega_2(f,\kappa)$ at $\kappa=f_0$ and $\kappa=f_0+\Delta f$. Dashed lines shows the division between domains where the function $\cos^{-1}\left[\Omega(f,\kappa = f_0)\right]$ alternates the sign.

Finally, by taking the results shown in Figures 6.3(b), 6.4(a) and 6.4(b), the phase increments can be calculated using equations 6.8 and 6.10 and from equations 6.9 and 6.11, the phases for both spectral components can be built up. Figures 6.5(a)-(b) show the calculated spectral phase obtained with our procedure.

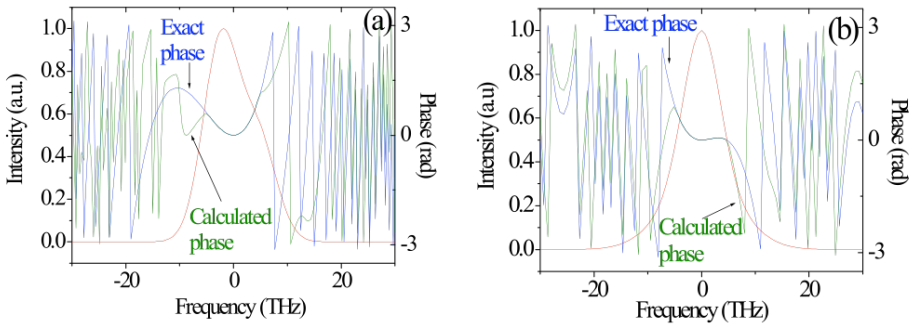

Fig. 6.5. Retrieved pulses (a) *E(f)* and (b) *G(f)* using equations (5.8) and (5.10) without alternate sign in when changing between the domains shown in Fig. 6.4.

As can be seen, the results only match with the exact phase within a certain region. This originates from not being able to determine the sign of the phase, which is caused by the sign indetermination related with the $\cos^{-1}(\Omega)$ function present in Eq. 6.8 and 6.10. Taking into account that $\cos^{-1}(\Omega)$ should change continuous along the frequency axis in the $[-\pi,\pi]$ range, the problem can be overcome identifying those points where $\Omega(f,\kappa)$ get close to 1 or -1 and there is an abrupt change in the slope. In these positions an alternate sign in the $\cos^{-1}(\Omega)$ function should be performed. The points dividing regions with different sign are highlighted in Figures 6.4(a) and 6.4(b) with dashed vertical lines.

After applying the criterion described above to equations 6.8 and 6.10, two possible solutions are available. Each solution corresponds to the positive or negative value of the sign chosen at the origin. However, care must be taken as only one of these solutions is correct. The correct solution, observed in Figures 6.6(a)-(b), results in the spectral phase correctly resembling the original phase, except for a small difference at negative frequencies. This difference is due to small errors in detecting the position of the sign change and can thus be easily improved. The second solution, when the alternative sign is chosen, greatly differs from the original phase (Fig. 6.6(c)-(d)). This second solution is a spurious solution of our equation system that correctly reproduces the component

at term $\kappa \approx f_0$ in Fig. 6.2(b). However, it is not solution of the complete interferometric trace. In particular, the pulses in Fig. 6.6(c)-(d) do not fulfils Eq. 6.4, that, as commented before, can be used as error-checking procedure. Experimentally, any source of errors, including the spurious solution, can be detected by numerically generating the interferometric trace using the retrieved pulses and comparing the result with the experimental trace. Equivalently, we can compare the interferometric correlations of the two solutions with the experimental one, which can be directly obtained from the interferometric trace time marginal. We have demonstrated this in Fig. 6.7. Here, the interferometric correlation corresponding to the solution in Fig. 6.6(a)-(b) is identical to the trace time marginal obtained by integrating the frequency axis of the interferometric trace in Fig. 6.2(a). Apart from the spurious solution, which can be rejected using the two checking procedures described above, we have not been able to detect other ambiguities as the ones present in XFROG and discussed in Ref. Seifert (2004).

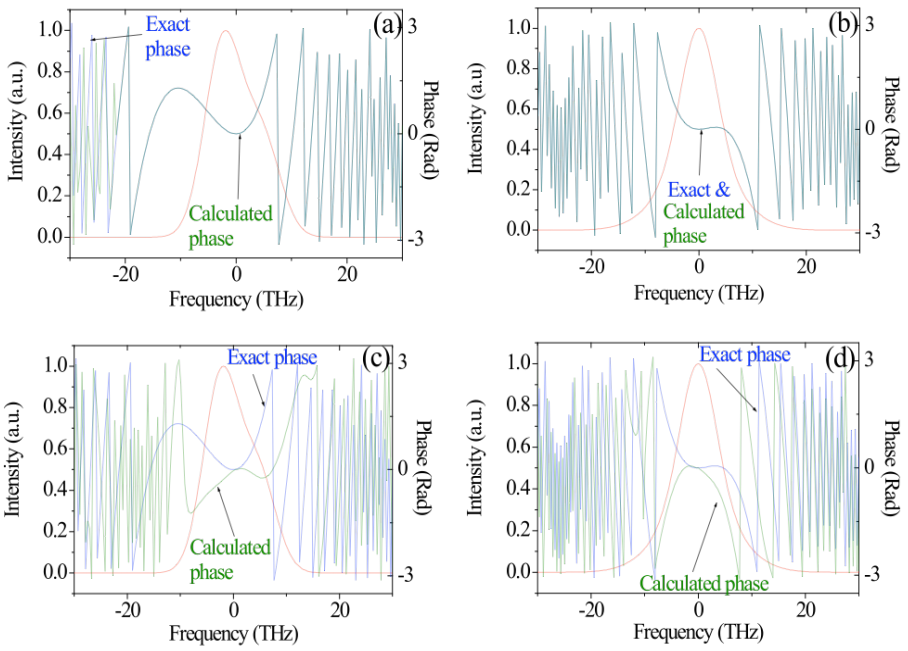

Fig. 6.6. Retrieved pulses alternating sign at the points shown in Fig. 4. Result (a) *E(f)* and (b) *G(f)* using the sign combination (+,-) in eq. (5.8) and (5.10). The spurious solution is shown in (c) *E(f)* and (d) *G(f)* using the (-,+) sign combination.

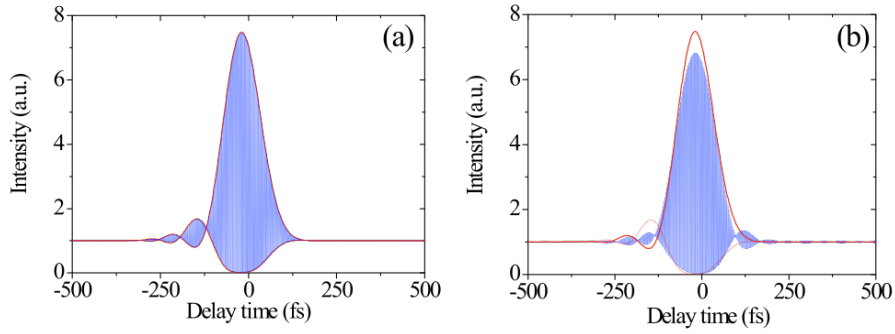

Fig. 6.7. *E(f)* and *G(f)* calculated interferometric correlations (blue) and envelope of the interferometric correlation obtained from Fig. 6.2(a) as the time marginal of the interferometric trace (red). (a) Result using the solution in Fig. 6.6(a)-(b). Here the red line coincides with the blue contour and is barely visible. (b) Result using the solution in Fig. 6.6(c)-(d)

The presence of noise in the experimental measurement can affect the phase extraction as noise increase the difficulty in determining the SSPs. As an example of the limits that noise impose to the technique we have added white Gaussian noise of 20 dB peak signal-to-noise ratio (SNR) to the slide R($f,\kappa \cong f_0$), shown in Fig. 5.3(a).

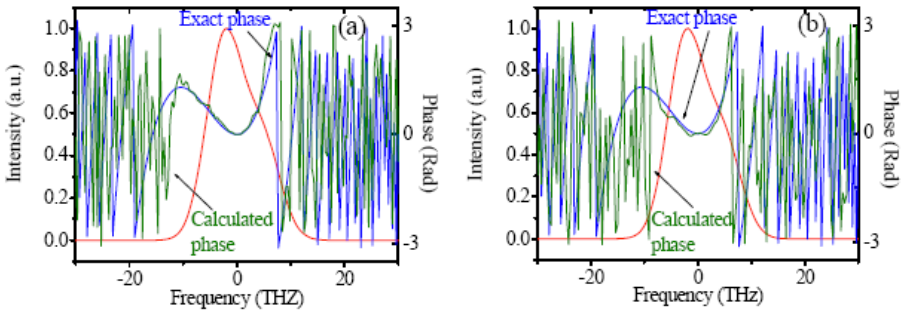

Fig. 6.8. Retrieved phase for a pulse with (a) 20 dB and (b) 13 dB SNR. Solution in (b) has been obtained by low band pass filtering the functions $\Omega_1(f,\kappa)$ and $\Omega_2(f,\kappa)$ in the frequency axis.

Under these conditions it was still possible to detect the SSPs and we were able to obtain the spectral phase inside the spectrum bandwidth Fig. 6.8(a). A further rising in the noise level, increased the difficulty in distinguishing the SSPs. To overcome this problem, we reject the high-frequency noise components by filtering the $\Omega_1(f,\kappa)$ and $\Omega_2(f,\kappa)$ functions in the f axis. This procedure allows the phase to be obtained at noise levels as high as 13 dB SNR, as shown in Fig. 6.8(b).

6.5 Other X-MEASUREMENTS

There are occasions in which one of the two pulses is known because it has been previously measured, and the algorithm can be simplified. Traditionally, this has been solved by using XFROG measurements.

The wealth of information contained within a collinear measurements allows finding several ways to obtain the unknown phase, which can be combined to better estimate the measured phase. Here, we present a few examples on how to proceed:

1. The direct approach is to follow the procedure reported by Reid (2000), and obtain the DC term of the collinear trace. Analytically and experimentally we have shown that this introduces a negligible error. Therefore, it is possible to apply the standard XFROG algorithm.

2. By exploiting the the component at the fundamental frequency $\kappa \approx f_0$ of $Y^{SHG}(f,\kappa)$ we can add an extra constrain, because we now know the gating pulse *g(t)*, to Equations 6.7(a) to 6.7(d) and solve Eq. 6.8 and 6.9 in a straight manner.

3. By exploiting the component at the second harmony frequency $\kappa \approx 2f_0$ of $Y^{SHG}(f,\kappa)$ we can directly solve equation 6.3.

6.6 Future directions of MEFISTO.

In Chapters 5 and 6 this dissertation presents MEFISTO, a new technique that offers an analytical and direct manner of measuring ultrashort laser pulses with a simple and general optical scheme. Last part of Chapter 5 focuses on describing a general formalism to unwrap the full pulse information of an unkown pulse from a single CFROG trace. This chapter 6 shows that it is possible extending such full characterization capabilities to two unkown pulses and it still maintains its analytical and directly measuring capabilities without any loss of generality.

Although one of the strengths of the MEFISTO is its ability of detecting errors in methodology through its extended marginals, it must be said

that the technique presented in this dissertation only utilizes two spectra to recover phase information. Therefore, one of the main advantages of the MEFISTO paradigm is that phase information is well repeated along all the fundamental term at $\kappa = f_0$, which would be similar to performing multiple SPIDER measurements. Therefore, more robust and more accurate techniques can be developed by using the best information available in the trace around this term, in this line, a later works was presented in 2007 (Hsu, 2007; Yang, 2009).

Similarly to the procedure explained in detail in 5.3 (Chapter 5, section 3) about CFROG (Amat-Roldan, 2004), for pulses that have a relatively narrow power spectrum compared to the optical wavelength, it is not necessary to resolve the interferometric fringes and apply Nyquist criteria on the delay step ($\Delta\tau < 1/4f_0$).

Importantly, this allows for a FAST-MEFISTO to be carried out at high rates without neither complex nor expensive set ups and without acquiring extensive datasets. As reported in the CFROG work, a simple undersampling criterion can be design to impose that $\kappa \approx f_0$ term is mostly preserved. Using a similar strategy, undersampling is used to demodulate the spectral terms of interest from Eq 6.6 and shown in Figure 6.2 (b), the new obtained sampling criterion is that substitutes Eq. 5.10:

$$\Delta\tau = (2n+1)/\left[2(f_0 \pm B_s)\right], \tag{6.18}$$

where n is an integer that will establish the reduction of required samples and B_s is the larger of the two pulse bandwidths to preserve the spectral term atr the fundamental delay frequency 5.13 as opposed to the DC term of section 5.3 of the previous Chapter.

As an example, two different pulses with 6.3*nm* and 5.*3nm* bandwidth at 800*nm,* following Nyquist criterion will require the use of a delay step $\Delta\tau = 0.65\ fs$. This results in a collection of 2151 spectra. However, by

undersampling at $\Delta\tau = 28.3\ fs$, only 50 spectra are acquired, a number of spectra 43 times lower (n=10 in Eq. 6.18), resulting in a fast and comparatively short dataset compared to the dataset obtained by following Nyquist.

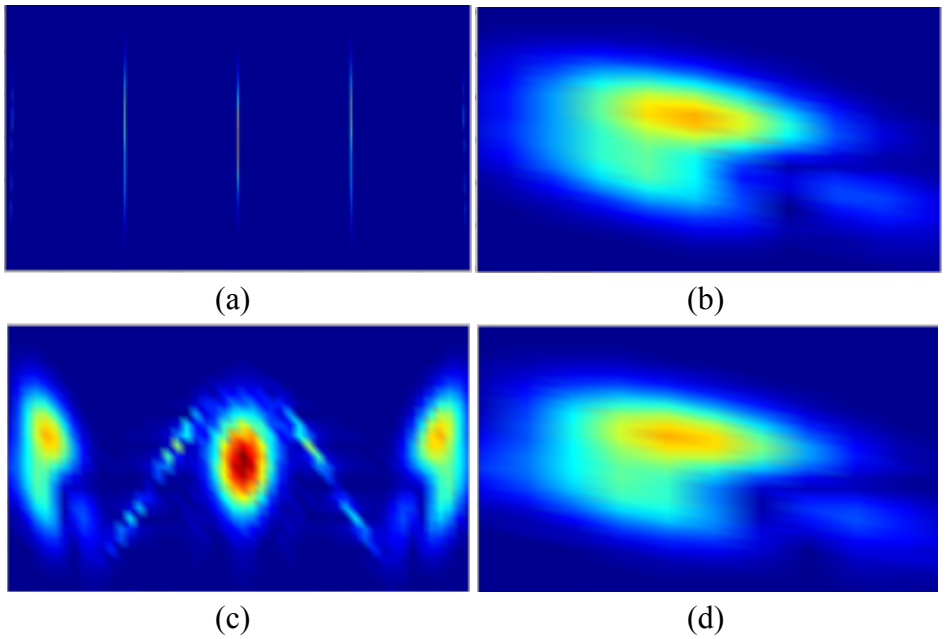

Fig. 6.9 Numerical results by computing MEFISTO at different sampling delay rates. (a) Transformed interferometric trace $Y^{SHG}(f,\kappa)$ and (b) the MEFISTO term, $Y^{SHG}(f,\kappa=f_0)$, when Nyquist criteria is applied (2151 spectra, 0.65 *fs* delay step). (c) Transformed interferometric trace $Y^{SHG}(f,\kappa)$ and (d) $Y^{SHG}(f,\kappa=f_0)$ when an undersampling using 28.3 *fs* delay step is performed (51 spectra, 43 times lower than following the Nyquist criteria).

Figure 6.9 shows how the transformed interferometric trace for the two cases and how the information for the MEFISTO term, i.e. Fig. 6.9(b) and (d), is preserved even after such a severe undersampling. Fig. 6.15 also shows how the maximum pulse bandwidth decreases when undersampling is performed, as the distance among different spectral terms of $Y^{SHG}(f,\kappa)$ become smaller.

6.7 Conclusions.

In this work we have outlined the theory and procedure of blind-MEFISTO and presented it as a method that allows the complex amplitude of two unknown ultrashort pulses with similar central frequency to be simultaneously obtained. Its time-frequency and interferometric ambivalent nature leads to a technique that possesses advantages and properties characteristic of interferometric techniques as SPIDER, as well as time-frequency measurements as FROG. In this sense, similar to interferometric techniques, the method enables the analytical extraction of pulse information without the need of an iterative retrieval algorithm. Similar to time-frequency techniques, it can be applied to simultaneously characterize two unknown pulses (blind MEFISTO) and enjoys extended error-checking capabilities. In addition, MEFISTO is based on a simpler experimental set up as it is based on a collinear arrangement.

MEFISTO techniques rely on Fourier analysis after obtaining a spectrally resolved interferometric correlation trace. In particular, we have described the general theory for blind-MEFISTO, pointing out the use of the different terms obtained during the theoretical development. Practical considerations have been discussed. These include spectral calibration, resolution (temporal and spectral), maximum bandwidth, sign uncertainty, possible problems with pulses whose spectra present abrupt changes, error checking procedures, and effect of noise. To manage these experimental limitations, a set of preliminary tools have been developed and explained. The analysis has also demonstrated that the method is not affected by some of the non-trivial ambiguities that are present in other techniques. The particular properties of the degenerate case have also been analyzed to highlight additional error-checking capabilities and self-calibrating techniques that help avoids errors entering the pulse measurement.

Finally, we want to stress that this is, to the best of our knowledge, the first analytical methodology capable to simultaneously characterize two unknown ultrashort laser pulses.

As future directions for MEFISTO we outline how to adapt the previously demonstrated methodology of FAST-CFROG. In this manner, FAST-MEFISTO can be also implemented in a similar manner to FAST-CFROG. A reduction of a factor of 40 has been showed which implies a faster characterization because it requires 40 times less samples (2150 to 50) and significantly smaller data sets which allows faster computation.
FAST-MEFISTO is then the final positive combination of interferometric and time-frequency techniques: direct phase measurement, robust error checking, self calibration and fast characterization. Future works beyond this thesis might include video rate characterization of pulses with appropriate optical set-up.

References

I Amat-Roldan, IG Cormack, EJ Gualda, D. Artigas, and P Loza-Alvarez. “Ultrashort pulse characterisation with SHG collinear-FROG,” *Opt. Express* **12** pp. 1169–1178 (2004a).

I Amat-Roldan, IG Cormack, P Loza-Alvarez, and D Artigas. “Starch-based second-harmonic-generated collinear frequency-resolved optical gating pulse characterization at the focal plane of a high-numerical aperture lens,” *Opt. Lett.* **29** pp. 2282–2284 (2004b).

I Amat-Roldan, IG Cormack, P Loza-Alvarez, and D. Artigas. “Measurement of electric field by interferometric spectral trace observation,” *Opt. Lett.* **30** pp. 1063-1065 (2005).

KW DeLong, R Trebino and WE White. “Simultaneous recovery of two ultrashort laser pulses from a single spectrogram,” *J. Opt. Soc. Am. B* **12** pp. 2463–2466 (1995).

C Hsu and S Yang. "Robustness Enhancement of Iteration-Free Spectral Phase Retrieval by Interferometric Second-Harmonic Trace," in *Conference on Lasers and Electro-Optics/Quantum Electronics and Laser Science Conference and Photonic Applications Systems Technologies*, OSA (2007).

AV Oppenheim and RW Schafer, Digital Signal Processing (Prentice-Hall, 1975).

DT Reid, P Loza-Alvarez, CTA Brown, T Beddard, and W Sibbett. "Amplitude and phase measurement of mid-infrared femtosecond pulses by using cross-correlation frequency-resolved optical gating," *Opt. Lett.* **25** pp. 1478–1480 (2000).

B Seifert, H Stolz, M Tasche. “Nontrivial ambiguities for blind frequency-resolved optical gating and the problem of uniqueness,” *J. Opt. Soc. Am. B* **21** pp. 1089-1097 (2004).

G Stibenz and G Steinmeyer, “Interferometric frequency-resolved optical gating,” *Opt. Express* **13** pp. 2617-2626 (2005).

S-D Yang, C-S Hsu, S-L Lin, Y-S Lin, C Langrock, and MM Fejer, "Ultrasensitive direct-field retrieval of femtosecond pulses by modified interferometric field autocorrelation," *Opt. Lett.* **34** pp. 3065-3067 (2009).

CHAPTER 7

Measuring ultrashort pulses inside a Multiphoton Microscope.

7 Measuring ultrashort pulses inside a Multiphoton Microscope.

7.1 Introduction.

The visualization of the internal structure of biological organisms is essential for the advance of life sciences. Great demands are placed on the field of microscopy to develop techniques that are able to image more complicated structures and find new sources of contrast. Multiphoton microscopy (Denk, 1990; Göppert-Mayer, 1931; Kaiser, 1961) has generated much interest within the scientific community because of its ability to generate new high-resolution, three-dimensional images with reduced phototoxic effects compared to one-photon confocal microscopes. This can be critical, especially in some applications, such as *in vivo* brain imaging. Remarkably, multiphoton microscopy is a promising and colourful tool due to its ability to find new sources of contrast, which are often label free, and with an extremely localized interaction, being then a contactless tool that has just emerged. Additionally, multiphoton processes can be employed to enhance current tools for microscopists and biomedical scientists, in order to produce new methods, which were previously unavailable (Potter, 1996; Denk, 1997; Zipfel, 2003): different types of imaging (Campagnola, 1999, 2003; Barad, 1997; Squier, 1998; Yelin, 1999; Débarre, 2006; Zumbusch, 1999; Cheng, 2002; Dudovich, 2002; Evans, 2008), accurate and delicate micro and nanosurgery (Berns, 1981; Koenig, 1995, 2000; Tirlapur, 2002; Uday, 2002; Sachihiro, 2004; Watanabe, 2004; Vogel, 2003; Shen, 2005; Heisterkamp, 2005), localized caging and uncaging of bioactive components (McCray, 1989; Callaway, 1993; Corrie, 1993; Denk, 1994; Katz, 1994; Pettit, 1997), electrical excitation of cells (Fork, 1971; Farber, 1983; Uzdensky, 1997; Smith, 2001, 2006; Hirase, 2002), gene transfection (Tirlapur, 2002; Zeira, 2003), optogenetics (Zemelman, 2002; Lima, 2005; Deisseroth, 2006; Miller, 2006; Arenkiel, 2007; Adamantidis, 2007; Zhang, 2008), etc.

Recent research regarding the underlying biophysics of multiphoton microscopy has shown how the temporal and spectral properties of the incident ultrashort pulse can have significant effects on the efficiency and selectivity of multiphoton processes (Dudovich, 2001; Kawano, 2003; Bardeen, 1999; Pastrick, 2003; Dela Cruz, 2004; Chen, 2002; Ogilve, 2006; Tang, 2006). In some of these works devoted to two photon excitation fluorescence (TPEF), the phase of an ultrashort pulse was arbitrarily altered until the desired two-photon fluorescence signal was optimized. Surprisingly, the optimum input pulse phase at the microscope objective contained a remarkable complex structure. This strongly suggests that the pulse at the sample was not transform limited (flat phase) as was thought. Yet little is known about this phase-dependent optimization process, and there is a great urgency to develop adequate tools to help in understanding it. Direct phase measurement of pulses at the sample plane of a microscope is thus required.

Under a context-free viewpoint, in which experimental set up is disregarded or pulse characterization, due to its complexity, is the experimental challenge by itself, sonograms are sometimes suggested as a better choice for full characterisation because the measurement occurs at detection. Although this can be extremely useful in some situations because it simplifies the optical setup; this actually imposes a limit in some others, such as characterization at the sample plane of a multiphoton microscope.

For example, sonograms would require putting a detector at the sample plane that seems a technological challenge. Instead, a spectrogram would require having some type of nonlinear response in a specimen to act as a probe. This confinement of the interactions, allows a simpler way to "select" what we want to measure. However, completely accurate measurements would require complete knowledge of the nonlinear response of the material, which might be also a challenge. In this chapter, we report a simple and efficient material as well as different characterisation techniques to overcome this situation.

7.1.1 The problem.

Two main problems arise when full characterization of pulses going through a high-numerical-aperture (NA) objective lens is desired. Firstly, a collinear geometry is imposed because the NA has to be completely filled in order to measure tightly focused traces and not cross correlations between different angular components that travel different thicknesses through all the optical system (Fittinghoff, 1998, 1999). The collinear geometry generally restricts the pulse measurements within multiphoton microscopy to the use of interferometric autocorrelation (Millard, 1999; Muller, 1995a, 1995b). This, however, provides no direct phase information on the pulse as seen in chapter devoted to the state of the art of ultrashort pulse characterization.

Secondly, severe requirements are imposed on the nonlinear medium as explained below. Pioneering research based on the well-known frequency-resolved optical gating (FROG) technique (Kane, 1993) showed how to characterize pulses at the sample plane by means of type II phase-matching collinear geometry is required and additional optical elements (Fittinghoff, 1998, 1999) as shown in the original's Fittinghaff's figure in Fig.7.1. In spite of using this complex setups, cross-polarization of the beams is never perfect and this leads to residual interference fringes appear that need to be filtered out, too.

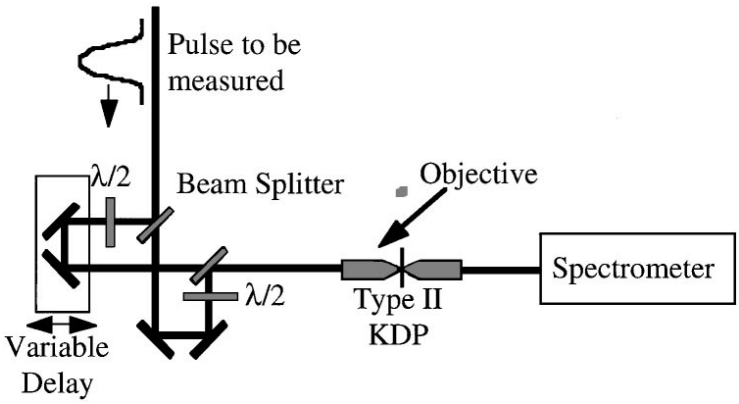

Figure 7.1. Schematic and figure acknowledged from Fitthinghoff (1998) to measure a collinear type II SHG FROG. This schematic is similar to an interferometric SHG FROG, ex- cept that there is a 90º polarization rotation between the two arms (achieved by placement of a half-wave plate in each arm) and that the device uses a type II crystal, potassium dihydrogen phosphate (KDP) in this experiment.

Therefore, CFROG is a more direct approach that avoids such complex setups and requires similar post-processing steps steps. Recently, CFROG has been used to measure one of the shortest pulses generated and has been published in Nature Photonics by other authors (Krauss, 2009).

Unfortunately, several additional difficulties are present when one tries to measure such a trace through a high-NA lens by using conventional nonlinear crystals. First, at the focal point the polarization of the fundamental beam is modified owing to the extremely steep convergence angles (Pawley, 1995). Second, there is an intrinsically large range of incident angles at the focal plane caused by high NAs. Finally, the large frequency bandwidth associated with ultrashort laser pulses requires the phase-matching bandwidth of the nonlinear medium to be large. All the problems cited above make the use of traditional nonlinear crystals error prone. To overcome these difficulties, the use of other nonlinear media has been explored. One of these options is the use of nonlinear fluorescent dyes (Quercioli, 2004). These dyes, however, are subject to photobleaching. It has also been reported that protein polymer chains,

such as bacteriorhodopsin, have been used to generate the required second-harmonic signal (Bouevitch, 1995). This technique, however, requires complex preparation of the medium.

7.1.2 Reported solution.

In this chapter we present MEFISTO (Amat-Roldan, 2005, 2006) and CFROG (Amat-Roldan, 2004) as simple and elegant techniques with which to characterize a pulse at the focal plane of a high-NA objective lens, solving the problems that we described above. These techniques are further complemented by the use of starch granules suspended in water as a novel nonlinear medium that overcomes the problems mentioned above.
The use of a recently reported data processing procedures (MEFISTO and CFROG) to successfully extract phase information from spectrally resolved collinear autocorrelations of an unknown pulse is explained in detail in the previous chapter.

Starch has been shown to have a naturally high $\chi^{(2)}$ coefficient (Fischer, 2000; Chu, 2002). Second-harmonic signals were previously generated from starch with ultrashort laser pulses with wavelengths of 700–1300 nm (Chen, 2002). These results are highly significant because they demonstrate the extremely large spectral range in which starch can be used. In this sense, the small sizes of these granules (approximately 5-10 μm) provide them with a naturally large bandwidth.
Furthermore, as starch is a chiral material: 1) it naturally possesses high $\chi^{(2)}$ coefficient, 2) it is possible to obtain efficient SHG at different polarizations and Numerical Apertures. Although this is not ideal, it allows obtaining an averaged measurement with a manifold of incident angles and polarizations. Together with these natural physical properties, it is also important to highlight a practical advantage: Starch is ideally suited for working within a microscope because a drop of the starch suspension in water can simply be sandwiched between two coverslips

and placed directly within the focal plane of a high-NA lens (or at the sample plane of the nonlinear microscope). All these properties make starch ideally suited for the high demands that are placed on a nonlinear medium that is being used to characterize pulses through a high-NA objective lens. To verify that starch can be successfully used for characterizing ultrashort pulses we proceeded to obtain a CFROG trace of pulses at the focal plane of high-NA objective lens. The general optical arrangement for measuring a starch-based second-harmonic generation (SHG) CFROG trace is shown in Fig. 7.2.

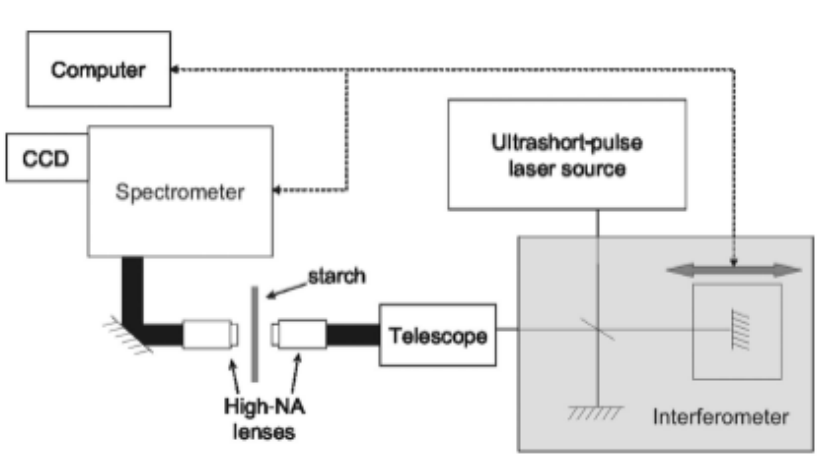

Fig. 7. 2 Schematic of the CFROG optical arrangement.

A telescope arrangement was used at the output of the interferometer and before the microscope objective to ensure that the beam filled the entire input aperture of the objective lens. A starch suspension in water was prepared and sandwiched between two coverslips. As the second-harmonic is generated from a single starch granule, precision in the preparation is not critical (a pinch of starch and a drop of water as shown in Fig. 7.3).

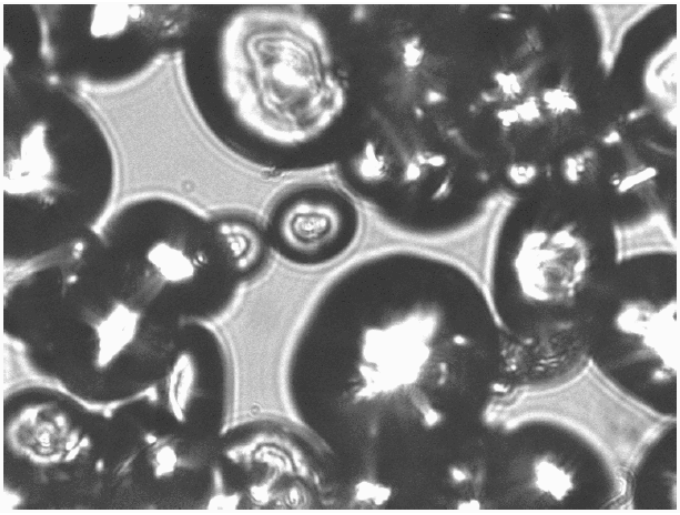

Fig. 7.3 Image of granule starch at focus from microscope using NA=1.25.

7.2 Forward characterization with CFROG.

In this experiment, we used CFROG to characterize the ultrashort laser pulse at the sample plane by acquirind the forward SHG signal generated from starch. The suspension of starch was placed at the focus of a high-NA (NA 1.25) lens. Refractive-index matching oil was used to ensure full use of the NA of the lens. Another lens was used to collimate the generated frequency-doubled signal, which was then sent to the spectrometer after passing through a BG39 filter. The interferometer and the spectrometer were both controlled by the computer. A backthinned CCD linear array (Hamamatsu HC230-1007), operated in vertical binning mode, was attached to the spectrometer to record the spectrum of the SHG signal. The pulses were generated from a Kerr-lens modelocked Ti:sapphire laser (repetition rate, 76 MHz) that was operating at a central wavelength of 835nm. The pulses entering the objective lens had an average power of 15 mW. The second-harmonic signal was generated only when the pulses were focused upon a granule of starch. We then acquired the CFROG trace (shown in Fig. 7.4(a)), obeying the

undersampling criteria outlined in (Amat-Roldan, 2004) corresponding to 220 sample points with delay steps of 7.58 *fs*. It should be noted that the CFROG trace is in fact an undersampled frequency-resolved interferometric autocorrelation.

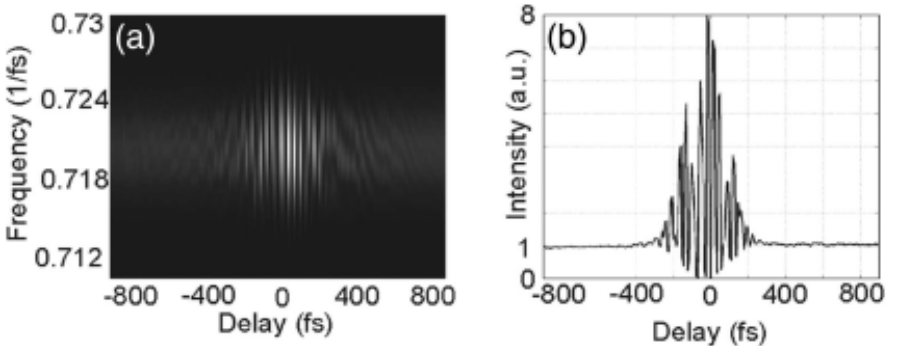

Fig. 7.4 (a) CFROG trace and (b) its time marginal spectrum obtained at the focus of a 1.25-NA lens.

Consequently, by integrating the CFROG trace in time (Fig. 7.4(b)) we can obtain the envelope of the interferometric autocorrelation and verify its validity by ensuring that there is the required 8:1 ratio. This result in itself demonstrates the effectiveness of starch as a nonlinear medium when high-NA lenses are used. The CFROG trace was then filtered (Amat-Roldan, 2004) and retrieved with a traditional SHG FROG retrieval algorithm explained in Chapter 5. The experimental and retrieved traces are presented in Fig. 7.5, along with the retrieved pulse and spectrum. We further checked the validity of the retrieved data by comparing them with the time marginal and the experimentally measured spectra. These spectra are shown in Fig. 7.6, where excellent agreement can be observed.

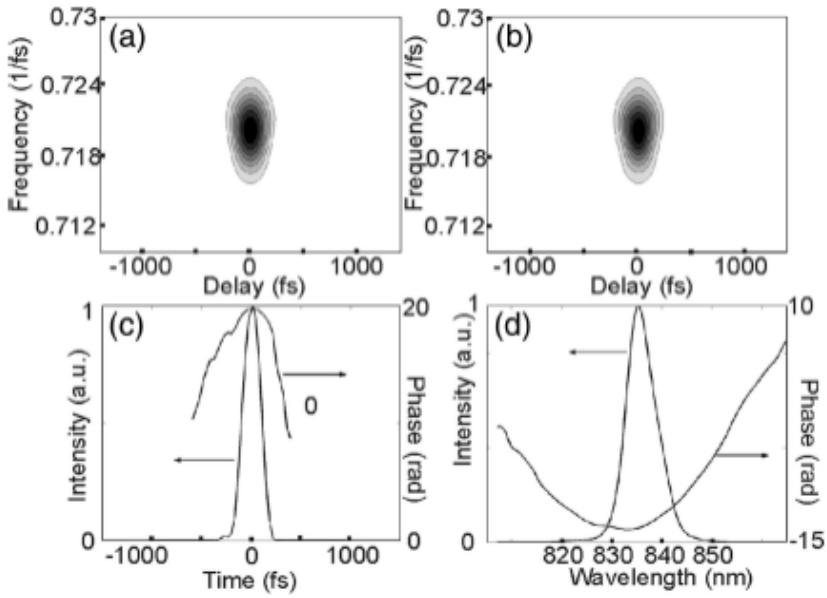

Fig. 7.5. Experimentally retrieved pulses at the focal plane of a 1.25-NA objective lens. (a) Fully f iltered CFROG trace, (b) retrieved trace, (c) amplitude and phase and (d) spectrum and phase of the retrieved pulse. The rms error of the traces is $G=8\cdot10^{-5}$.

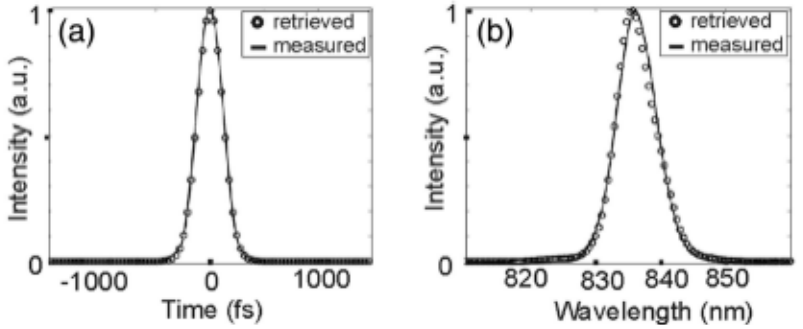

Fig. 7.6 Comparison of experimental and retrieved pulses (λ = 835 nm) at the focal plane of a 1.25-NA lens. (a) Time marginal and retrieved intensity autocorrelation. (b) Measured and retrieved spectra.

To further investigate the use of starch as a nonlinear medium we proceeded to characterize the output pulses from a home-made

synchronously pumped optical parametric oscillator (Loza-Alvarez, 1999) operating at 1100 nm shown in Figure 7.7. To do this, we used an objective lens with a NA of 0.85. In this case we used a delay step of 42.6 fs and produced 96 samples. The resultant CFROG trace was again filtered to produce a non-collinear SHG FROG trace and then retrieved. The result of this retrieval is shown in Fig. 7.8. As above, to validate the data we compared the retrieved results with externally measured data. Figure 7.9 shows the excellent agreement obtained.

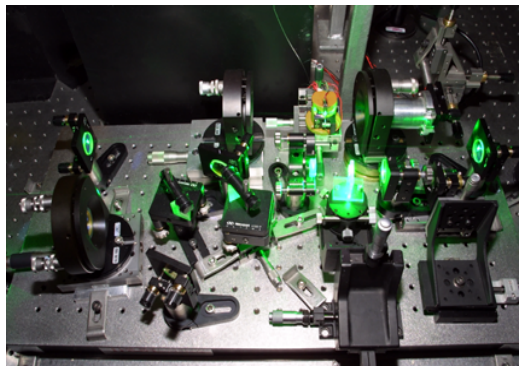

Fig. 7.7 Custom-made synchronously pumped optical parametric oscillator operating at 1050 – 1150 nm pumped with the Coherent Mira 900.

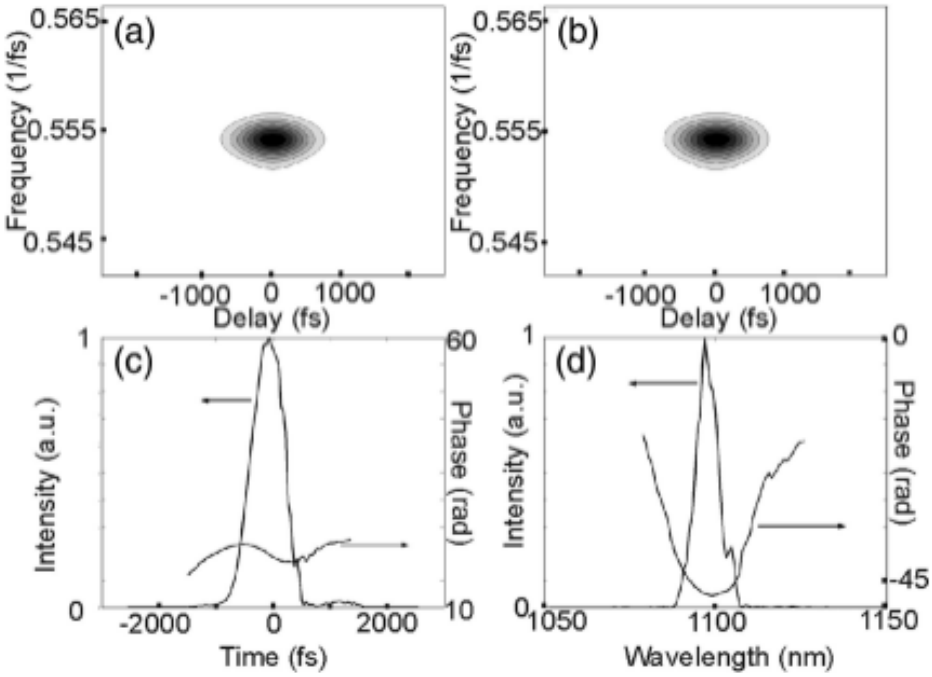

Fig. 7.8 Experimentally retrieved pulses at the focal plane of a 0.85-NA objective lens. (a) Fully filtered CFROG trace, (b) retrieved trace, (c) amplitude and phase, and (d) spectrum and phase of the retrieved pulse.

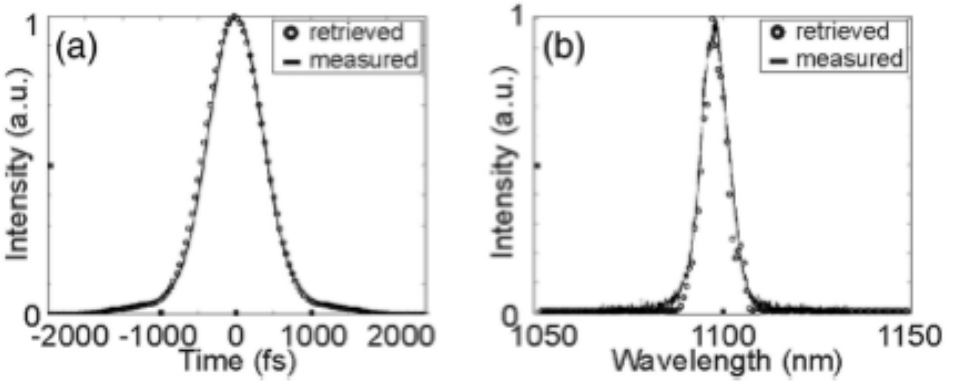

Fig. 7.9 Comparison of experimental and retrieved pulses (λ = 1100nm) at the focal plane of a 0.85-NA lens. (a) Measured time marginal and retrieved intensity autocorrelation. (b) Measured and retrieved spectra.

The results of both experiments confirm that starch can be successfully used with a wide range of wavelengths to characterize pulses with different characteristics at the focal plane of a high-NA lens in an easy and quick way.

7.3 Relevance of the forward characterization.

Prior to this forward characterization was released (Amat-Roldan, 2004b), several important groups were trying to measure ultrashort pulses at the sample plane. Initially, some of them reported measurements, in general autocorrelations at the focus (Cannone, 2003; Müller, 1998). However, their successful measurements required assuming different constraints on the pulse working at high NA objectives, such as quadratic phase modulation (linear chirp).

The first successful characterization with no assumptions of a tightly focused ultrashort pulse was done by David Fittinghoff from Trebino's group. In 1998, they published an excellent work titled "Collinear type II

second-harmonic-generation frequency-resolved optical gating for use with high-numerical-aperture objectives" where they used type II phase-matching to partially remove the interferometric fringes from a collinear FROG trace (Fittinghoff, 1998). They performed an immaculate FROG retrieval on 22 *fs* pulses at NA=0.4, which is just above paraxial approximation. One year later, another excellent work was reported by Fittinhoff were an actual high NA=1.25 microscope objective from Carl Zeiss was employed and pulses passing through it were successfully retrieved (Fittinghoff, 1999). This technique, however, has a critical limitation: type II phase matching condition. This importantly adds important drawbacks: 1) addition of optical elements is a source of experimental errors, 2) future polarization resolved measurements are not possible or can become too complex (Brixner, 2001; Suzuki, 2004; Silberberg, 2004), 3) it still requires digital filtering to complete remove some remanent interferometric fringes, otherwise, FROG algorithm might stagnate or give an erroneous retrieval, and the most important, 4) a type II nonlinear crystals are difficult to be found in a biomedical lab (toxicity, easy to break, very expensive,...). On the contrary, starch is disposable, extremely cheap, non-toxic, polarization sensitive, among other virtues to be foreseen.

7.4 Backwards characterization with specimen and comparing CFROG and MEFISTO.

In this section, we report the significant SHG signal generated from starch granules in the backward direction and its use to obtain information of ultrashort pulses interacting with the specimen inside a high resolution (high NA) multiphoton microscope. Backward SHG provides an extremely simple way to measure the SHG-autocorrelation trace from an unmodified TPEF microscope. With the simple addition of a spectrometer to the output port of the microscope, which is unnecessary in some commercial models, it is possible to spectrally resolve the

autocorrelation trace. This frequency-resolved SHG autocorrelation can then be processed to fully characterize the pulse. This can be done using several techniques such as CFROG (Amat-Roldan, 2004) or IFROG (Stibenz, 2005). However, these need an iterative retrieval algorithm to obtain the pulse information, adding complexity to the methodology. We decided to use the MEFISTO (Amat-Roldan, 2005, 2006) technique, which allows direct extraction of the pulse in an analytical way and it has more potential to be carried out at video rates.
The use of backward propagating SHG from starch granules is especially important in multiphoton microscopy because the same epi-detection scheme can be used to collect both the TPEF and SHG signals making starch ideally suited to work with in a TPEF microscope. Additionally, there are several significant practical advantages of using starch as a nonlinear medium. Apart from being cheap, and non photo-bleaching, it is also non soluble and non-toxic, so it can be added into the culture medium where the specimen is.

Importantly, preparation of the experiment was mainly carried out by Anisha Thayil as reported in her work (Thayil, 2008) and her thesis but pulse measurement was carried out by the author of this thesis.
In order to show that *in-situ* pulse information can be obtained while imaging, two different situations were examined. In the first one, we added a very small quantity of starch granules into a dish of live HeLa cancer cells (GFP labeled). In the second, starch granules were placed alongside a more complex organism, a C. elegans that was prepared for in-vivo neuron imaging (GFP labeled on D-type neurons). The granules embedded in this way were 5 approximately 5-10μm in size. The non-toxic and non soluble nature of starch allows it to be among living cells or the organisms without affecting them in any way. A schematic diagram of the optical arrangement used in this experiment is shown in Fig. 7.10.

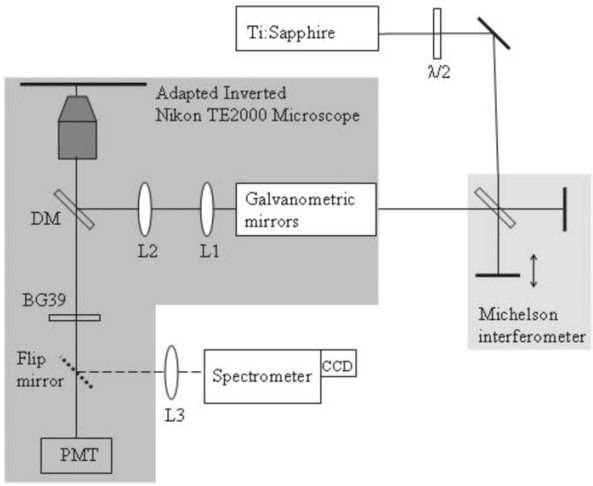

Fig. 7.10. A schematic diagram of the experimental set-up (image acknowledged from Thayil 2008).

Imaging was performed on an adapted inverted microscope (Nikon TE2000-U) with the optical scanning being performed by a pair of galvanometric mirrors. A X60 oil immersion objective lens (NA 1.4, Nikon Plain Apo-Achromatic) was used throughout the experiment. The ultrashort laser pulses were produced from a mode locked Ti: Sapphire laser (MIRA 900f) which was set at a central wavelength of 840 nm and a repetition rate of 80 MHz. The pulses were sent through a Michelson interferometer before entering the microscope. A telescope arrangement was used to ensure that the beam filled the entire aperture of the objective lens. The generated TPEF signal from the cells and the backward SHG from the starch granules were collected in the backward direction via the same objective lens. The signals were then passed through the hot mirror, a BG39 filter and onto the photomultiplier tube.

In order to compare the SHG signal from starch granules emitted in the forward and backward (epi-) directions we used an additional mount for forward direction as well. This mount was equipped with a collecting objective (1.25NA), a band pass filter centered at 420nm and a photomultiplier tube. Fig. 7.11 shows the combined forward and backward collected SHG images of the starch granules for different

polarizations of the fundamental beam. The images correspond to a plane passing through the center of the granule. In this plane, the signal in the backward direction originates only from the edges of the granule and does not overlap with the forward signal originate from inside the granules. Interestingly, both, the forward and backward SHG signal can be generated in starch for any laser polarization. Compared to the use of crystals, which would require perfect alignment for satisfying phase-matching conditions, this more relaxed polarization dependence makes starch ideal for pulse characterization inside a microscope.

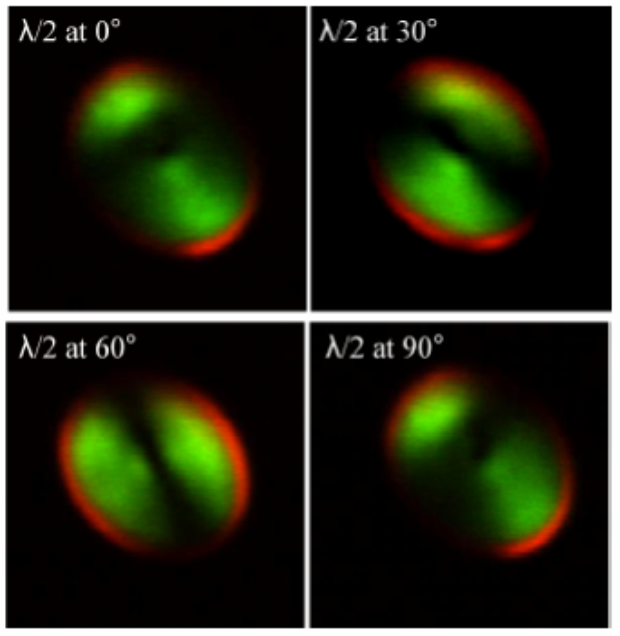

Fig. 7.11 SHG images of starch granules detected in the forward (green) and backward (red) directions for different polarizations (image acknowledged from Thayil 2008).

This observation of backward SHG signal from starch granules could be due to backward scattering, since starch is a highly scattering medium (Mertz, 2001). In addition, the possibility of backward phase matching in starch (possessing semi-crystalline shells of approximately 10 nm of thick 7 amylopectin side chain clusters (Gallant, 1997) , cannot be neglected as it has been shown that nearly equal forward and backward

phase matching occurs when objects have an axial size less than $\lambda_{SHG}/10$, which is approximately 40 nm (Moreaux, 2000; Williams, 2005; Psilodimitrakopoulos, 2007). However, these fail to explain the lack of a signal generated in the forward direction. The exact nature of the backward SHG signal from starch granules is not within the scope of this contribution and needs further investigation (Psilodimitrakopoulos, 2007, 2008).

Having a better understanding of the capabilities of starch to generate SHG signal in the backward direction, we proceeded to perform *in-situ* pulse characterization and imaging. Removing the forward collecting mount (experimental arrangement as depicted in Fig. 7.10) and blocking one of the interferometric arms, it was possible to simultaneously acquire both the backward SHG and the TPEF to obtain image of both the starch and the cells. Cancer cells are highly prone to contaminations but we found that the addition of starch granules do not affect them in anyway, strongly supporting the use of starch for this kind of applications. Figure 7.12(a) shows a photograph of the cell and starch mixture which has been overlaid with the summed SHG and TPEF image. We confirmed that the SHG signal (at 420 nm) was only generated when the laser was focused upon a granule of starch and the TPEF signal from the cancer cells was observed with a central wavelength of 510 nm (Fig. 7.12(a)). Similarly, we simultaneously epi-detected the TPEF signal from the neurons of C.elegans and SHG signal from starch granules (Fig. 7.12(b)). To show the contour of the granules, images taken with different polarizations had been added. Here again, presence of starch granules in the culture medium of the C.elegans does not affect the development of the organism. To check that we were indeed observing the combined signals we replaced the PMT with a spectrometer (Jobin Yvon, Triax 180) and a back-thinned CCD linear array (Hamamatsu, HC 230-1007) to measure the different spectra that was being generated. Importantly, in both cases, the two signals were well separated from one another as shown in Fig. 7.12(c). (c) The spectra of the observed signals; TPEF (red) and SHG (green).

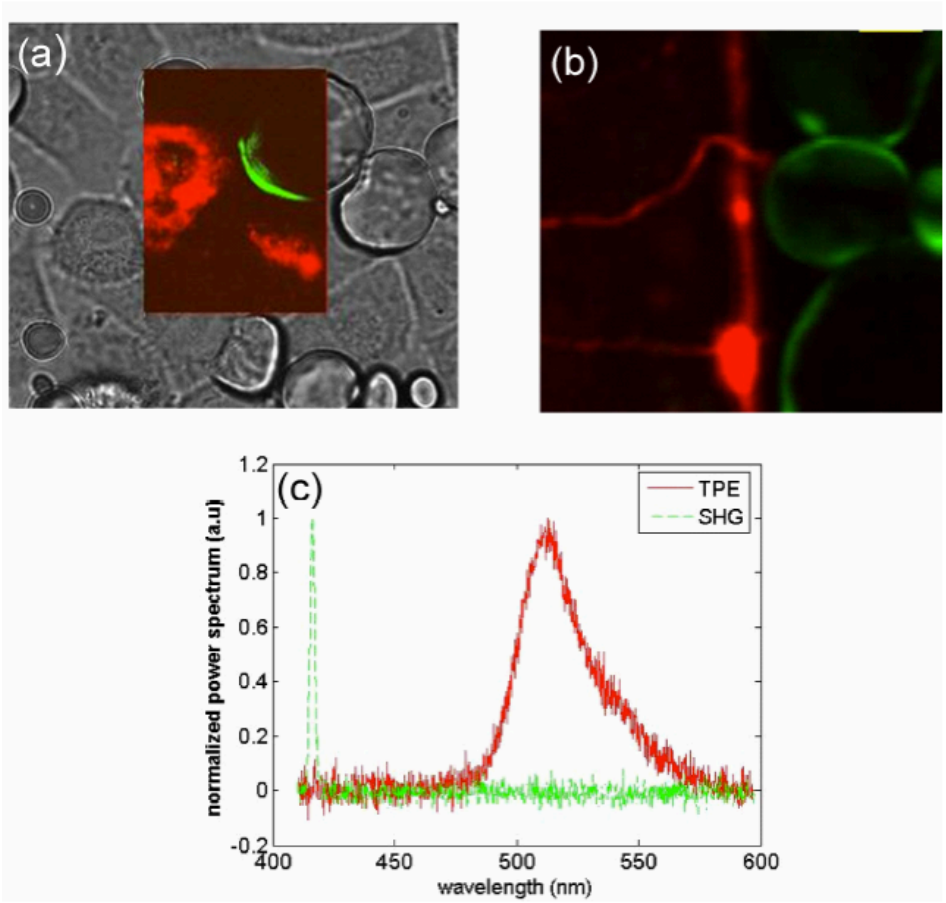

Fig. 7.12 (a) Image of the HeLa cells together with the starch granules. The inset shows the TPEF signals from cancer cells (red) and the backward directed SHG signals (green) from a starch granule. (b) The epi-detected TPEF image of the C.elegans neurons (red) and SHG image of the starch granules (green).

To characterise the pulses, we focused the beam onto one of the starch granules that lies on top of the living cells or besides the C. elegans. SHG autocorrelation can be directly measured by rapidly scanning one of the interferometric arms while recording the output voltage of the PMT. To fully characterize the pulse, we used a spectrometer at the output port of the microscope to obtain the interferometric spectrally resolved autocorrelation. This trace is then treated in order to be able to use the MEFISTO technique to retrieve the pulses. To support the effectiveness

of the MEFISTO technique we compared the results with the more conventional Collinear SHG-FROG (CFROG) technique. The same experimental data is used in both cases. Fig. 7.13 shows the numerical interferometric autocorrelations obtained from MEFISTO and the CFROG techniques and are compared with the experimentally acquired one. In both cases there is an excellent overlap showing the validity of both retrievals.

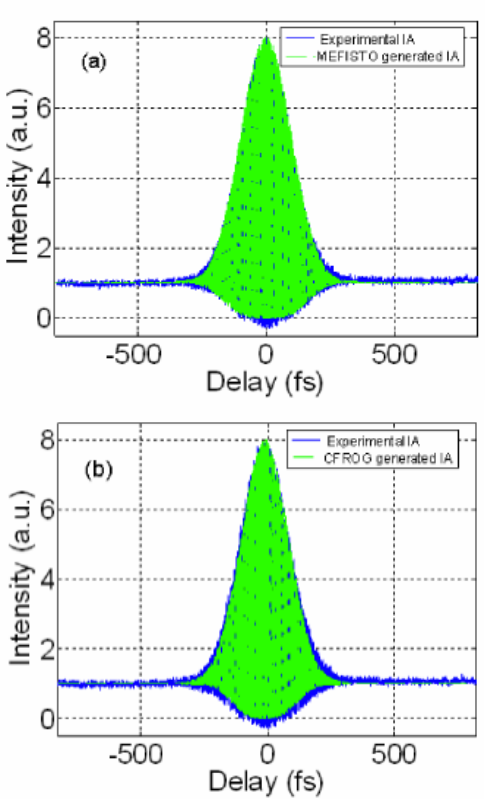

Fig. 7.13. Interferrometric autocorrelations. (a) from MEFISTO and (b) from CFROG.

The retrieved temporal intensity, spectral intensity and phase profiles of the pulse at the sample plane of the microscope are displayed in Fig. 7.14. The results obtained using both characterization techniques are in good agreement except for the spectral intensity and phase profiles. Retrieved spectral intensity profiles were validated by comparing them with experimentally measured data (Fig. 7.14(b)). The spectral intensity

profile obtained by using MEFISTO technique shows a better agreement with the measured spectrum. The small disagreement of the spectrum obtained with CFROG might be attributed to the averaging effect introduced by the iterative algorithm.

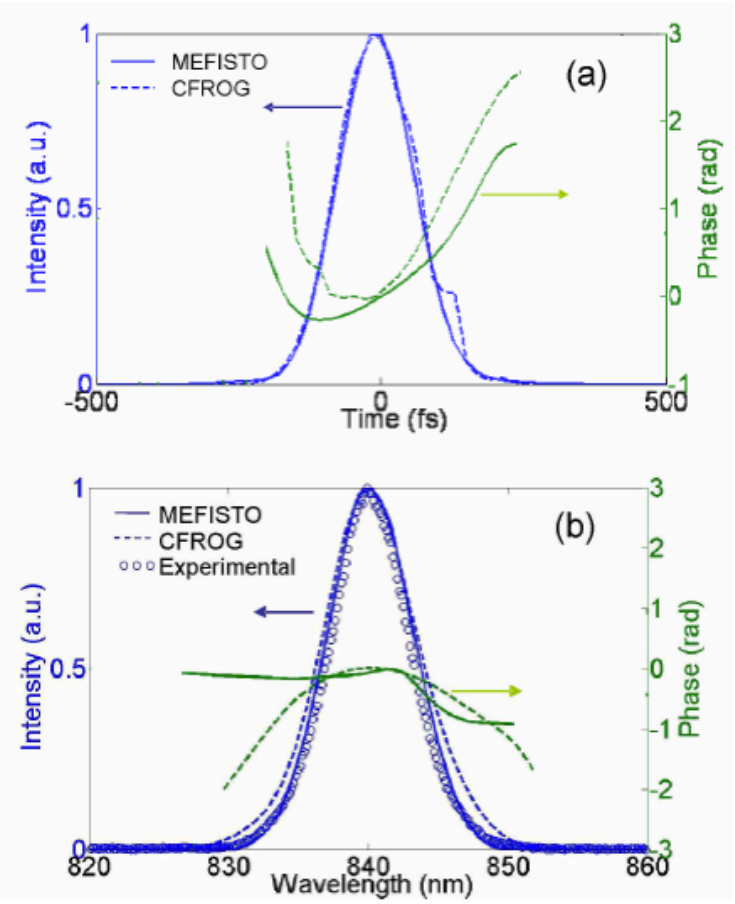

Fig. 7.14. Retrieved phase and intensity profiles of the pulse at the sample plane of the microscope obtained with MEFISTO (solid line) and standard CFROG procedure (dashed line): (a) temporal intensity and phase. The temporal width (FWHM) of the pulse at the sample plane is 163fs. (b) The measured spectrum (circles) and the retrieved spectral intensity and phase profiles

7.5 Conclusions.

In conclusion, in this chapter we have demonstrated a few successful full characterizations of ultrashort pulses at the focal plane of a high-NA objective lens in forward and backward directions and at different wavelengths with a clear potential to be included in a biomedical lab.

In the forward direction, we achieved this goal in two steps: first, by the use of CFROG, a recently reported method that permits the use of collinear geometry and second, by introducing the use of starch as a nonlinear medium.

In the backward direction, we also succeeded in detecting SHG signal from starch with no additional optical mounts in a commercial microscope and using more recent ultrashort pulse measurement technique: MEFISTO, and also CFROG, both reported in this thesis.

The use of a starch-in-water suspension has been shown to be highly suitable for the characterization of pulses at the focal plane of high-NA lenses. This is possible because the generation of the nonlinear signal in such a medium is not highly dependent upon polarization and angle at a single spot location. Smooth changes in the nonlinear tensor can occur, as shown by the SHG polarization dependence of starch in Figure 7.11, due to small motions of the starch granule, which are seldom and can be averaged out by the behaviour of the whole trace. Although it is not perfect, starch granules also average different angular and polarization components to provide an averaged estimation of the pulse. More accurate measurements, if needed, can be readily designed by simply taking into account strict angular and polarization dependence of the SHG signal in starch granules.

Moreover, we have shown the large bandwidth of starch by characterizing ultrashort pulses at two different wavelengths, confirming earlier reports that it can be successfully used from 700 to 1300 nm. The proven characteristics of starch will allow the technique to characterize pulses with far larger bandwidths than described here, even with the large acceptance angles that a high NA objective lens possesses.

In summary, starch importantly overcomes all inherent difficulties associated with thin nonlinear medium used in previous techniques; this material is a simple, nontoxic, easy-to-store, nonphotobleaching, easy-to-obtain, cheap, and easy-to-handle medium for the full characterization of ultrashort pulses at the sample plane of a multiphoton microscope. Remarkably, from the life sciences viewpoint, the addition of starch to the sample of study, being a nontoxic and non-soluble material, does not affect living cells or organisms allowing the pulse characteristics to be measured in-situ, without the need to move back and forth the sample, which is a source of errors and an important limitation to achieve video rate measurements.

The final procedure presented in this chapter, in which backward SHG signals from starch granules are collected, is a nearly ideal approach for pulse characterization within a TPEF microscope at the current state of the art. Both the fluorescence and SHG signals can be collected using the same epi-detection scheme, helping to considerably simplify the experimental arrangement. This importantly means that no alteration to a standard TPEF microscope is required for a complete characterization of pulses at focus, making it handy with no bulky parts required.

We further highlight the use of MEFISTO technique as a simple (non iterative) and self-consistent method specially suited for characterizing pulses in a multiphoton microscope with a clear potential to achieve video rates regime.

All these developed means, offer different approaches to characterise ultrashort pulses at the sample plane of a multiphoton microscope. This was the focus of this thesis as the subsequent step is to accurately shape the pulses and exploit multiphoton processes in different manners as explained at the begining of the chapter. Spatiotemporal shaping of pulses holds a big promise to control light-matter interactions in both accurate and precise manner. There are many articles that describe how selective fluorescence can be achieved, enhancement of SHG, even CARS can be achieved by pulse shaping. Other works relate shaped light to quantum control and tuning of chemical reactions. Although these are

extraordinarily challenging and difficult goals, they remain out of reach for researchers at subcellular level (or diffraction limited) without the necessary means to characterize pulses at high NA. In this sense, MIIPS, the technique explained in the state-of-the-art combines both pulse characterization and shaping. However, it is still an iterative algorithm and requires compensating the pulse to achieve full characterization. Additionally, MEFISTO can be implemented with a Spatial Light Modulator (SLM) after minor modifications and allow pulse characterization and shaping in a more direct manner. In the latter years, pulse characterization at the sample plane of multiphoton microscopy has not experienced any significant advance. Most microscopists that understand the unique features of ultrashort pulses simply compensate second order dispersion (maybe third in some cases) to achieve temporally narrow pulses at the focal plane, or simply approach to maximize detected signal. This is probably because SLM are still complex to use and most microscopist address biological problems, which are complex and currently have a more specific impact.

References

AR Adamantidis, F Zhang, AM Aravanis, K Deisseroth, L de Lecea. Neural substrates of awakening probed with optogenetic control of hypocretin neurons. *Nature* **450** pp. 420-424 (2007).

I Amat-Roldan, IG Cormack, P Loza-Alvarez, and D Artigas. "Measurement of electric field by interferometric spectral trace observation," *Opt. Lett.* **30** pp.1063-1065 (2005).

I Amat-Roldan, D Artigas, IG Cormack, and P Loza-Alvarez. "Simultaneous analytical characterisation of two ultrashort laser pulses using spectrally resolved interferometric correlations," *Opt. Exp.* **14** pp. 4538-4551 (2006).

I Amat-Roldan, IG Cormack, E Gualda, D Artigas, and P Loza-Alvarez. "Ultrashort pulse characterisation with SHG collinear-FROG," *Opt. Express* **12** pp. 1169-1178 (2004a).

I Amat-Roldan, IG Cormack, D Artigas, and P Loza-Alvarez. "Starch-based second – harmonic–generated collinear frequency-resolved optical gating pulse characterization at the focal plane of a high-numerical-aperture lens," *Opt. Lett.* **29** pp. 2282-2283 (2004b).

BR Arenkiel, J Peca, IG Davison, C Feliciano, K Deisseroth, GJ Augustine, MD Ehlers, G Feng. In vivo light-induced activation of neural circuitry in transgenic mice expressing channelrhodopsin-2. *Neuron* **54** pp. 205-18 (2007).

Y Barad, H Eisenberg, M Horowitz and Y Silberberg. Nonlinear scanning laser microscopy by third harmonic generation. *Appl. Phys. Lett.* **70** pp. 922-924 (1997).

CJ Bardeen, VV Yakovlev, JA Kent, R Wilson, SD Carpenter and PM Weber. Effect of Pulse Shape on the Efficiency of Multiphoton Processes: Implications for Biological Microscopy. *J. Biomed. Opt.* **4** pp. 362-367 (1999).

MW Berns, J Aist, J Edwards, K Strahs, J Girton and P McNeil et al., Laser microsurgery in cell and developmental biology, *Science* **213** pp. 505–513 (1981).

O. Bouevitch and A. Lewis, Autocorrelating femtosecond pulses with thin bacteriorhodopsin films. *Opt. Commun.* **116** p. 170 (1995).

T Brixner and G Gerber. "Femtosecond polarization pulse shaping," *Opt. Lett.* **26** pp. 557-559 (2001).

EM Callaway and LC Katz, "Photostimulation using caged glutamate reveals functional circuitry in living brain slices," *Proc. Natl. Acad. Sci. USA **90*** pp. 7661–7665 (1993).

PJ Campagnola, M Wei, A Lewis and LM Loew. High-Resolution Nonlinear Optical Imaging of Live Cells by Second Harmonic Generation. *Biophys J* **77** pp. 3341-3349 (1999).

PJ Campagnola and LM Loew. Second-harmonic imaging microscopy for visualizing biomolecular arrays in cells, tissues and organisms. *Nature Biotechnology* **21** pp.1356 - 1360 (2003).

F Cannone, G Chirico, G Baldini, and A Diaspro. "Measurement of laser pulse width on the microscope objective plane by modulated autocorrelation method," *J. Micros.* **210** pp. 149-157 (2003).

IH Chen, SW Chu, CK Sun, PC Cheng and BL Lin, "Wavelength dependent damage in biological multi-photon confocal microscopy: A micro-spectroscopic comparison between femtosecond Ti:sapphire and Cr:forsterite laser sources," *Opt. Quantum Electron.* **34** pp. 1251-1266 (2002).

JX Cheng, A Volkmer, A., XS Xie, "Theoretical and experimental characterization of coherent anti-Stokes Raman scattering microscopy," *JOSA B* **19** p. 1363 (2002).

SW Chu, IH Chen, TM Liu, CK Sun, SP Lee, BL Lin, PC Cheng, MX Kuo, DJ Lin, and HL Liu. "Nonlinear bio-photonic crystal effects revealed with multimodal nonlinear microscopy," *J. Microsc.* **208** pp. 190-200 (2002).

JET Corrie, and DR Trentham, Caged Nucleotides and Neurotransmitters. In *Bioorganic Photochemistry*, H. Morrison, ed. (New York: Wiley), pp. 243–305. (1993)

D Débarre, W Supatto, A-M Pena, A Fabre, T Tordjmann, L Combettes, M-C Schanne-Klein1 and E Beaurepaire. "Imaging lipid bodies in cells and tissues using third-harmonic generation microscopy," *Nature Methods* **3** pp. 47 - 53 (2006).

K Deisseroth, G Feng, AK Majewska, G Miesenböck, A Ting, and MJ Schnitzer "Next-Generation Optical Technologies for Illuminating Genetically Targeted Brain Circuits," *The Journal of Neuroscience* **26** pp. 10380 –10386 (2006).

Dela Cruz J.M., Pastirk I., Comstock M., Lozovoy V.V., Dantus M., "Use of coherent control methods through scattering biological tissue to achieve functional imaging," *Proc Natl. Acad. Sci.* **101** pp. 16996–17001 (2004).

W Denk, JH Strickler and WW Webb. "Two-photon laser scanning fluorescence microscopy," *Science* **248** pp. 73-76 (1990).

W Denk. "Two-photon scanning photochemical microscopy: mapping ligand-gated ion channel distributions," *Proc. Natl. Acad. Sci. USA* **91** pp. 6629–6633 (1994).

W Denk and K Svoboda. "Photon Upmanship: Why Multiphoton Imaging Is More than a Gimmick," *Neuron*, **18** pp. 351–357 (1997)

N Dudovich, B Dayan, SMG Faeder and Y Silberberg. “Transform limited pulses are not optimal for resonant multiphoton transitions,” *Phys. Rev. Lett.* **86** pp. 47-50 (2001).

N Dudovich, D Oron and Y Silberberg. “Single-pulse Coherently Controlled Nonlinear Raman Spectroscopy and Microscopy,” *Nature* **418** pp. 512-514 (2002).

CL Evans and XS Xie. “Coherent Anti-Stokes Raman Scattering Microscopy: Chemical Imaging for Biology and Medicine,” *Annu. Rev. Anal. Chem.* **1** pp. 883–909 (2008).

IC Farber and A Grinvald. “Identification of presynaptic neurons by laser photostimulation,” *Science* **222** pp. 1025–1027 (1983).

P Fischer, DS Wiersma, R Righini, B Champagne, and AD Buckingham. “Three-Wave Mixing in Chiral Liquids,” *Phys. Rev. Lett.* **85** pp. 4253-4256 (2000).

DN Fittinghoff, JA Squier, CPT Barty, JN Sweetser, R Trebino, and M Muller. “Collinear type II second-harmonic-generation frequency-resolved optical gating for use with high-numerical-aperture objectives,” *Opt. Lett.* **23** pp. 1046-1048 (1998).

DN Fittinghoff, AC Millard, JA Squier, and M Muller. “Frequency-resolved optical gating measurement of ultrashort pulses passing through a high numerical aperture objective,” *IEEE J. Quantum Electron.* **35** pp. 479-486 (1999).

RL Fork. “Laser stimulation of nerve cells in Aplysia,” *Science **171*** pp. 907–908 (1971).

DJ Gallant, B Bouchet and PM Baldwin. “Microscopy of starch: evidence of a new level of granule organization,” *Carbohydrate Polymers* **32** pp.177-191 (1997).

M Göppert-Mayer. “Über Elementarakte mit zwei Quantensprüngen,” *Annalen der Physik* **401** pp. 273-294 (1931).

A Heisterkamp, IZ Maxwell, E Mazur, JM Underwood, JA Nickerson, S Kumar et al. “Pulse energy dependence of subcellular dissection by femtosecond laser pulses,” *Opt. Express* **13** pp. 3690–3696 (2005).

H Hirase, V Nikolenko, JH Goldberg and R Yuste. “Multiphoton stimulation of neurons,” *Journal of Neurobiology* **51** pp. 237-247 (2002).

W Kaiser and CGB Garrett. “Two-photon excitation in CaF_2:Eu^{2+},” *Phys. Rev. Lett.* **7** pp. 229–231 (1961).

DJ Kane and R Trebino. “Characterization of Arbitrary Femtosecond Pulses Using Frequency Resolved Optical Gating,” *IEEE J. Quantum Electron.* **29** pp. 571-579 (1993).

LC Katz and MB Dalva. “Scanning laser photostimulation: a new approach for analyzing brain circuits,” *J. Neurosci. Methods* **54** pp. 205–218 (1994).

H Kawano, Y Nabekawa, A Suda, Y Oishi, H Mizuno, A Miyawaki, and K Midorikawa. “Attenuation of photobleaching in two-photon excitation fluorescence from green fluorescent protein with shaped excitation pulses,” *B.B.R.C.* **311** pp. 592-596 (2003).

K Koenig, I Riemann, P Fischer, and K Halbhuber, “Intracellular nanosurgery with near infrared femtosecond laser pulses,” *Cell. Mol. Biol.* **45** pp. 192–201 (1995).

K Koenig. “Multiphoton microscopy in life sciences,” *J. Microsc*. **200** pp. 83–104 (2000).

G Krauss, S Lohss, T Hanke, A Sell, S Eggert, R Huber, A Leitenstorfer. “Synthesis of a single cycle of light with compact erbium-doped fibre technology”, *Nature Photonics* **4**, 33-36 (2009).

SQ Lima and G Miesenböck. “*Remote control of behavior through genetically targeted photostimulation of neurons*”. *Cell* **121** pp.141–152 (2005).

P Loza-Alvarez, CTA. Brown, DT Reid, W Sibbett, and M Missey. "High-repetition-rate ultrashort-pulse optical parametric oscillator continuously tunable from 2.8 to 6.8 μm," *Opt. Lett.* **24** pp. 1523-1525 (1999).

JA McCray and DR Trentham. “Properties and Uses of Photoreactive Caged Compounds,” *Annual Review of Biophysics and Biophysical Chemistry* **18** pp. 239-270 (1989).

J Mertz and L Moreaux. “Second-harmonic generation by focussed excitation of in homogeneously distributed scatterers,” *Opt. Comm.* **196** pp. 325-330 (2001).

AC Millard, DN Fittinghoff, JA Squier, M Muller, and AL Gaeta. *“"Using GaAsP photodiodes to characterize ultrashort pulses under high numerical aperture focusing in microscopy," J. Microsc.* **193** pp. 179-181 (1999).

G Miller. “Optogenetics. Shining new light on neural circuits,” *Science* **314** pp.1674-1676 (2006).

L Moreaux, O Sandre, and J Mertz. “Membrane imaging by second-harmonic generation microscopy,” *J. Opt. Soc. Am. B* **17** pp. 1685-1694 (2000).

M Muller, J Squier, and GJ Brakenhoff. “Measurement of femtosecond pulses in the focal point of a high-numerical-aperture lens by two-photon absorption,” *Opt. Lett.* **20** pp. 1038-1040 (1995a).

M Muller and GJ Brakenhoff. “Characterization of high-numerical-aperture lenses by spatial autocorrelation of the focal field,” *Opt. Lett.* **20** pp. 2159 (1995b).

M Muller, J Squier, R Wolleschensky, U Simon, and GJ Brakenhoff. “Dispersion pre-compensation of 15 femtosecond optical pulses for high-numerical-aperture objectives,” *J. Micros* **191** pp. 141–150 (1998).

JP Ogilvie, D Débarre, X Solinas, JL Martin, E Beaurepaire and M Joffre. “Use of coherent control for selective two-photon fluorescence microscopy in live organisms,” *Opt. Expr.* **14** pp. 759-766 (2006).

I Pastrick, JM Dela Cruz, KA Walowicz, VV Lozovoy and M Dantus. “Selective two-photon microscopy with shaped femtosecond pulses,” *Opt. Express* **11** pp. 1695-1701 (2003).

JP Pawley, Handbook of Biological Confocal Microscopy, 2nd ed. (Plenum, New York, 1995).

DL Pettit, SS-H Wang, KR Gee and GJ Augustine. “Chemical Two-Photon Uncaging: a Novel Approach to Mapping Glutamate Receptors,” *Neuron*, **19** pp. 465–471 (1997).

SM Potter. “Vital imaging: Two photons are better than one,” Current Biology **6** pp. 1595–1598 (1996).

S Psilodimitrakopoulos, I Amat-Roldan, M Mathew, AN Thayil, D Zalvidea, D Artigas, and P Loza- Alvarez. “Starch granules as a probe for the polarization at the sample plane of a high resolution multiphoton microscope,” BIOS’08, Photonics west 2008. *Proc. of SPIE*, Multiphoton Microscopy in the Biomedical Sciences VIII, 68600-E1-14. San José, California, USA.

F Quercioli, A Ghirelli, B Tiribilli, and M Vassalli. “Ultracompact autocorrelator for multiphoton microscopy,” *Microsc. Res. Tech.* **63** pp. 27-33 (2004).

M Sachihiro, H Tsunehito, F Kiichi, I Keisuke, I Kazuyoshi. “Femtosecond laser disruption of subcellular organelles in a living cell,” *Opt Express* **12** pp. 4203–4213 (2004).

N Shen, D Datta, CB Schaffer, P Le Duc, DE Ingber and E Mazur. “Ablation of cytoskeletal filaments and mitochondria in live cells using a femtosecond laser microscissors,” *Mech. Chem. Biosyst*. **2** pp. 17–26 (2005).

Y Silberberg. “Ultrafast physics: Quantum control with a twist,” *Nature* **430** pp. 624-625 (2004)

NI Smith, K Fujita, T Kaneko, K Kato, O Nakamura, T Takamatsu and S Kawata. “Generation of calcium waves in living cells by pulsed-laser-induced photodisruption,” *Appl. Phys. Lett*. **79** pp. 1208-1210 (2001).

NI Smith, S Iwanaga , T Beppu, K Fujita, O Nakamura, S Kawata. “Photostimulation of two types of Ca2+ waves in rat pheochromocytoma PC12 cells by ultrashort pulsed near-infrared laser irradiation,” *Laser Physics Letters* **3** pp. 154-161 (2006).

J Squier, M Muller, G Brakenhoff and KR Wilson. “Third harmonic generation microscopy,” *Opt. Express* **3** pp. 315-324 (1998).

T Suzuki, S Minemoto, T Kanai and H Sakai. “Optimal Control of Multiphoton Ionization Processes in Aligned I2 Molecules with Time-Dependent Polarization Pulses,” *Phys. Rev. Lett.* **92** 133005 (2004).

G Stibenz, G Steinmeyer. “Interferometric frequency-resolved optical gating,” *Opt. Express* **13** pp. 2617-2626 (2005).

S Tang, TB Krasieva, Z Chen, G Tempea, and BJ Tromberg. “Effect of pulse duration on two-photon excited fluorescence and second harmonic generation in non-linear optical microscopy,” *J. Bio. Opt.* **11** 020501-1-3 (2006).

AKN Thayil, EJ Gualda, S Psilodimitrakopoulos, IG Cormack, I Amat-Roldan, M Mathew, D Artigas and P Loza-Alvarez, “Starch-based backwards SHG for in-situ MEFISTO pulse characterization in multiphoton microscopy,” *J. of Microscopy* **230** pp.70-75 (2008).

UK Tirlapur and K Koenig. “Femtosecond nearinfrared laser pulses as a versatile non-invasive tool for intratissue nanoprocessing in plants without compromising viability,” *Plant. J.* **31** pp. 365–374 (2002a).

UK Tirlapur and K Koenig. “Targeted transfection by femtosecond laser,” *Nature* **448** pp. 290–291 (2002b).

AB Uzdensky and VV Savransky. “Single neuron response to pulse-periodic laser microirradiation. Action spectra and two-photon effect,” *J. Photochem. Photobiol. B Biology* **39** pp. 224-228 (1997).

A Vogel and V Venugopalan. “Mechanisms of pulsed laser ablation of biological tissues,” *Chem. Rev.* **103** pp. 577–644 (2003).

W Watanabe, N Arakawa, S Matsunaga, T Higashi, K Fukui, K Isobe et al. “Femtosecond laser disruption of subcellular organelles in a living cell,” *Opt Express* **12** pp. 4203–4213 (2004).

RM Williams, WR Zipfel, and WW Webb. “Interpreting second-harmonic generation images of collagen I fibrils,” *Biophy. J.* **88** pp. 1377-1386 (2005).

B Xu, JM Gunn, JMD Cruz, VV Lozovoy, and M Dantus, "Quantitative investigation of the multiphoton intrapulse interference phase scan method for simultaneous phase

measurement and compensation of femtosecond laser pulses," *J. Opt. Soc. Am. B* **23** pp. 750-759 (2006).

D Yelin and Y Silberberg, "Laser scanning third-harmonic-generation microscopy in biology," *Opt. Express* **5** pp. 169-175 (1999).

E Zeira, A Manevitch, A Khatchatouriants, O Pappo, E Hyam, M Darash-Yahana, E Tavor, A Honigman, A Lewis and E Galun. Femtosecond infrared laser—an efficient and safe in vivo gene delivery system for prolonged expression. *Molecular Therapy* **8** pp. 342–350 (2003).

BV Zemelman, GA Lee, M Ng, G Miesenböck. "Selective photostimulation of genetically chARGed neurons," *Neuron* **33** pp. 15-22 (2002).

F Zhang, LP Wang, ES Boyden, K Deisseroth, "Channelrhodopsin-2 and optical control of excitable cells," *Nat. Methods* **3**(10) pp. 785-792 (2006).

F Zhang, M Prigge, F Beyriere, SP Tsunoda, J Mattis, O Yizhar, P Hegemann, and K Deisseroth. "Red-shifted optogenetic excitation: a tool for fast neural control derived from Volvox carteri," *Nat Neurosci* **11** pp. 631 - 633 (2008).

WR Zipfel, RM Williams, and WW Webb "Nonlinear magic: multiphoton microscopy in the biosciences," *Nature Biotechnology* **21** pp. 1369 - 1377 (2003).

Zumbusch, A.; Holtom, G. R.; Xie, X. S., "Vibrational mircoscopy using coherent anti-Stokes Raman scattering," *Phys. Rev. Lett.* **82** 4014 (1999).

CHAPTER 8

Summary of this thesis.

8 Summary of this thesis.

8.1 Major contributions.

In this thesis I have presented a series of "new tools" to fully characterise ultrashort laser pulses and I have achieved specific "milestones" that show its performance in real applications like *in-vivo* multiphoton microscopy. In summary, major contributions of this work can be numbered as: (1) developing two new families of techniques able to fully measure ultrashort laser pulses under a collinear scheme which were named CFROG and MEFISTO, (2) specifically, MEFISTO can directly measure one unknown pulse in an analytical way, (3) both techniques, CRFOG and MEFISTO, were experimentally demonstrated in a range of scenarios ranging from simple to more complex pulses, (4) fast-CFROG and fast-MEFISTO, which do not require large datasets neither long acquisitions, have both been demonstrated, (5) theoretical demonstration of the blind-MEFISTO technique, able to simultaneously characterize two unknown pulses in an analytical way, (6) suggesting and demonstrating the use of starch granules as a natural nonlinear material for characterising ultrashort laser pulses at the sample plane of a multiphoton microscope and (7) by exploiting backwards second harmonic generation from starch granules it is possible to characterise pulses without additional nor bulky mechanical mount on any commercial system.

CFROG measurements were derived from extending the non-collinear theoretical framework of pulse measurement to a collinear scheme, which showed good performance experimentally even in its "fast" version at undersampling regimes. This progress was a mandatory step in our strategy to develop an ultrashort pulse measurement technique fully compatible with pulse measurement in a nonlinear microscope. Importantly, developing a general method based on collinear geometry by itself enables a simpler and more reliable scheme to carry out pulse measurements. For this reason, CFROG is now being employed for more

demanding applications. In fact, CFROG was the method of choice for one major contribution published in *Nature Photonics* (Krauss, 2009) to characterise single optical cycle ultrashort pulsed laser, which is basically at the physical limit of an ultrashort pulse at a given wavelength.
MEFISTO was then developed to overcome an additional limitation of the current state-of-the-art mainly represented by FROG, which is the required iterative algorithm to seek for a solution through recursively estimating the retrieved phase. The fundamental objection of this procedure is that it shows specific flaws in front of some non-trivial ambiguities and the additional fact that it has been shown to give different retrievals with different initial conditions. In this sense, MEFISTO performs a direct measurement on the collinear measurement and it possess solely one possible outcome. MEFISTO has been shown to retrieve ultrashort laser pulses with small quadratic phase modulation mainly caused by an optical isolator, or complex pulses which suffered a number of nonlinear effects while propagating through multimodal fibers, additional pulses undergoing optical components of a multiphoton microscope have been characterised.
This methodology has the potential to become a sound gold standard but this requires further refinement of some aspects of the technique. Main positive aspects that require to be emphasised are:
MEFISTO is a highly sensitve technique that can measure very subtle phase changes, but it requires a very good system calibration and convenient acquisition.
MEFISTO has the potential to obtain phase information in the low SNR regime. This could be solved by the development of a multi-slice approach. This has been in fact preliminary demonstrated by other authors (Hsu, 2007), but a complete analysis is still required.

In this thesis rather than trying to solve such (mathematical) problems, we have decided to points out other theoretical scenarios of MEFISTO. For example, after developing the BlindMEFISTO technique we have numerically computed blindMEFISTO under different SNR regimes so to assess its feasibility for an experimental demonstration. Additionally

we have focus our attention in fastMEFISTO and we have shown that it contains the very same information of the classical trace if Nyquist criterion is followed, which dramatically reduces acquisition time.

Starch has been suggested and demonstrated as a suitable natural nonlinear material, which is very convenient for generating the SHG signal required for characterising ultrashort laser pulses of the tightly focused light in a microscope. Specifically, starch possess a relaxed phase-matching that occur not only at a broad spectral range experimentally demonstrated from 700 to 1300nm (in this thesis at 830nm and 1100nm by means of a home-made SP-OPO), but also at the large angles and the different polarizations which are produced an average representation of the focused light that has passed through optical components of a multiphoton microscope in a different manner. For example, the outermost part of the objective introduces less dispersion because it is thinner than the innermost part, which is the thickest. After this works were published, another technique named MIIPS was presented by Dantus and co-workers, but this methodology possess major differences with ours: (1) it is still an iterative algorithm which converges after a sequence of approximations, (2) it requires to compensate the ultrashort pulse to characterise it, (3) it requires an Spatial Light Modulator, which is expensive and more complex if compared to a Michelson Interferometer, (4) it is dedicated to characterise optical components or schemes rather than characterise light at the focal plane, and (5) it did not reported any suitable material like starch.

Therefore, the important remarks are that our techniques previously solved the issue of measuring an ultrashort laser pulse at the sample plane of a multiphoton microscope by providing a double answer: technique and material. MIIPS occurred in the middle of this work and were reported years later. Also, it should be highlighted that CFROG was the first general method that accurately measured the ultrashort laser pulse compared to previous attempts described in the thesis.

Finally, pulse characterisation is measured at the focal plane of a commercial microscope *in-vivo* with no additional mechanical mounts and epi-detection of SHG is experimentally shown in starch.
Therefore, a wide range of "new tools" and techniques has been shown to be suitable to fully characterise ultrashort laser pulses, which was the main aim of this thesis.

As I said at the beginning of this dissertation, these new tools for measurement of ultrashort pulses will be part of the existing basis of laser technologies for development of improved tools for biomedicine and other disciplines. The exquisite control on light matter interactions offered by pulse shaping can be only achieved if we can actually measure our ultrashort light pulses anywhere and anytime. Coherent control is an exciting concept that might offersan unbelievable opportunity for science and technology, but it requires development of many disciplines and realistic control to perform biomedical experiments in a direct manner might be available in very few sites of the world or none. In this long way, one of the first requirements to be acomplisshed is to ensure that pulse characterisation is accurate, robust, flexible and handy. The intention of this thesis was to build solid and specific progress in this direction, and we have successfully achieved that. Characterising ultrashort pulses in a microscope will be of high interest in life sciences but also in many other fields, because life sciences offer a difficult arena with added complications such as the fragility of life. Also, from the microscopy prospective coherent imaging should be the logical extension of this thesis to be able to exploit new contrast mechanisms by tailoring the shape of ultrashort light pulses to particular molecules or chemical environments and enhancing specificity of multiphoton imaging, which is lost for unshaped pulses and represents a major disadvantage when compared to linear confocal microscopy from the biomedical viewpoint. Furthermore, accurate control of temporal properties of light, will enable producing even shorter events, and more controllable attosecond pulses and understand much better ultrafast phenomena that occurs well below picoseconds and femtoseconds in the near future, hopefully.

In this line, the work presented in this thesis has continued in a number of projects: a European Project, named STELUM, SpatioTemporal Engineering of Light: Ultimate Multiphoton-microscopy, in which pulse characterization is followed by pulse shaping; another PhD student used MEFISTO to characterise ultrashort laser pulses in her experiments like the one reported in chapter 6; and an undergraduate student is currently programming a graphic user interface for using MEFISTO in a fully automated manner.

No major evolutions on pulse measurement have been carried out in the recent years beyond those reported in chapters 3. Reamarkably, authors of Hsu (2007) has solved MEFISTO trace using the frequency delay axis (Li-Fan, 2010) which was mentioned in the paper but never carried out experimentally, which shows that this technique is further evolving in other research groups around the world.

My major contributions to the research group led by Prof. Loza-Alvarez are the adaptation of a standard microscope to a multiphoton system with a custom-made chamber for keeping cells alive, detection of Second Harmonic and Two-Photon Microscopy, use of starch as nonlinear medium, solution of direct pulse measurements in collinear conditions, characterization of the pulses and this can be then reported in the works submitted for journals, characterization of the dispersion introduced by the optical elements of the setup and some pulse shaping with prisms and a Spatial Light Modulator (SLM). Currently the group is using this initial knowledge to continue the work and extend it to the spatial domain. They are currently using adaptive optics to compensate wavefront aberrations when progating through heterogeneous media. These methodologies allow for correct focusing at deep layers and maximization of the detected signal, which again enables to minimize phototoxic effects when imaging biological specimens. However, adaptive optics also encounter similar technical difficulties to those with pulse shaping as they both rely on SLMs. SLMs are very interesting components from the theoretical prospective, but in practical terms they are highly complex to use and require a very detailed study to efficiently use them.

8.1.1 List of papers related to this thesis.

I Amat-Roldan, IG Cormack, E Gualda, D Artigas, P Loza-Alvarez. "Ultrashort pulse characterisation with SHG collinear-FROG", *Optics Express* **12** pp. 1169-1178 (2004).
I Amat-Roldan, IG Cormack, D Artigas, P Loza-Alvarez. "Starch-based SHG-CFROG pulse characterisation at the focal plane of a high numerical aperture lens", *Optics Letters* **29** pp. 2282-2284 (2004).

I Amat-Roldan, IG Cormack, D Artigas, P Loza-Alvarez. "Measurement of electric field by interferometric spectral trace observation", *Optics Letters* **30** pp. 1063-1065 (2005).

I Amat-Roldan, D Artigas, IG Cormack, and P Loza-Alvarez. "Simultaneous analytical characterisation of two ultrashort laser pulses using spectrally resolved interferometric correlations", *Optics Express* **14** pp. 4538-4551 (2006).

AKN Thayil, EJ Gualda, S Psilodimitrakopoulos, IG Cormack, I Amat-Roldan, M Mathew, D Artigas, P Loza-Alvarez. "Starch-based backwards SHG for in-situ MEFISTO pulse characterization in multiphoton microscopy", *Journal of Microscopy* **230** pp. 70-75 (2008).

8.1.2 List of papers with the research group.

IG Cormack, P Loza-Alvarez, L Sarrado, S Tomas, I Amat-Roldan, L Torner, D Artigas, J Guitart, J Pera, J Ros. "Lost writing uncovered by Laser two-photon fluorescence provides a terminus post quem for Roman colonization of Hispania Citerior," *Journal of Archaeological Sciences* **34** pp. 1594-1600 (2007).

M Mathew, I Amat-Roldan, R Andres, IG Cormack, D Artigas, E Soriano, P Loza-Alvarez. "Influence of distant femtosecond laser pulses on growth cone fillopodia," *Cytotechnology* **58** pp. 103-111 (2008).

S Psilodimitrakopoulos, SICO Santos, I Amat-Roldan, AKN Thayil, D Artigas, P Loza-Alvarez. "In vivo, pixel resolution mapping of thick filaments

orientation in non-fibrilar muscle using polarization sensitive second harmonic generation microscopy," *Journal of Biomedical Optics* **14** 014001 (2009).

S Psilodimitrakopoulos, D Artigas, G Soria, I Amat-Roldan, AM Planas, P Loza-Alvarez . "Quantitative discrimination between endogenous SHG sources in mammalian tissue based on their polarization response," *Optics Express* **17** pp. 10168-10176 (2009).

S Psilodimitrakopoulos, V Petegnief, G Soria, I Amat-Roldan, D Artigas, AM Planas, P Loza-Alvarez. "Estimation of the effective orientation of the SHG source in cortical neurons," *Optics Express* **17** pp. 14418-14425 (2009).

M Mathew, I Amat-Roldan, R Andres, SICO Santos, D Artigas, E Soriano, P Loza-Alvarez. "Signalling effect of NIR Pulsed Lasers on Axonal growth," *Journal of Neuroscience Methods* **186** pp. 196-201 (2009).

S Psilodimitrakopoulos, I Amat-Roldan, P Loza-Alvarez, D Artigas. "Estimating the helical pitch angle of amylopectin in starch using polarization second harmonic generation microscopy," *Journal of Optics* **12** pp. 084007 (2009).

I Amat-Roldan, S Psilodimitrakopoulos, P Loza-Alvarez, D Artigas. "Fast image analysis of Polarization SHG microscopy," *Optics Express* **18** pp. 17209-17219 (2010).

S Psilodimitrakopoulos, I Amat-Roldan, P Loza-Alvarez, D Artigas. "Effect of molecular organization on the image histograms of polarization SHG microscopy," *Biomed Opt Express* **3** pp. 2681-2693 (2012).

8.1.3 Public patents with the research group.

P Loza-Alvarez, I Amat-Roldan, R Andres, D Artigas, IG Cormack, M Mathew, E Soriano, and L Torner. "Method and device for the control and analysis of nerve cell growth," ICFO- The Institute of Photonic Sciences and Universitat Politècnica de Catalunya. WO/2008/043808. Spain, 13.10.2006.

I Amat-Roldan, P Loza-Alvarez, D Artigas, “Device for multispectral and spatial shaping”, ICFO- The Institute of Photonic Sciences and Universitat Politècnica de Catalunya. WO/2010/060460. Spain, 25.11.2008.

References

G Krauss, S Lohss, T Hanke, A Sell, S Eggert, R Huber, A Leitenstorfer. “Synthesis of a single cycle of light with compact erbium-doped fibre technology”, *Nature Photonics* **4**, 33-36 (2009).

C Hsu and S Yang, "Robustness Enhancement of Iteration-Free Spectral Phase Retrieval by Interferometric Second-Harmonic Trace," in *Conference on Lasers and Electro-Optics/Quantum Electronics and Laser Science Conference and Photonic Applications Systems Technologies*, OSA, 2007.

L-F Yang, S-L Lin, and S-D Yang, "Ultrashort pulse measurements by interferometric spectrogram," *Opt. Express* **18**, 6877-6884 (2010).